Experimental and Numerical Study of Particle Heating Using DC Discharge

by

Olawale Ajuwon

A thesis submitted in partial fulfillment of the requirements for the degree of

Master of Science

in

Chemical Engineering

Department of Chemical and Materials Engineering

University of Alberta

©Olawale Ajuwon, 2015

Abstract

The main aim of this work is experimental and numerical study of heat and mass transfer in fixed beds by the Joule heating effect, which is a volume-based type of heating rather than surface-based. This is aimed at looking more into energy storage technologies where electrical energy is stored as chemical energy i.e. **Energy to Chemicals (E2C) concept**. Experiments were carried out for fixed bed heating with and without gas flowing through the bed and temperature measurements with time were taken at the center and outlet of the bed for solid and gas temperatures respectively. The experiments were carried out with 15 W, 22.5 W and 42 W powers and also with four mass flow rates ranging from 1.27 $\times 10^{-7}$ to 6.13 $\times 10^{-7}$ kg/s. The experimental results were then validated against numerical and computational fluid dynamics (CFD) models. It was observed that since the bed was not insulated, heat was lost at the wall and also that the gas temperature increases at the outlet with mass flow rate. This was attributed to the fact that for lower mass flow rates, the gas tends to moves along the wall from the inlet to the outlet of the bed. Based on this knowledge of heat and mass transfer in fixed beds with electrical heating, a preliminary study of energy storage, in particular, steam reforming of methane, was then carried out.

Acknowledgements

I would like to extend my thanks and gratitude towards my research supervisors, Dr Rajender Gupta and Dr. Petr Nikrityuk, for their continuous help and support throughout my masters degree. I am very grateful to them for giving me the privilege of working under their mentorship.

I would also like to thank Dr Moshfiqur Rahman for his help and encouragement for my research. I would like to thank my colleagues, Pankaj Kumar Sahu, Md Omar Reza, Hemant Bansal, for their valuable insight and technical assistance. I would also like to thank Sebastian Schulze for his help.

I would like to acknowledge the financial support of Canadian Centre for Clean Coal/Carbon and Mineral Processing Technology (C5MPT), Helmholtz-Alberta Initiative (HAI) and NSERC Canada.

Contents

List of Figures

List of Tables

Abbreviations

1D	**O**ne **D**imensional
2DPF	**T**wo **D**imensional **P**lug **F**low
2DADPF	**T**wo **D**imensional **A**xially **D**ispersed **P**lug **F**low
3D	**T**hree **D**imensional
CFD	**C**omputational **F**luid **D**ynamics
DC	**D**irect **C**urrent
DRM	**D**ry **R**eforming **M**ethane
E2C	**E**nergy **T**o **C**hemicals
MP	**M**elting **P**oint
MRI	**M**agnetic **R**esonance **I**maging
PSD	**P**article **S**ize **D**istribution
SRM	**S**team **R**eforming **M**ethane
WGS	**W**ater **G**as **S**hift

Physical Constants

Emissivity	ϵ_σ	=	0.99
Particle density	ρ_{nickel}	=	8900 kg/m^3
Fluid density	ρ_{air}	=	1.225 kg/m^3
Specific heat	C_{nickel}	=	460.6 J/kgK
Porosity (void fraction)	ε	=	0.67

Nomenclature

A, A_{sur}	surface area	m^2
A_k	pre-exponential factor	
c, C_p	heat capacity of component	J/kgK
D	tube diameter	m
d_p	particle diameter	m
ΔE_{st}^{tot}	total energy stored	J
E_a	activation energy	J/kg.mol
E_{in}	inflow energy	J
E_{out}	outflow energy	J
E_g	energy generated	J
ΔH_i	enthalpy of reaction i	kJ/mol
I	current	A
k	rate constant	
L	bed length	m
$\dot{m}$	mass flow rate	kg/s
N_p	number of particles	
Nu	Nusselt number	
Pr	Prandtl number	
r	radial position inside reactor	m
Re	Reynolds number	
R	universal gas constant	J/kgK
T	temperature	K
T_{cfd}	CFD estimated temperature	K
T_{exp}	measured temperature	K

t	time	s
v, U_V	velocity	m/s
U	voltage	V
V	volume	m^3
Y	mass fraction	

Greek symbols

α	heat transfer coefficient	W/m^2K
α_w	wall heat transfer coefficient	W/m^2K
β	temperature exponent	
ϵ_σ	emissivity	
ε	porosity	
λ	thermal conductivity	W/mK
μ	fluid dynamic viscosity	kg/(m· s)
$\mu_{t\varepsilon}$	macroscopic turbulent viscosity	kg/(m· s)
ρ	density	kg/m^3
ϱ	electrical resistivity	ohm.m
σ	Stefan-Boltzmann constant	W/m^2K^4
ϕ	particle sphericity	

Superscripts

0	initial
tot	total

Subscripts

ax	axial
e	effective
f	fluid
g	generated
in	inlet
out	outlet
p	particle
r	radial
s	solid
st	stored
w	wall

Dedicated to the author and finisher of my faith, the Lord Jesus Christ and to my parents and siblings

Chapter 1

Introduction

1.1 Background

The environmental and climatic impacts of fossil fuels have necessitated the search for cleaner and cheaper alternative energy sources [1]. These energy sources (e.g. wind, sunlight, tidal and geothermal) are renewable and produce electricity which can be used to convert energy from fossil fuels into storable chemical energy. This energy conversion and storage is usually carried out in a fixed bed, which is regarded to be more economical due to its ease of operation and lower operating cost especially for large production amounts [2, 3]. Fixed beds can be used for various kinds of reaction,which includes gasification ($C + CO_2$), water gas reaction ($C + H_2O$ & $C + CO_2$), steam and dry reforming reaction ($CH_4 + H_2O$ & $CH_4 + CO_2$). These reactions have a wide range of application in the chemical and process industries. Their application includes drying [2, 4, 5] reactors for the production of chemicals [2, 4, 6], porous media in storage of thermal energy and oil recovery [2, 7], filters and heat exchangers[1].

The wide range of fixed bed applications (which includes heat removal from exothermic reaction or for heat supply for endothermic reactions) [8], necessitates the study of the transport phenomena within the bed. This would allow for a better

approach for treating reactions as either homogeneous or heterogeneous especially when simulations are carried out.

1.2 Literature Review on Fixed Beds Technologies

Although much studies have been done on the transport properties of fixed beds, very few of them have been on fixed bed heating with electricity. This electric fixed bed heating can be used in processes like gasification and steam reforming, whose end product can be stored as chemical energy for energy generation at a later time.

The performance of fixed beds depends on heat transfer parameters such as fluid-particle heat transfer and heat transfer coefficient [4, 9–14]. This can be studied using one phase homogeneous models or two phase heterogeneous models [15, 16] depending temperature difference between phases. One phase homogeneous model would be appropriate for small temperature differences between phases, while two phase heterogeneous model should be used when there is considerable temperature difference between phases[4]. Therefore, the Biot number defined as *the ratio of the thermal resistance within the packed particle to that between the fluid and packed particle*,[4] can be used to select the appropriate model.

1.2.1 DC heating of Fixed Beds

Glaser and Thodos [17] carried out a study to establish the heat transfer coefficient for gases flowing through a fixed bed of randomly packed granular particles in the absence of mass transfer effects [18–26]. They proposed the possibility of evaluating the analogy between heat and momentum transfer from the pressure drop data. In their work, electric current was passed through a bed of metallic particles and a steady generation of heat is achieved. The heat was continuously

removed by gas flowing through the bed and the temperature measurements of the gas and solid taken. From the temperature measurements, the local heat transfer coefficient, α_g was obtained.

Colburn [27] developed a correlation for the heat transfer factors for different types of bed. A plot of heat transfer factor, j_h against modified Reynolds number shows a good correlation for different bed sizes and shapes. The correlations were found to differ as the shape and size of bed changes. *The lack of a single correlation for all types of packing was then attributed to the fact that the ratio of particle size to column diameter exceeds the recommended limit of 0.125*[17]. From the pressure drop measurement, the friction factors, f_k, were then calculated from the Ergun [28] equation and it has been found that the friction factor increases with decreasing particle size, which is opposite to the behaviour observed for the heat transfer factor. The momentum and heat transfer are not related in packed beds because momentum transfer involves surfaces, corners and edges whereas heat transfer involves just the surfaces.

1.2.2 Heat and Mass Transfer in Fixed Beds

Despite the fact that fixed beds have become one of the most commonly used reactors in the industry, understanding the fluid flow and heat transfer in these beds is still a major concern, especially for low tube to particle diameter ratio, in the range of 3-8 [29]. The heat transfer behaviour of these types of bed is still yet to be understood [30–32]. Correlations in literature for the effective heat transfer parameters have not been able to give a good comparison with experimental data [31, 33]. Therefore, there is a need for better understanding of the fluid flow and heat transfer in fixed bed, to obtain better model results.

Kutsovsky et al. [34] and Sederman et al. [35] have recently used magnetic resonance imaging (MRI) to map out the velocity profile within the fixed bed. However, this approach does not allow temperature profile investigation. Computational fluid dynamics (CFD) is now been used to investigate both the fluid flow

and temperature profile in fixed beds. This approach is very complex due to the need mesh creation around the contact points and the high gradients [29].

Logtenberg et al. [29] simulated the fluid flow and heat transfer in a fixed bed using CFD, assuming the fluid to be incompressible and Newtonian with temperature dependent properties. Although this study was done for laminar and turbulent flow in steady state, the Reynolds number at which turbulent eddies start to form in the fixed bed is uncertain [36, 37]. The standard $\kappa - \varepsilon$ model was used for the turbulence model.

The work by Logtenberg et al. [29] was aimed at improving on the work done by Logtenberg and Dixon [38, 39] and Derkx and Dixon [40] by including wall-particle and particle-particle contact points in the CFD models for fluid flow and heat transfer in fixed beds. They found out that there was a strong radial components of flow near the vicinity of wall-particle contact, which leads to high rates of effective radial heat transfer. Also, they found that as the Reynolds number increased, eddies start to form. These eddies are as a result of the strong radial flow from the middle towards the wall which goes both in the upward and downward axial flow at the wall [34]. A decrease in local radial heat transfer cause increased axial flow and reduced radial flow at the wall, and a temperature jump near the wall [29]. Also, an increase in Reynolds number increases velocity, which in turn increases the convective heat transfer. The wall Nusselt number was found to change with the height of the bed and dependent on the structure and flow profile near the wall.

Due to the extensive use of fixed bed in the industries, a concise knowledge of the heat transfer in fixed bed is required. Most researchers express the heat transfer properties in fixed beds as effective thermal conductivities which is *an average transfer parameter describing the total thermal performance of a medium* [41–48]. Some authors have expressed it as the heat transfer coefficient [49–55]. Previous works on the heat transfer in fixed beds have been based on some form of empirical and semi-empirical correlations, many of which do not yield the same results. This is believed to be as a result of the different experimental conditions used to arrive

at the correlations. Also, this disagreement can be attributed to the experimental measurement technique and most importantly improper system modeling [41].

One very important parameter when studying heat transfer is the heat transfer coefficient. This has been studied extensively by various researchers to determine the most accurate way of approximating this very important parameter. Wen and Ding [4] studied heat transfer behaviour of a gas flowing through a packed bed. The experimental data for both the transient and steady-state study under constant wall temperature conditions were compared to a two-dimensional numerical model. The two-dimensional model with either a plug flow or an axially dispersed plug flow assumption was used [56]. The model can be classified into one-phase homogeneous model or two-phase heterogeneous model depending on the temperature difference between the packed bed and flowing fluid [15, 16].

Previous studies on the heat transfer in packed beds have measured radial temperature at the inlet and outlet of the bed[33, 57–63]. Therefore, the temperature profile in the interior of the bed is generally unknown. Some researchers have shown that using variable effective radial thermal conductivity and wall-fluid heat transfer coefficient parameters, allows the two-dimensional homogeneous model to predict the temperature inside the bed more accurately[60, 62–64]. They found out that the particle-gas temperature difference increases with Reynolds number. Also, the higher the Reynolds number, the more no-uniform the temperature distribution is, since temperature distribution depends on Reynolds number. The temperature distribution was also found to have little dependence on the radial position.

Wakao et al. [65] computed the axial effective thermal conductivity. By comparing experimental data and modeling results, they concluded that effective thermal conductivity is not constant but depend on heating length. Also, the two-dimensional axially dispersed plug flow (2DADPF) model assumes a uniform porosity distribution in packed beds and neglects radial flow distribution. This assumption applies very well for beds with large bed to particle diameter ratios but for beds with small ratios gives significant deviations. Large voidage at the wall leads to

a large temperature drop at the wall region. Therefore, in order to have a better agreement between experimental data and modelling, the non- uniform radial flow assumption has to be used.

Previous studies by Li and Finlayson [30] and Paterson and Carberry [66] for two-dimensional plug flow (2DPF) model suggest that the effective thermal conductivities and the wall heat transfer coefficient decreases with increasing heating length and approach a constant value when the flow is fully developed. Dixon [60] suggested that the use of 2DADPF model eliminated the length-dependent effect.

1.2.3 Materials conversion

Studies have been carried out to understand the influence of heterogeneous fuel bed properties on the fuel conversion [67]. To model this system, the Lagrangian tracking approach or the Eulerian continuum approach could be used. The Lagrangian tracking approach involves tracking each particle as the process proceeds and this is used with the Eulerian representation for the fluid [68, 69]. The Eulerian continuum approach on the other hand is such that the both the particle and fluid phase are represented by Eulerian representation [70–81]. The Eulerian continuum approach has been employed in their study due to the high computational cost for using the Lagrangian tracking approach. For spherical particles, the assumption is that the fuel bed shrinks smoothly and the particles are assumed to slide down perfectly when the mass beneath them is consumed but this is seldom the case as most particles are rarely spherical and are often times rough on the surface. The conversion of fuel particles represented as cylinders are modelled according to the shrinking core model. The model results show that heterogeneous bed porosity could result in channelling in the fuel bed, which leads to uneven combustion. The channelling tendency can then be reduced by grates of higher flow resistance[67].

1.2.3.1 Steam-Methane Reforming

Sadooghi and Rauch [1] carried out a study on steam reforming of methane in the presence of catalyst particles. Electricity was used to provide the heat needed for the reaction. A pseudo heterogeneous model was used in this study to represent the diffusion phenomena inside the reactor. The model was used to solve for both the flow phase and within the catalyst pellets. Heat and mass transfer equations were coupled with the reaction mechanism and modeled under the steady state assumption.

The model was a two-dimensional heterogeneous steady-state model, with explicit description of velocity, concentration and temperature distribution inside the surface bed reactor system. This consists of equations for material, energy and momentum balance; and an equation for physical properties of the reactants. Steam reforming of methane consist of three reversible reactions: two strongly endothermic reforming reactions and one mildly exothermic water-gas shift reaction[82].

The correlation by Froment and Hofmann [83] and Dixon et al. [84] was used for calculating effective thermal conductivity and effective radial diffusivity. The planar geometry was used and this changed the continuity equation for both methane and carbon dioxide. The model showed that the increasing the outlet temperature increases the reaction temperature. This in turn increases the methane conversion and hydrogen yield. Also, higher temperature led to more uniform temperature profile distributions in the axial direction and this result in a more efficient usage of the reactor. Also, high temperature favours methane conversion.

1.2.3.2 Coal Gasification

Luckos and Bunt [85] studied the pressure drop across a coal bed gasifier, using the Ergun equation [28, 86, 87] for pressure drop measurements. It was found that the Ergun equation gave good prediction for non-reacting isothermal packed beds with particles of uniform size. Also, it was found that good predictions were obtained from the equation when the particles were either spherical or nearly spherical. So

for a coal bed gasifier where there are four zones, namely, drying, devolatilization, reduction (gasification) and combustion zones, the physical properties (such as average particle size, particle size distribution (PSD), sphericity and density) and chemical properties (such as temperature, density and viscosity) are different in each zone. This therefore means that the pressure drop across the bed will not be the same. The total pressure drop will then be the sum of the pressure drops in all the zones. The main aim of their study is to evaluate the prediction accuracy of the Ergun equation for pressure drop in a fixed bed gasifier. It was determined from this work that pressure drop determination depends on the bed voidage and so a precise estimation of the bed voidage is required for accurate calculation of the pressure drop. The voidage depends on the PSD, particle sphericity and surface roughness, the packing method and vessel size relative to the particle diameter[88–102]. Hicks [103] argued that the usage of Ergun equation without flow range restriction may not be applicable for values of $Re/(1–\varepsilon)$ greater than 500. Although, previous experiments show that pressure drop increases as bed PSD spread and particle size decreases, CFD results suggest otherwise. It was found from their work that pressure drop in the gasification and combustion region accounts for over 70% of the total pressure drop across the bed. They explained this by citing low bed voidage and the value of $Re/(1–\varepsilon)$ in the drying and devolatilization region which is higher than the 500 limit suggested by Hicks [103]. Therefore, they concluded that the Ergun equation cannot be used to determine pressure drop within these regions.

1.2.4 Modeling of heat transfer

To reduce the discrepancy between the methods used by different researchers, Bhattacharyya and Pei [41] suggested that a better approach is to correlate the heat transfer as a contribution of the different mechanisms in terms of the properties which would most likely affect the heat transfer. This was done by assuming the contributions are independent of each other and that they are additive. A model which separates the heat transfer into two parts was proposed by Yagi and

Kunii [47], namely those *independent of and dependent of fluid flow*. The equation representing this correlation consist of contributions to heat transfer which are independent and dependent of fluid flow respectively on the right hand side of the equation[41].

Bhattacharyya and Pei [41] suggested that heat transfer can be described by two mechanisms, namely:

- Fluid-to-particle heat transfer which describes the convective heat transfer between the particle and its surrounding fluid
- Particle-to-particle heat transfer which describes the heat conduction between solids through the points of contact. This may also be dependent on fluid flow

Researchers [104–109] have studied the conductive heat transfer alone for bed of spheres. They found that predicting the effective thermal conductivity of the beds, the resistance must be considered as a *combination of macroscopic conductive resistance of the contact points, microscopic constriction resistance at the contact areas due to surface roughness and the film resistance between the contacts*. Due to fluid flow through the bed, the film thickness between the bed changes and this affects the thermal conductivity of the bed. Therefore, fluid flow does not only influence the convective heat transfer but also the conductive heat transfer.

The study by Bhattacharyya and Pei [41] was aimed at separating the two mechanisms of heat transfer and studying them separately. This was achieved using microwave power to heat the bed to achieve a constant uniform solid temperature and eliminate conductive heat transfer. They also predicted the fluid flow effect on the conductive heat transfer. They concluded that the convective heat transfer coefficient, α_{fp} or α_{conv} can be estimated from the heat balance equation. From their study, it was found that irrespective of the size, shape, density and thermal conductivity of the particle, convective heat transfer coefficient reaches a peak value with increase in Reynolds number. This Reynolds number was investigated

and found to correspond to the *fluidization Reynolds number*. Fluid-to-particle heat transfer coefficient was also correlated using the Colburn heat transfer factor.

Bhattacharyya and Pei [41] extrapolated the conductive heat transfer alone from other studies in literature [49–53, 110]. This was then compared to the predicted value. This was done by taking the difference of total heat transfer and the convective heat transfer for all the studies considered. This resulted in the conductive heat transfer which was represented as the conductive Nusselt number, Nu_c, which was extrapolated as the Reynolds number approaches zero ($\mathrm{Re}_{pm} \rightarrow 0$, $\lambda_e^0/\lambda_f = \alpha_{cond}\mathrm{d}_p/\alpha_f$ for no flow). It was found that there was good agreement between the predicted values and the true values. The difference between and Nu_c and λ_e^0/λ_f will therefore represent the contributions of fluid flow on the conductive mode of heat transfer denoted by h_{fc}. The conductive heat transfer due to fluid flow was found to depend on "contact resistance" as studied previously [104, 107–109], Bhattacharyya and Pei [41] and suggested that contact resistance may be functions of the following:

- *total area of contact, i.e. shape and number of solids per unit volume (related to the void fraction and particle diameter)*;
- *velocity of fluid flow (causing variation of film thickness between adjacent solids)*;
- *volumetric specific heat of the solid, $\rho_p \cdot C_{pp}$ (heat capacity per unit volume)*;
- *compactness of the packing due to gravity force (heavier are the solids better is the contact)*;
- *surface properties of the packing (rougher surface cause higher drag and consequently heat transfer rate increases)*;
- *porosity of individual particles (part of fluid may flow through the solid); etc.*

They therefore expressed the conductive heat transfer with respect to fluid flow using the Colburn heat factor correlation excluding the porous materials and data with extremely high temperature, small tube to particle ratio and shallow beds. They concluded that the total heat transfer in a bed is made up of three modes, namely: conductive heat transfer with motionless fluid, conductive heat transfer with fluid flow effect and convective heat transfer.

The modelling of fixed bed reactors depends on the industrial objective for which the reactor is needed. This also requires a better understanding of a parameters involved which are the effective diffusivity and the overall heat transfer coefficient [111–114]. Martinez et al. [111] analyzed the experimental methods for estimating the overall heat transfer coefficient and derived a relationship to express it in terms of the parameters in the two-dimensional heterogeneous reactor model. They did this by relating the heat transfer parameter in a one-dimensional pseudo-homogeneous model to that of the two-dimensional heterogeneous model. They proposed that this can be done in two ways: *through the heterogeneous one-dimensional model or through the pseudo-homogeneous two-dimensional model*[115].

- *Via the heterogeneous one-dimensional model*

  This model incorporates the *radial heat transfer through the solid phase*[114]. Equating the heat transferred to the surrounding for both the one-dimensional and two-dimensional heterogeneous models, the one-dimensional coefficients can then be calculated. This represents a system without axial dispersion and therefore represent the limiting case[116]. For systems with axial dispersion, expression by Dixon and Cresswell [117] can be used.

- *Via the pseudo-homogeneous two-dimensional model*

  This approach of relating the pseudo-homogeneous one-dimensional coefficient to the parameters in the heterogeneous two-dimensional model has been studied more in literature and it is usually done in two steps:

  1. Relating the parameters in the pseudo-homogeneous two-dimensional model to those in the corresponding heterogeneous model, and

2. Evaluating the pseudo-homogeneous one-dimensional heat transfer coefficient with the parameters on the corresponding two-dimensional model

Relating the parameters in the pseudo-homogeneous two-dimensional model to those in the corresponding heterogeneous model has been studied by several authors, but there has not been a consensus about the temperature in the pseudo-homogeneous model. The temperature of the pseudo-homogeneous model can be either be set as the fluid temperature or the solid temperature depending on whether the convective term in the energy balance equation or the reactive term in considered respectively [111]. Olbrich [118] was able to obtain criteria of equivalence by comparing the two models for heat exchangers. This was later expanded upon by Dixon and Cresswell [117] when they included axial dispersion and matched the fluid-phase temperature to the pseudo-homogeneous temperature. This was contested by Vortmeyer and Berninger [119] since a different relationship has been found from a previous study by Vortmeyer and Schaefer [120] from which the solid-phase temperature was concluded to be equal to the pseudo-homogeneous temperature. Cresswell and Dixon [121] attributed the disparity between the work by Dixon and Cresswell [117] and Vortmeyer and Schaefer [120] to the fact that they were studied under steady and non-steady state respectively. Therefore, for the purpose of this study, Martinez et al. [111] assumed that solid, fluid and pseudo-homogeneous temperatures are all equal since the pseudo-homogeneous assumption requires that the difference between the solid and fluid temperature be very small and therefore came up with an expression for the parameters.

Solving the pseudo-homogeneous two-dimensional model and assuming that the heat transferred to the surroundings is equal for both models, a simple expression was obtained. The correlations used by [111] are the same as those used by Duarte et al. [122]. Also, experimental data by Leva et al. [123] and Verschoor and Schuit [45] were used for comparison and very good agreement were found for operating conditions ranging from $150 < \mathrm{Re} < 2250$ and $4 < \mathrm{d}_t/\mathrm{d}_p < 14$.

The axial experimental methods of determining the overall heat transfer coefficient were found to reach a certain asymptotic value after certain minimum bed length and this length was found to increase with Reynolds number. Also, the radial methods were found to reach asymptotic values much slower than the axial methods

Johansson et al. [73] investigated the influence of intra-particle gradients on modeling fixed bed combustion. This was been done by comparing the porous media approximation, neglecting intra-particle gradient for modeling fixed bed combustion to that in which the intra-particle gradients have been taken into account by a two-dimensional particle model. Wurzenberger [124] described the conversion of particles in the bed using a one-dimensional model which accounts for intra-particle gradients. They compared with results from a porous bed model for simulation of drying and pyrolysis in flow of hot nitrogen. From their comparison, they discovered that the temperature profiles from both models are similar but the drying and pyrolysis fronts in the bed are extended when intra-particle gradients are considered. The bed is assumed to consist of particles which are spherical in shape and of the same size. The bed porosity is 0.5 and assumed to be constant throughout the entire conversion. The system is described by transport equations for energy and mass in the gas and solid phases.

The particle model accounts for the conversion of particles in the bed. The surface temperature of the solid phase from the porous bed model serves as the boundary condition of the particle model. The boundary condition considers the dependence of surface temperature on time and position on the particle surface. The bed model is then linked to the particle model through three parameters, which include a heating ratio, Φ, an effective drying temperature, and an effective devolatilization temperature. The effective drying and devolatilization temperature of the bed are calculated form the Arrhenius expressions for moisture and volatile release. The heating ratio is given by Froment and Bischoff [113].

Turbulence model for flow in a rigid and fixed bed have been proposed and this has been extended to moving porous bed [125–141]. For all such studies, only the

isothermal flow has been considered. The aim of the study by de Lemos and Saito [142] is to extend the previous works to study the energy transfer between the fluid and the moving porous bed. They only considered the case where the solid phase velocity is kept constant. Governing equations were obtained by taking the volumetric average of the entire equation set.

Kuwahara et al. [143] proposed a numerical correlation for the interfacial convective heat transfer coefficient for laminar flow. Saito and De Lemos [144] and de Lemos and Saito [142] extended the work and proposed the expression for both low and high Reynolds number turbulence models. The control volume technique was applied for the numerical solution. The study shows that as the inlet velocity of the fluid decreases, the temperature of the fluid increases faster in the axial direction. This leads to a lower drop in solid temperature. As the Reynolds number increases, the cooling effect is more prominent and it is mostly at the beginning of the channel where the greater temperature drop occurs.

Porosity and pebble geometry are very important since they determine the flow pattern and local flow conditions in a packed bed [145–150]. It has been found from previous works that porosity enhances the heat transfer and increases the pressure drop as well but using highly porous material with large particle diameter reduces the pressure drop [151, 152]. Hadad and Jafarpur [153] in their study presented the convection heat transfer as a summation of two heat transfer limits i.e. the conduction limit which includes the conduction heat transfer between the body and its surrounding fluid and the convection Nusselt number that can be obtained from the laminar boundary layer solution and involves heat transfer due to fluid bulk motion. Yovanovich and Vanoverbeke [148] and Yovanovich [149] proposed a more detailed model for the model by Hadad and Jafarpur [153]. Three different beds (spherical, cylindrical and conical beds) have been used in their study. The conduction limit depends on geometry of pebbles and porosity. The model was only valid in the laminar flow regime in porous media ($Re \leqslant 300$). From previous studies, model was proposed for the forced laminar convection heat transfer for different pebble geometry [11, 17, 125, 154–164] The proposed model predicts

very well at both low and high Reynolds numbers and at all practically possible porosities.

1.2.5 Objective of the study

The main background-objective of this work is to study energy storage by either gasification or reforming process in fixed beds heated by DC discharge. The heating is based on the Joule heating effect from electrical current passed through the fixed bed. This electricity can also be generated from renewable sources of energy. This is aimed at the storage of energy in form of chemical energy (**E2C**) which can later be converted back to electricity. Therefore, for this study, a mini-gasifier was built and fitted in both ends with the Nichrome rod to serve as electrodes. The gasifier was then filled with coal particles and connected to the electric source. It was observed that the coal particles were not heated up and this was explained due to the low conductivity of coal particles. It was then concluded that, to carry out the study with coal particles, large volt of electricity would be needed and this was not feasible in the laboratory. Therefore, the study was modified to better understand the energy generation and transfer in the fixed bed. The modification involves substituting the coal particle with metallic spheres which in this case was nickel spheres of diameter 3 mm. The experiment was then carried out with the nickel spheres in the fixed bed with and without gas flowing through the bed. The fixed bed used for the experiment is made of quartz and its of 1 cm diameter. The experiment without gas flow gave more insight onto the heat transfer and loss from the bed. The results from both experiments were then validated against the CFD-Simulation. Also, models were developed for both the experiment conditions. This knowledge of the bed for both experimental conditions can then be used to simulate the heterogeneous reaction that occurs during gasification of coal or steam reforming of methane in a fixed bed using electricity as the source of heat. For the purpose of this study, steam reforming of methane has been simulated numerically using CFD-based model (where methane reforming reaction was

simplified) for conditions where the heat is been produced by Joule heating and also when the bed is heated up by the wall of the bed.

Chapter 2

Experimental and Numerical Study of fixed bed heating using DC discharge

2.1 Experiment

A tube made of quartz constructed by the glass shop (Chemistry department, University of Alberta) was used as the fixed bed. This was filled with nickel balls (Cu<2500 ppm, Fe<4000 ppm, Mg<2000 ppm, Mn<3500 ppm, Si<1500 ppm, Ti<1000 ppm, C<1500 ppm, S<100 ppm, Total purity includes Cobalt). Nickel-Chromium rods (Al 1000 ppm, Cr 18 - 20% ppm, Fe 2000 ppm, Mn 2000 ppm, Si 1.5% ppm, Ni + Co balance) obtained from Goodfellow, which were fitted to the quartz fitting were used as electrodes to conduct electricity from the B& K precision 1901 DC power supply (32 V, 30 A rating) to heat up the fixed bed. The electrodes were connected to the power supply by 10 g. a. wires of 30 A service. High temperature thermocouple (Type K, diameter 0.040", length 20", ungrounded) obtained from Omega was used. The thermocouple was calibrated at the instrument shop (Chemical Engineering department, University of Alberta). Fluke thermometer 54 IIB ($80PK-1$, Bead probes, Accuracy: $above-100^oC$;

$0.05\% + 0.3^oC$ for J, K, T, E and N types) was used to read the temperature measured by the thermocouples. Traceable stopwatch obtained from Fisher Scientific was used to monitor the temperature measurement with time. Gas cylinder containing compressed air obtained from Praxair was used for experiment involving gas flow, with air serving as the gas. Flow rate meter obtained from Cole Palmer was used to measure the flow rate for experiments involving gas flow

2.1.1 Scheme of the Fixed bed

The fixed bed is made up of quartz tube which filled with nickel balls of about 400. The quartz tube has nickel-chromium (Nichrome) electrodes fitted on both ends of the tube. These electrodes are attached to 10ga wire which is then connected to the power supply. The schematic diagram of the tube with the nickel balls inside without the passage electricity is as shown below in figure 2.1

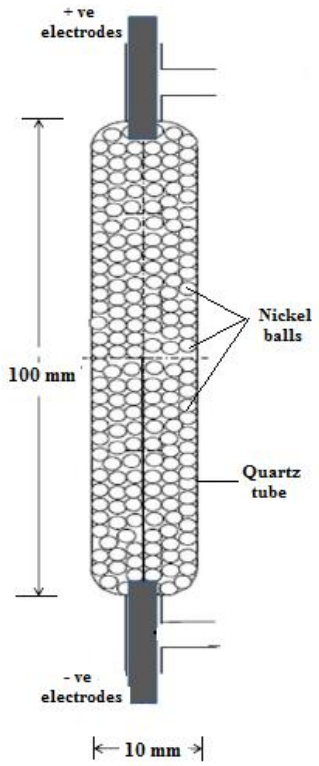

FIGURE 2.1: Schematic diagram of the packing of nickel balls in the quartz cylindrical tube

2.1.1.1 Experimental Set-up

The experimental set-up used for the experiments is as shown below. The dimensions of the quartz tube used for the experiment and the set-up during the experiment with and without gas flow are as shown.

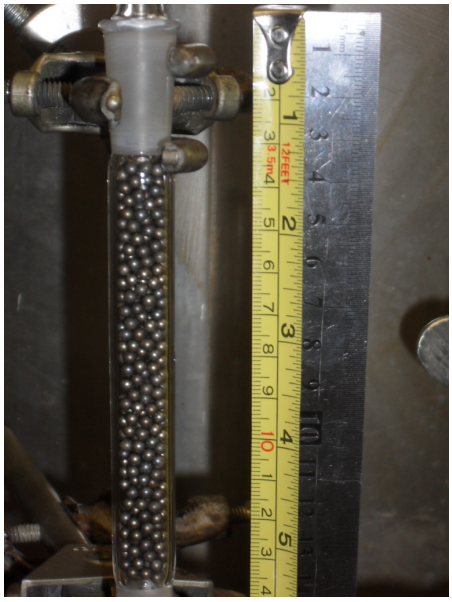

(A)

(B)

FIGURE 2.2: Dimensions of tube (quartz) used for experiment showing: (a) Length of tube, and (b) Outer diameter of tube

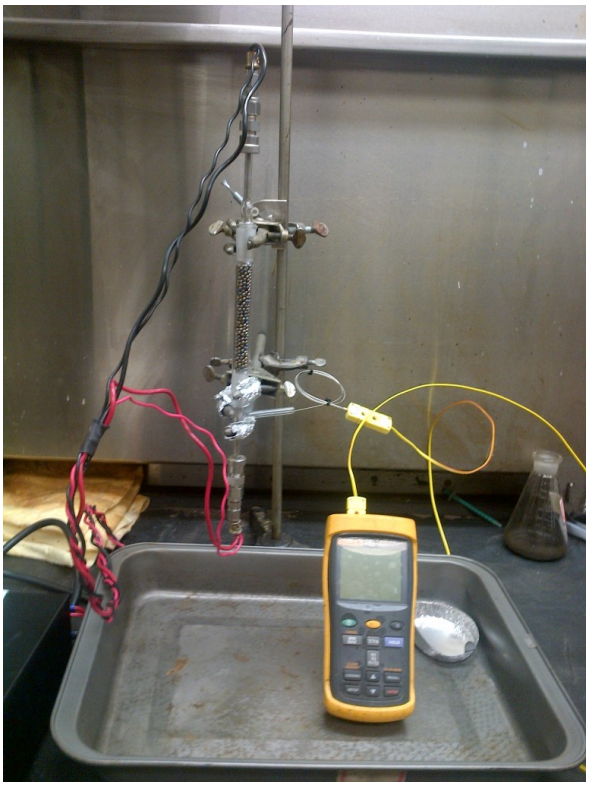

(A)

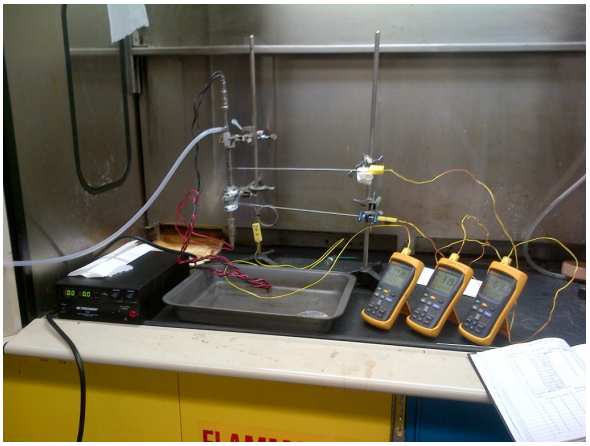

(B)

(C)

FIGURE 2.3: Experimental Set-up showing: (a) Set-up without gas flow, (b)

2.1.1.2 Properties of the bed

The fixed bed consist of quartz tube, nickel balls, Nickel-Chromium electrodes and thermocouples. Below in tables 2.1 to 2.3 are some of the properties of the materials which make up the fixed bed.

TABLE 2.1: Quartz tube properties

Properties	Value	Unit
D	0.01	m
L	0.1	m
MP	about 1600	^0C

TABLE 2.2: Nickel-Chromium rod properties

Properties	Value	Unit
ϱ	1.08	μohmm
ρ	8400	kg/m^3
MP	1400	^0C
λ	13.4	$W/m \cdot K$

TABLE 2.3: Nickel balls properties

Properties	Value	Unit
d_p	0.003	m
N_p	374	–
ϕ	5.08	μm
ρ	8900	kg/m^3
Purity	99 %	–
Tolerance	$\pm$ 25.4	μm
MP	1453	^0C
λ	90.9	$W/m.K$

2.1.2 Temperature measurement

The quartz tube was held in a vertical position by two clamps on a retort stand to enhance the contact between the nickel balls. With one end closed with the fitted nichrome electrode into the quartz fitting, the tube was filled with nickel balls up to the top and closed with the other quartz fitting fitted with electrodes. This is then connected to a power supply by wires (10 g.a.) at both ends through the nichrome electrodes as shown below in figure 2.4

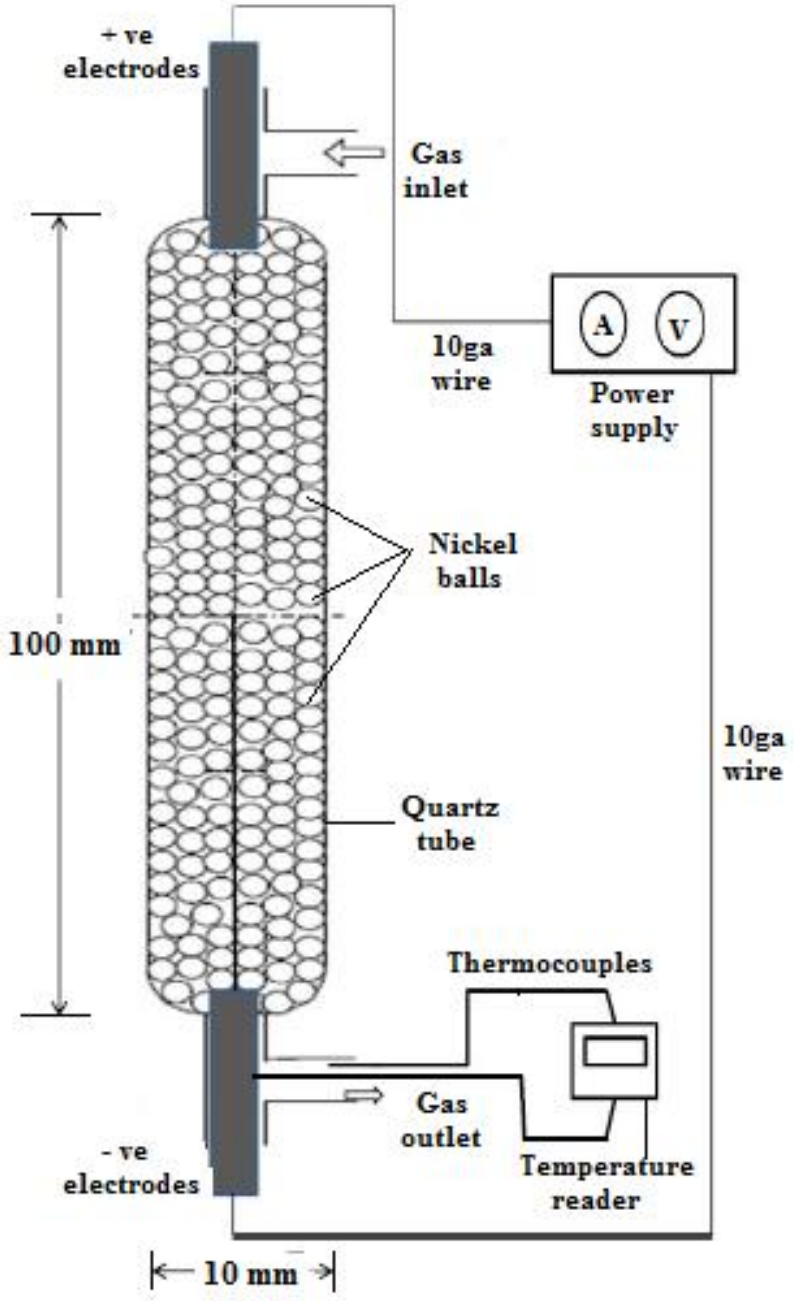

FIGURE 2.4: Schematic diagram of the heating of fixed bed with joule heating by DC discharge

2.1.2.1 Temperature measurement in the fixed bed without gas flow

This experiment was carried out without the gas flowing through the tube. A thermocouple was inserted halfway into the quartz tube to measure the temperature inside the tube. This thermocouple was connected to a temperature reader.

Once the set-up is ready, the power supply was turned on and checked to be sure if working properly. Once this is done, the current knob of the power supply is then turned to the desired current. The power supply then regulates it voltage output and once the desired current is attained, stopwatch is started.

The temperature is taken for 10 minutes at 1 minute interval. This is done for three different currents which include 5.0 A, 7.5 A and 10.0 A. The voltage output for all the current used ranges for 3.0 – 4.5 V. The experimental results are as shown in figures 2.13 to 2.15 represented with symbols.

2.1.2.2 Temperature measurement in the fixed bed with gas flow

The same experiment as discussed above was also carried for the fixed bed with gas flowing through the bed. Due to the introduction of gas flow through the fixed, there was a need to measure the temperature of the gas. The gas was introduced into the bed from the top and it flows out through the outlet valve at the bottom as shown above. A thermocouple was then placed at the outlet position to measure the temperature of the gas at the outlet. This thermocouple was connected to another temperature reader. The gas used for the experiment was compressed air. The experimental data for both the temperature inside the tube and the outlet temperature of air flowing through the tube during the experiment is as shown below in figure 2.5 for the different experimental conditions i.e. three electrical power and four mass flow rate.

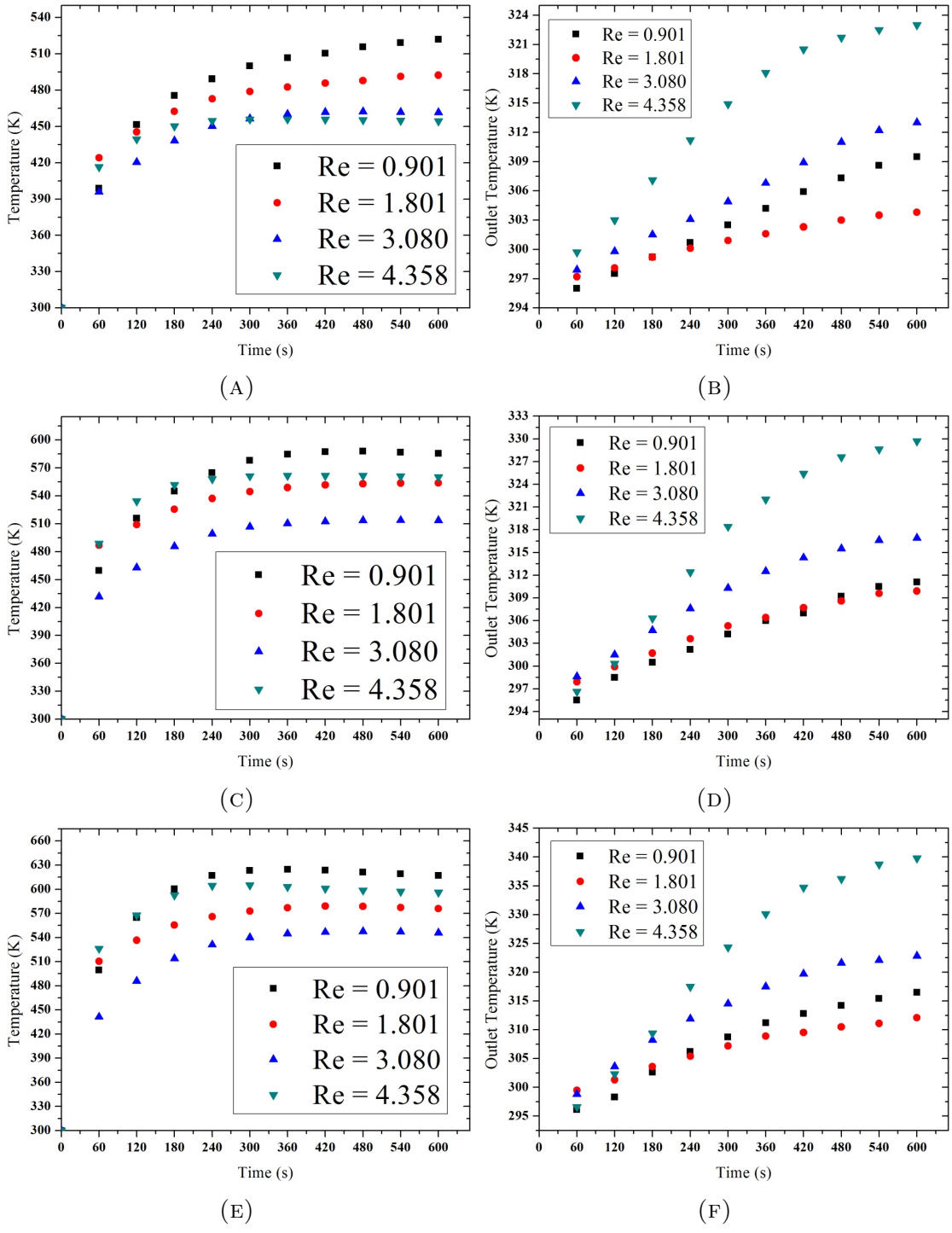

FIGURE 2.5: Temperature measurement inside the tube and the outlet air temperature respectively: (a) and (b) at 15 W power, (c) and (d) at 22.5 W power, (e) and (f) at 42 W power

From the experiment, the results were found to approach steady state at around 10 minutes, therefore, table 2.4 and 2.5 below summarizes the experimental data as it approaches steady state:

TABLE 2.4: Temperature inside the tube at steady state

I, A	U, V	$\dot{m}$, kg/s	$T_{steady\ state}$, K
5	3	0	474.6
		1.27E-07	521.9
		2.53E-07	492.4
		4.33E-07	461.5
		6.13E-07	454.4
7.5	3	0	526.3
		1.27E-07	585.5
		2.53E-07	553.8
		4.33E-07	513.6
		6.13E-07	560.2
10	4.2	0	643.7
		1.27E-07	617.1
		2.53E-07	576.0
		4.33E-07	545.8
		6.13E-07	596.0

TABLE 2.5: Air Outlet temperature at steady state

I, A	U, V	$\dot{m}$, kg/s	$T_{steady\ state}$, K
5	3	1.27E-07	309.5
		2.53E-07	303.8
		4.33E-07	313.0
		6.13E-07	323.0
7.5	3	1.27E-07	311.1
		2.53E-07	309.9
		4.33E-07	316.9
		6.13E-07	329.7
10	4.2	1.27E-07	316.5
		2.53E-07	312.1
		4.33E-07	322.8
		6.13E-07	339.8

2.2 Modeling of fixed bed without gas flow

The fixed bed which was made up of nickel spheres of diameter 3 mm, was modeled and the result validated against experimental data of temperature which was measured through the thermocouple inserted halfway into the fixed bed. This was done for the three different electrical powers used during the experiment. A semi-empirical model was developed for the heat transport in the fixed bed without gas flow and this was then solved through the use of MATLAB commercial software.

2.2.1 Modeling

Once the heat transfer parameter between the wall of the fixed bed and its surrounding has been established through the use of ANSYS commercial software 14.0, the parameters obtained were then used in the model developed. The model was developed by applying the *first law of thermodynamics* over a time interval (Δt) which states that *the increase in the amount of energy stored in a control volume (CV) must equal the amount of energy that enters the control volume, minus the amount of energy that leaves the control volume (CV) i.e. the total energy of a system is conserved*. Energy can enter and leave the control volume due to heat transfer through the boundaries, work done on or by the control volume, and energy advection. When the first law of thermodynamics is applied to a closed system, energy can either enter or leave the system by heat transfer through the boundaries and work done on or by the system[150]. Therefore, the first law of thermodynamics is therefore expressed as:

$$\Delta E_{st}^{tot} = Q - W \tag{2.1}$$

The energy conservation applied to the thermal and mechanical energy over a time interval (Δt) states that *the increase in the amount of thermal and mechanical energy stored in the control volume must equal the amount of thermal and mechanical energy that enters the control volume, minus the amount of thermal and mechanical energy that leaves the control volume, plus the amount of thermal and mechanical energy that is generated within the control volume*[150]. This is expressed mathematically as:

$$\Delta E_{st} = E_{in} - E_{out} + E_g \tag{2.2}$$

At an instant, the energy conservation for the thermal and mechanical energy can be stated as *the rate of increase of thermal and mechanical energy stored in the control volume must equal the rate at which thermal and mechanical energy*

enters the control volume, minus the rate at which thermal and mechanical energy leaves the control volume, plus the rate at which thermal and mechanical energy is generated within the control volume[150]. This is expressed mathematically as:

$$\dot{E}_{st} = \frac{dE_{st}}{dt} = \dot{E}_{in} - \dot{E}_{out} + \dot{E}_g \tag{2.3}$$

2.2.2 Numerical Model and results

For the model formulation, some assumptions have been made, this includes:

- Solid temperature, T_s is equal to the gas temperature, T_g i.e. $T_s = T_g$
- There is no flow present in the bed (no flow)
- Wall thickness has been considered for the simulation
- One dimensional homogeneous model has been developed

For the fixed bed without gas flow in this study, the three basic phenomena heat transfer includes energy generation by the electrical current, energy lost by convection and radiation and change of the total energy during the time (heating). Using energy conservation law, the energy balance for the fixed bed of length, L, has the form:

$$\dot{E}_{st} = \dot{E}_g - \dot{E}_{out} \tag{2.4}$$

Here, the energy generated ($\dot{E}_g$) in the fixed bed is the thermal energy generation which is due to the electric resistance heating and its given by:

$$\dot{E}_g = I\,U \tag{2.5}$$

The energy outflow ($\dot{E}_{out}$) from the surface of the fixed bed is as a result of the convection and net radiation from the surface of the fixed bed. This is expressed as:

$$\begin{aligned} \dot{E}_{out} &= \alpha A\left(T - T_{\infty}\right) + \epsilon_{\sigma}\sigma A\left(T^4 - T_{sur}^4\right) \\ A &= \pi D L \end{aligned} \tag{2.6}$$

The energy stored ($\dot{E}_{st}$) in the fixed bed is associated with the rate of change in the internal thermal energy in the fixed bed and its expressed as:

$$\begin{aligned} \dot{E}_{st} &= \frac{dU}{dt} = \frac{d}{dt}\left(\rho V c T\right) \\ V &= \pi\frac{D^2}{4}L \end{aligned} \tag{2.7}$$

Therefore, equations 2.5 to 2.7 are then substituted into equation 2.4 to give the following heat equation, equation 2.8 below, which is then used to model the heat transfer in fixed bed in the absence of gas flowing through the fixed bed.

$$\frac{d}{dt}\left(\rho V c T\right) = I U - \left[\alpha A\left(T - T_{\infty}\right) + \epsilon_{\sigma}\sigma A\left(T^4 - T_{sur}^4\right)\right] \tag{2.8}$$

Equation 2.8 can be rearranged as follows:

$$\frac{dT}{dt} = \frac{I U - \left[\alpha A\left(T - T_{\infty}\right) + \epsilon_{\sigma}\sigma A\left(T^4 - T_{sur}^4\right)\right]}{\rho V c} \tag{2.9a}$$

$$V = \pi\frac{D^2}{4}L \tag{2.9b}$$

$$A = \pi D L \tag{2.9c}$$

$$\frac{dT}{dt} = \frac{I U - \alpha A\left(T - T_{\infty}\right) - \epsilon_{\sigma}\sigma A\left(T^4 - T_{sur}^4\right)}{\rho V c} \tag{2.9d}$$

The results that were obtained from the use of MATLAB commercial software were not in agreement with the experimental data. Due to the discrepancy between the results obtained from the model and the experimental data, it was observed that the heat transfer parameter used in the model developed was not accurate enough and this resulted in the difference between the model and results from experiment. And this was explained due to the heat loss from the wall of the fixed bed to its surrounding.

2.2.3 Convective Heat transfer coefficient

Therefore, to obtain a better evaluation of the temperature inside the tube with time from the model developed, a more accurate heat transfer parameter was needed. This parameter was then obtained through the use of ANSYS commercial software 14.0. This was done by developing a 2D-axisymmetric geometry of the wall of the fixed bed and its surrounding representative of that from the experiment. The geometry used for the evaluation of the heat transfer coefficient between the wall of the bed and its surrounding is as shown in figure 2.7. The mesh used for the simulation consists of 163670 cells, 328195 faces and 164526 nodes. This was carried out on a 4 core computer with 3.5 GHz, 32 Gb RAM. For discretization of the convective heat transfer coefficient between the wall of the bed and its surrounding, the energy and Viscous (Standard k-ω) models have been used with the standard k-ω options of shear flow corrections. The SIMPLE scheme has been employed for pressure-velocity coupling and the spatial discretization method includes least squares cell based method for gradients, PRESTO! for pressure and the QUICK method for turbulent kinetic energy, specific dissipation rate, energy and momentum. The simulation was carried out for different wall temperatures ranging form $350 - 750$ K. It was observed that as the wall temperature increased to about 500 K, the solution did not converge. The solution did not converge because the flow around the wall became turbulent. To obtain a converged solution, the standard $\kappa - \omega$ model was then employed for higher wall temperatures and this gave a converged solution. To obtain a converged solution

for both the laminar and turbulent flow around the wall of the fixed bed, the different mesh sizes were employed as the mesh closer to the wall are finer than those further away from the wall. This increased the computational cost for the simulation but was necessary to obtain a converged and more accurate solution for the heat transport properties of the wall to its surrounding. The equations solved using ANSYS Fluent 14.0 is as shown in table 2.7[1]. The values for the convective heat transfer coefficient and heat flux at the wall of the fixed bed is as shown in table 2.6. Some of the assumptions made include:

- Wall thickness has not been considered
- A no-slip conditions at the wall of the bed.
- Uniform wall temperature

TABLE 2.6: Heat transport properties of wall of fixed bed to its surrounding

	T_w, K	α_w, W/m^{2}K	q, W/m^2
Laminar flow	350	7.818	390.910
	400	9.027	902.666
	450	9.819	1472.824
	500	10.449	2089.741
Turbulent flow	550	11.117	2779.251
	600	11.616	3484.761
	650	11.994	4197.781
	700	12.475	4989.977
	750	12.792	5756.227

The convective heat transfer coefficient which was about 11 to 14 W/m^{2}K used for the model developed depends on the electric power been considered. This was because as seen from the results in table 2.6 for the simulation carried out to determine the convective heat transfer coefficient between the wall of the fixed bed and its surrounding, it was observed that as the wall temperature increases, the heat transfer coefficient increases also.

[1]The simulation was carried out under the steady state condition, i.e. $(\frac{\partial}{\partial t} = 0)$

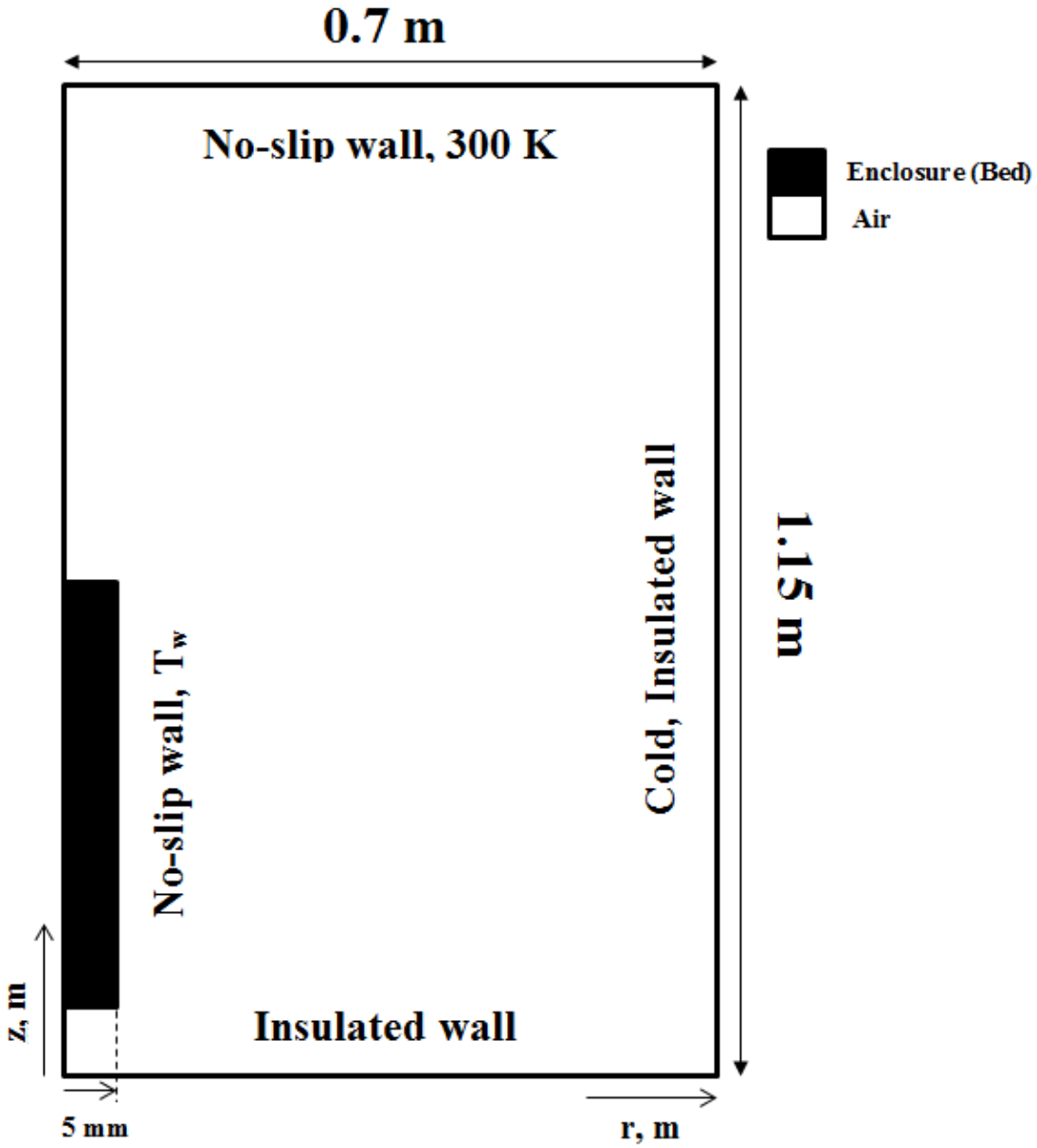

FIGURE 2.6: 2D Axisymmetric Geometry for estimating heat transfer coefficient with boundary conditions for $350 \leqslant T_w \leqslant 750$

TABLE 2.7: Equations solved for the simulation from ANSYS FLUENT 14.0

	Equations
Conservation of mass	$\nabla \cdot \left(\rho \overrightarrow{v}\right) = 0$
Conservation of momentum	$\nabla \cdot \left(\rho \overrightarrow{v}\, \overrightarrow{v}\right) + \nabla p = \nabla \cdot \left(\overline{\overline{\tau}}\right) = \rho \overrightarrow{g} + \overrightarrow{F}$
Stress tensor	$\overline{\overline{\tau}} = (\mu + \mu_t)\left[\left(\nabla \overrightarrow{v} + \nabla \overrightarrow{v}^T\right) - \frac{2}{3}\nabla \cdot \overrightarrow{v}\, I\right]$
Conservation of energy	$\nabla \cdot \left(\overrightarrow{v}\,(\rho E + p)\right) + \nabla \cdot j_{q,j} = \nabla \cdot \left(\overline{\overline{\tau}}_{eff} \cdot \overrightarrow{v}\right) + S_h$
	$E = h - \frac{p}{\rho} + \frac{v^2}{2}$
Diffusive heat transport $j_{q,j}$	$j_{q,j} = -\left(\lambda + \frac{c_p \mu_t}{Pr_t}\right)\nabla T + \sum_{i=1}^{N_g} h_i j_{i,j}$
Turbulence kinetic energy, k	$\frac{\partial}{\partial x_i}(\rho k u_i) = \frac{\partial}{\partial x_j}\left(\Gamma_k \frac{\partial k}{\partial x_j}\right) + G_k - Y_k + S_k$
Specific dissipation rate, ω	$\frac{\partial}{\partial x_i}(\rho \omega u_i) = \frac{\partial}{\partial x_j}\left(\Gamma_\omega \frac{\partial \omega}{\partial x_j}\right) + G_\omega - Y_\omega + S_\omega$
Effective diffusivity of k and ω	$\Gamma_k = \mu + \frac{\mu_t}{\sigma_k} \qquad \Gamma_k = \mu + \frac{\mu_t}{\sigma_k}$
Turbulent viscosity, μ_t	$\mu_t = \alpha^* \frac{\rho k}{\omega}$
Production of turbulence kinetic energy, G_k	$G_k = -\rho \overline{u_i' u_j'} \frac{\partial u_j}{\partial x_i} \qquad G_k = \mu_t S^2$
	$S \equiv \sqrt{2 S_{ij} S_{ij}}$
Production of ω, G_ω	$G_\omega = \alpha \frac{\omega}{k} G_k$
	$\alpha = \frac{\alpha_\infty}{\alpha^*}\left(\frac{\alpha_0 + Re_t/R_\omega}{1 + Re_t/R_\omega}\right) \quad , \alpha^* = \alpha_\infty^*\left(\frac{\alpha_0^* + Re_t/R_k}{1 + Re_t/R_k}\right)$
	where
	$R_\omega = 2.95 \qquad Re_t = \frac{\rho k}{\mu \omega} \qquad R_k = 6 \qquad \alpha_0^* = \frac{\beta_i}{3} \qquad \beta_i = 0.072$

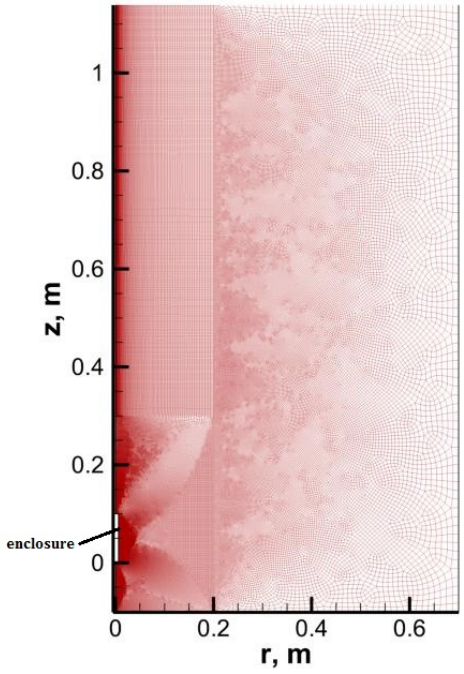

(A)

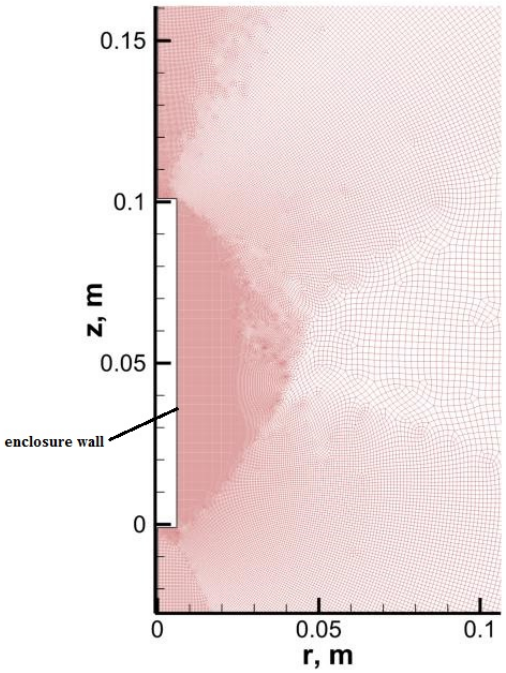

(B)

FIGURE 2.7: Geometry and mesh used for wall heat transfer coefficient to its surrounding: (a) Geometry and (b) Zoomed Geometry

The heat transfer coefficient obtained from the simulations form ANSYS commercial software was then used in the model developed to solve for the homogeneous temperature profile with time in the fixed bed without the gas flow. The temperature and velocity profile for the surrounding of the wall of the fixed as obtained from the simulation carried out through the use of ANSYS commercial software 14.0 for two wall temperatures are as shown in figures figures 2.8 to 2.11. Also, as the temperature of the wall of the fixed bed increases, the flow around the wall became turbulent and so the turbulent viscosity ratio profile was also obtained as shown in 2.12.

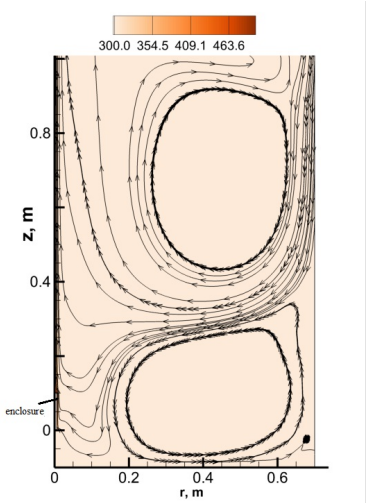

(A)

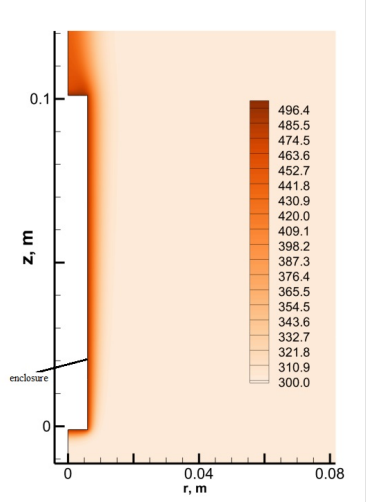

(B)

FIGURE 2.8: Temperature distribution between the fixed bed wall and its surrounding at a wall temperature of 500 K: (a) Temperature for Laminar flow with streamlines, and (b) Temperature for Laminar flow (zoomed)

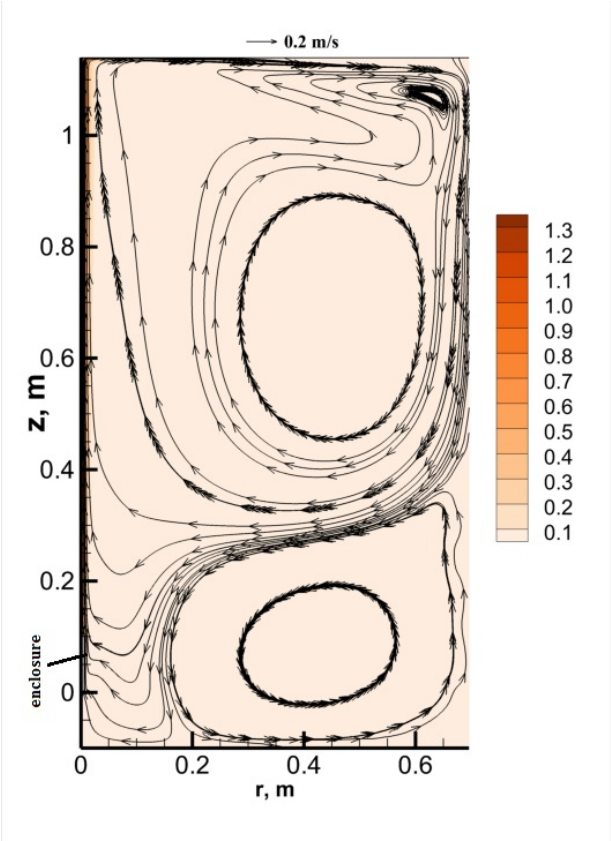

(A)

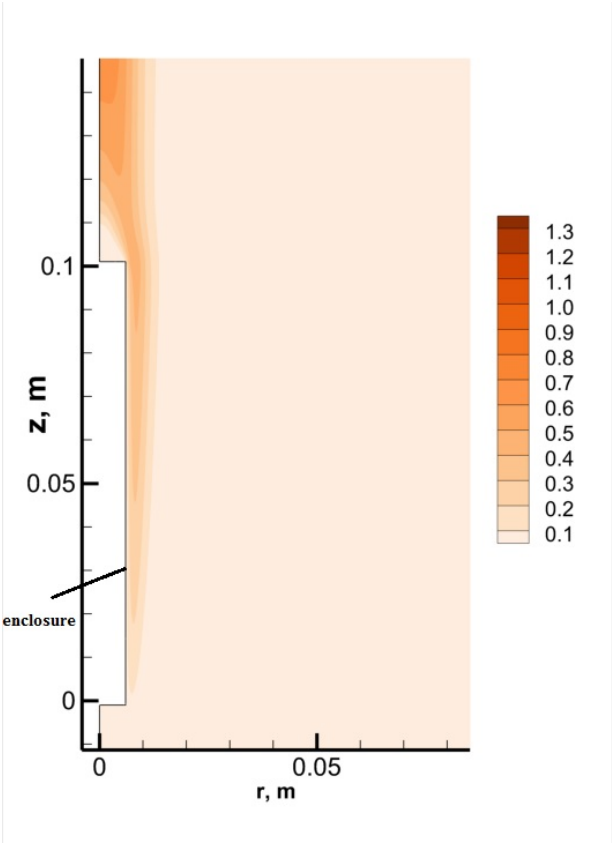

(B)

FIGURE 2.9: Velocity distribution between the fixed bed wall and its surrounding at a wall temperature of 500 K: (a) Velocity for Laminar flow with stream-

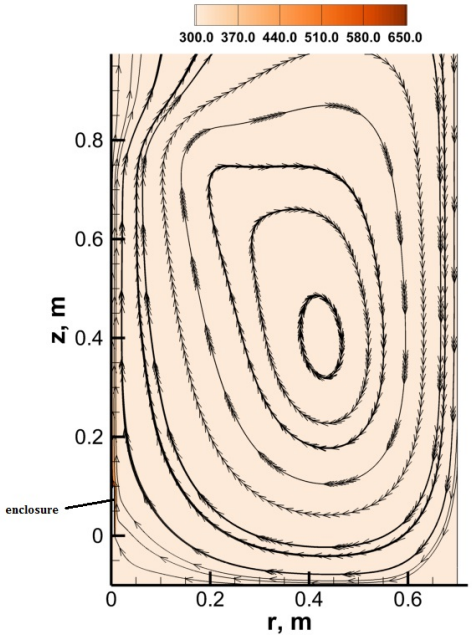

(A)

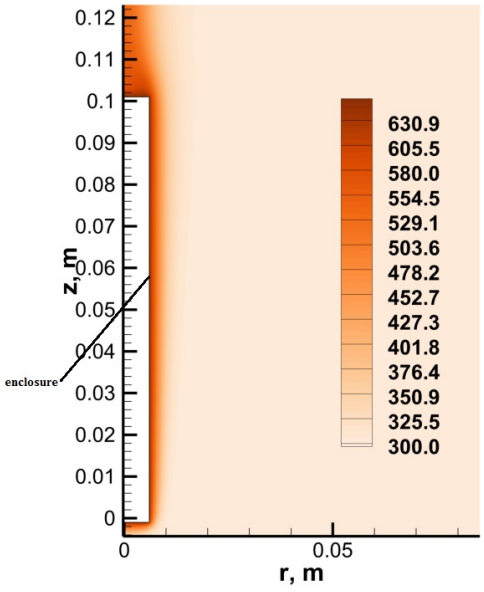

(B)

FIGURE 2.10: Temperature distribution between the fixed bed wall and its surrounding at a wall temperature of 650 K: (a) Temperature for turbulent flow with streamlines, and (b) Temperature for turbulent flow (zoomed)

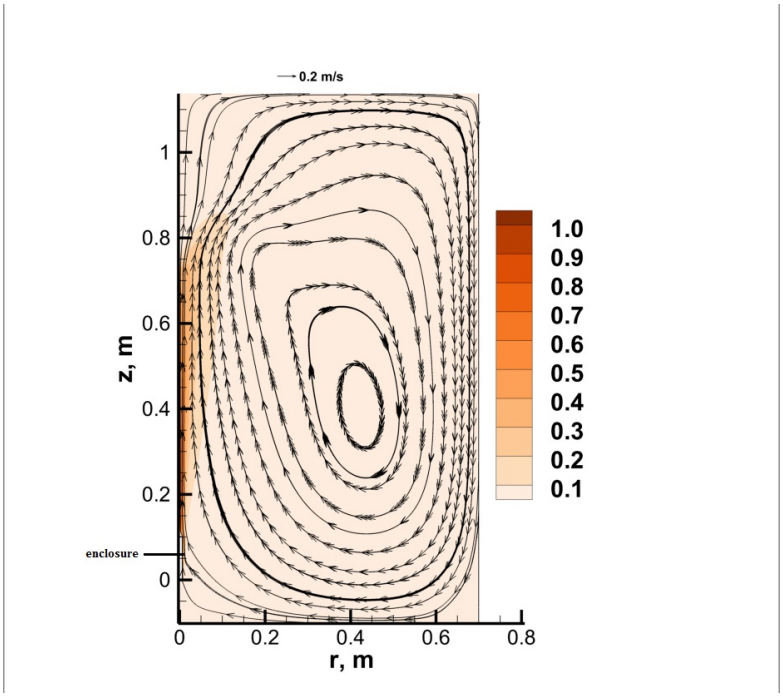

(A)

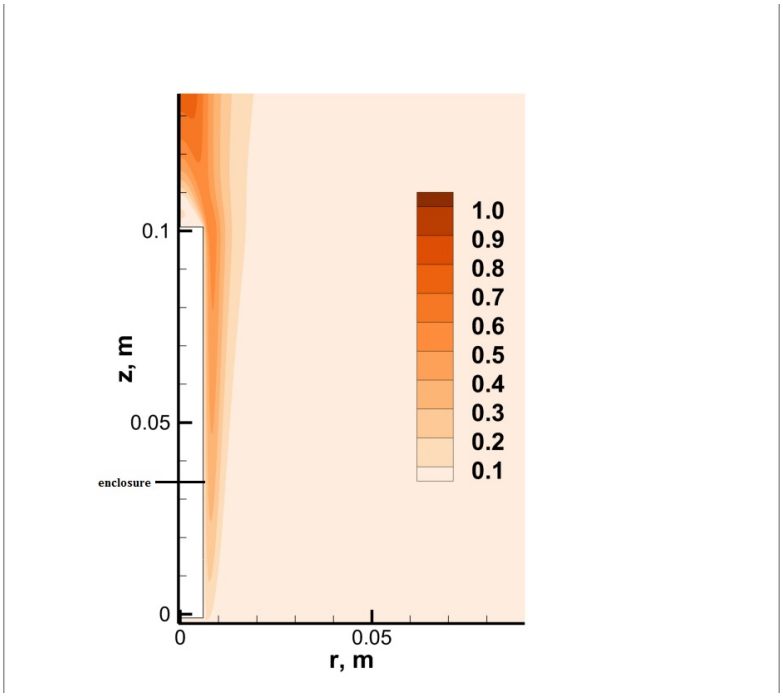

(B)

FIGURE 2.11: Velocity distribution between the fixed bed wall and its surrounding at a wall temperature of 650 K: (a) Velocity for turbulent flow with streamlines, and (b) Velocity for turbulent flow (zoomed)

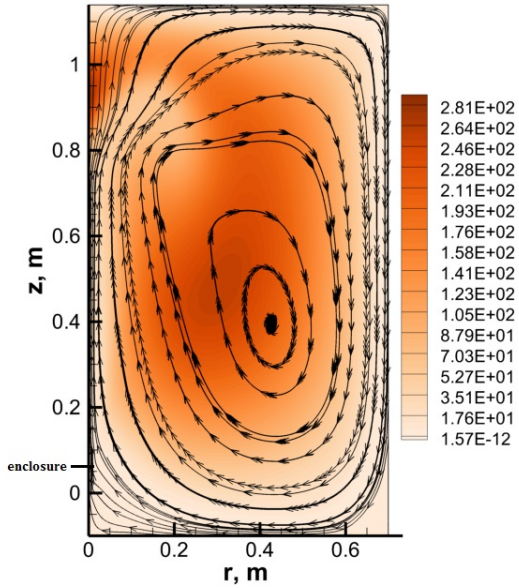

(A)

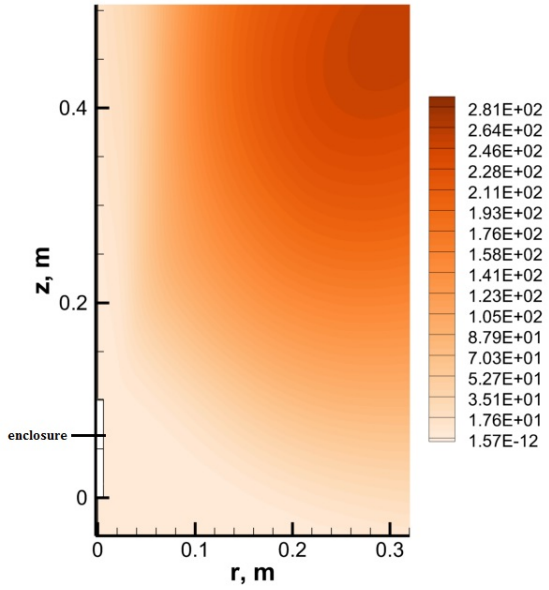

(B)

FIGURE 2.12: Turbulent Viscosity ratio distribution between the fixed bed wall and its surrounding at a wall temperature of 650 K: (a) Turbulent Viscosity ratio with streamlines, and (b) Turbulent Viscosity ratio

2.2.4 Modeling vs. Experiment

Equation 2.9 was then solved using the built-in functions in MATLAB commercial software by making some assumptions. The code for solving the heat transfer equation in the fixed bed in the absence of gas flow is as shown in Appendix A. Some of the assumptions made are as follows:

Assumptions:

$$\begin{aligned} T_\infty = T_{sur} &= 300\,K \\ C_p &= \varepsilon C_{nickel} \\ \rho &= \varepsilon \rho_{nickel} + (1-\varepsilon)\,\rho_{air} \\ \epsilon_\sigma &= 0.99 \\ \rho_{nickel} &= 8900\,kg/m^3 \\ \rho_{air} &= 1.225\,kg/m^3 \\ C_{nickel} &= 460.6\,J/kgK \\ \varepsilon &= 0.67 \end{aligned} \tag{2.10}$$

The results obtained from solving the heat transfer equation 2.9 and applying the assumptions listed above were then validated against the experimental data. This gave a good fit with the experimental data. This was done for all the three electrical power used to obtain the experimental data. The results are as shown in figures 2.13 for 15 W power, 2.14 for 22.5 W power and 2.15 for 42 W power.

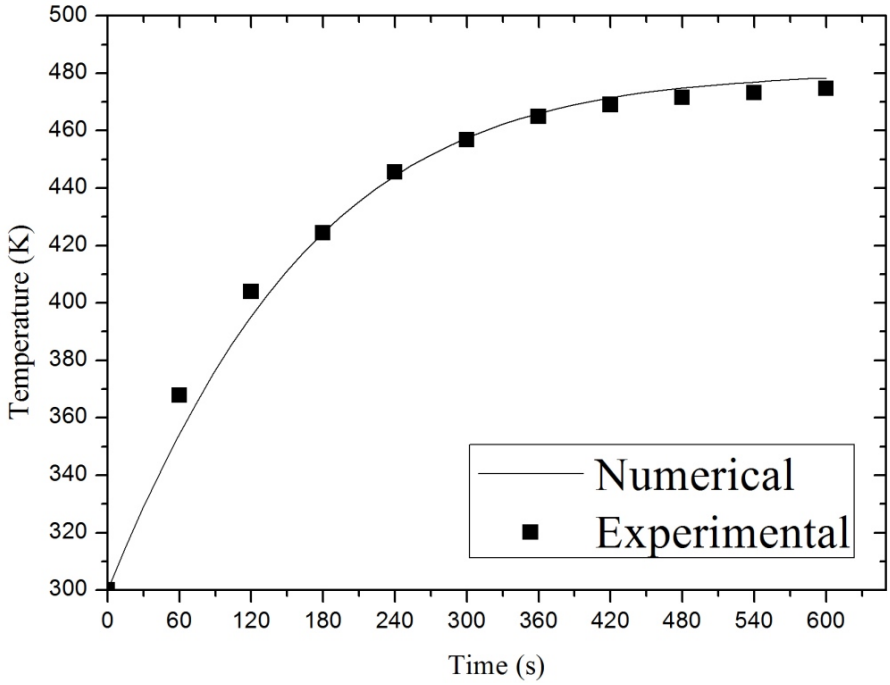

FIGURE 2.13: Experimental and Numerical temperature result for heating of fixed bed without gas flow at 15 W power

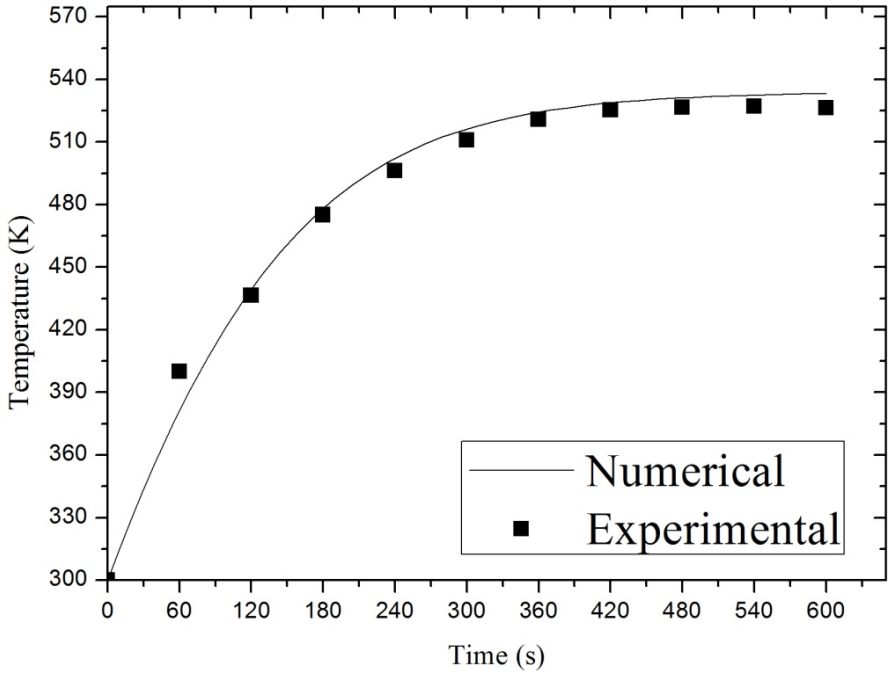

FIGURE 2.14: Experimental and Numerical temperature result for heating of fixed bed without gas flow at 22.5 W power

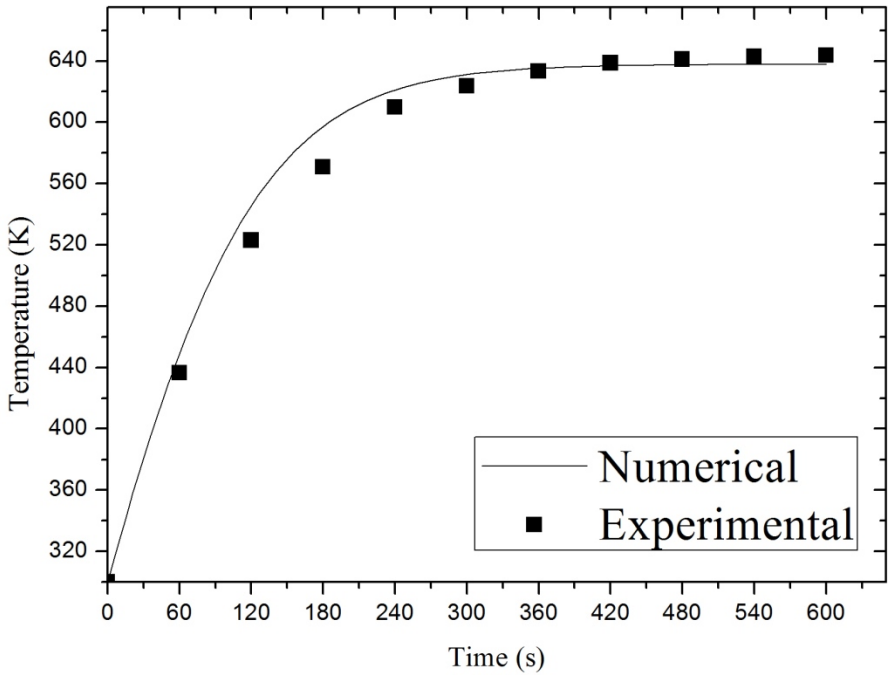

FIGURE 2.15: Experimental and Numerical temperature result for heating of fixed bed without gas flow at 42 W power

Chapter 3

Heating of Fixed bed with gas flow: Modeling

3.1 Heating of Fixed bed with gas flow

Here, the fixed bed which consists of nickel spheres of diameter 3 mm was used and the bed was heated by the use of electrodes placed at both ends of the tube and connected to an electric source. The bed was placed vertically to allow for better contact between the nickel spheres and therefore better conduction of heat through the bed. Pressurized air from a cylinder was then passed through the bed from the top and allowed to escape at the bottom end of the tube. Thermocouples were used to measure the temperature of the bed and the exiting air temperature. Four different mass flow rate and therefore Reynolds number of air were studied here and it's as shown in the table 3.1 below:

TABLE 3.1: Showing mass flow rate and Reynolds number of flow

$\dot{m} \times 10^{-7}$, kg/s	Re
1.27	0.901
2.53	1.801
4.33	3.080
6.13	4.358

The experiment was carried out with three different electrical power, for all the mass flow rates of air passing through the bed and the temperature measurement was recorded. To validate the experimental data, a steady state heterogeneous model was developed to evaluate the temperature inside the bed, temperature of the gas at the outlet of the bed and the wall temperature. This model was developed by taking into account the heat generation and heat transfer between particles and the air passing through the bed.

3.1.1 Numerical Model and results

Taking into account the generation of heat and the transfer of heat in the fixed bed, a heterogeneous model to validate the experimental results was developed. This was done by assuming that the solid particles are first heated up by the electricity passed through the electrodes to the nickel spheres (particles) in the bed. The heat generated is then removed by the gas (air) passing through the bed which gets heated up also. Another way through which heat is been removed from the bed is through the wall of the bed by radiation and convection. Based on this knowledge, semi-empirical models were then developed and the model equations as follows;

Solid temperature equation:

$$\frac{1}{r}\frac{\partial}{\partial r}\left(r\varepsilon\lambda_s\frac{\partial T}{\partial r}\right)+\dot{q}-\dot{A}_\Sigma\alpha\left(T-T_g\right)=0 \tag{3.1}$$

where

$$\dot{A}_\Sigma=\frac{A_\Sigma}{\Delta z\pi r_0^2} \tag{3.2a}$$

$$A_\Sigma=N_p\cdot 4\pi r_p^2 \tag{3.2b}$$

$$\dot{q}=\frac{I\cdot U}{\varepsilon_s\left(L\cdot\pi r_0^2\right)} \tag{3.3}$$

Boundary condition:

$$r = 0, \quad \frac{\partial T}{\partial r} = 0 \tag{3.4a}$$

$$r = r_0, \quad T = T_s \tag{3.4b}$$

Gas temperature equation:

$$\rho_g C_p u_g \frac{dT_g}{dz} = \dot{A}_\Sigma \alpha \left(\overline{T} - T_g \right) \tag{3.5}$$

where $\overline{T}$ is the averaged (over the radius) temperature of the solid phase:

$$\overline{T} = \frac{2}{r_0^2} \int_0^{r_0} T r dr$$

$$\alpha = \frac{Nu \cdot \lambda_{air}}{d_p}$$

where Nusselt number used is as given by Gunn

$$Nu = \left(7 - 10\varepsilon_s + 5\varepsilon_s^2\right) \left(1 + 0.7 Re^{0.2} Pr^{1/3}\right) + \left(1.33 - 2.4\varepsilon_s + 1.2\varepsilon_s\right) Re^{0.7} Pr^{1/3}$$

$$Re = \frac{\rho_f v D}{\mu}, \qquad Pr = \frac{\mu c_p}{\lambda}$$

To account for the heat loss through the wall since the bed is not insulated and therefore not adiabatic; an correlation to evaluate the temperature at the wall was developed as follows:

Surface (wall) temperature equation:

$$\alpha_{out} \left(T_s - T_\infty\right) + \varepsilon_\sigma \sigma \left(T_s^4 - T_\infty^4\right) = -\lambda_s \left. \frac{\partial T}{\partial r} \right|_{r=r_0} \tag{3.6}$$

where h_{out} is the heat transfer coefficient characterizing heat transfer between the wall of the bed and its surroundings.

The heterogeneous model was then solved using MATLAB commercial software. The discretization method and MATLAB code used to solve the heterogeneous model is as shown in Appendix B. The results obtained showed that the temperature inside the tube and that of the gas is the same throughout the whole length of the bed. It also yielded that the surface (wall) temperature is slightly lower than the temperature inside the tube. The disparity between the result obtained for the gas temperature for the experiment and model led to questioning the validity of the model developed. Therefore, an alternate approach was needed to further verify and therefore validate the experimental results.

The results shown in tables 3.2 and 3.3 obtained from the numerical model does not give a good correlation with the experimental results. Although, the correlation between the model and experiment is not good, we were able to conclude from the numerical results that the gas is heated at the center of the bed and also that the heat is been lost at the wall of the fixed bed.

TABLE 3.2: Temperature inside the bed predicted using semi-empirical model

RUN	Velocity, m/s	Experimental, K ±0.3 K	Numerical, K	% Error
1	0.0013	521.9	455.3	12.77
	0.0064	454.4	455.3	0.19
2	0.0013	585.5	536.5	8.37
	0.0064	560.2	536.5	4.23
3	0.0013	617.1	736.2	19.30
	0.0064	596.0	736.2	23.52

TABLE 3.3: Outlet temperature predicted using semi-empirical model

RUN	Velocity, m/s	Experimental, K ±0.3 K	Numerical, K	% Error
1	0.0013	309.5	455.2	47.08
	0.0064	323.0	427.3	32.30
2	0.0013	311.1	536.4	72.43
	0.0064	329.7	495.0	50.13
3	0.0013	316.5	736.0	132.55
	0.0064	339.8	661.3	94.61

3.2 CFD-Simulation and results

Since the numerical solution of the heterogeneous model and experimental data, especially the gas temperature, do not agree, there was the need to find other methods to validate the experimental data. Computational fluid dynamics emerged as a viable method to simulate and better understand the process of heat and mass transfer occurring in the bed. To do this, a domain representative of the experimental set-up was developed. This domain developed consists of the nickel spheres and the quartz tube, all in three-dimension (3D). The domain as seen in figure 3.1 consists of 8098058 cells, 1667646 faces and 16832121 nodes. The energy and viscous (laminar) models were used here. This was solved using the SIMPLE scheme for pressure-velocity coupling. The spatial discretization used includes least squares cell based method for gradient, standard for pressure and QUICK for energy and momentum. All transport properties used are temperature dependent. This was carried out on a 4 core computer with 3.5 GHz, 32 Gb RAM.

The simulation was then carried out using ANSYS commercial software 14.0 for the three different electrical power used for the experiment. Also, for each electrical power used, simulations were carried out for the slowest and fastest mass flow rate as used during the experiment for comparison with the experimental results. The simulations were carried out for the steady state case and this was because an unsteady state simulation requires more computational cost and time.

The grid in figure 3.1 was created numerically with particle packing was done using the discrete element method (DEM)[165]. The grid inside and outside the particles was developed.

3.2.1 Model Formulation

This model used here was formulated based on the assumptions that:

- No contact between the particles in the geometry used.

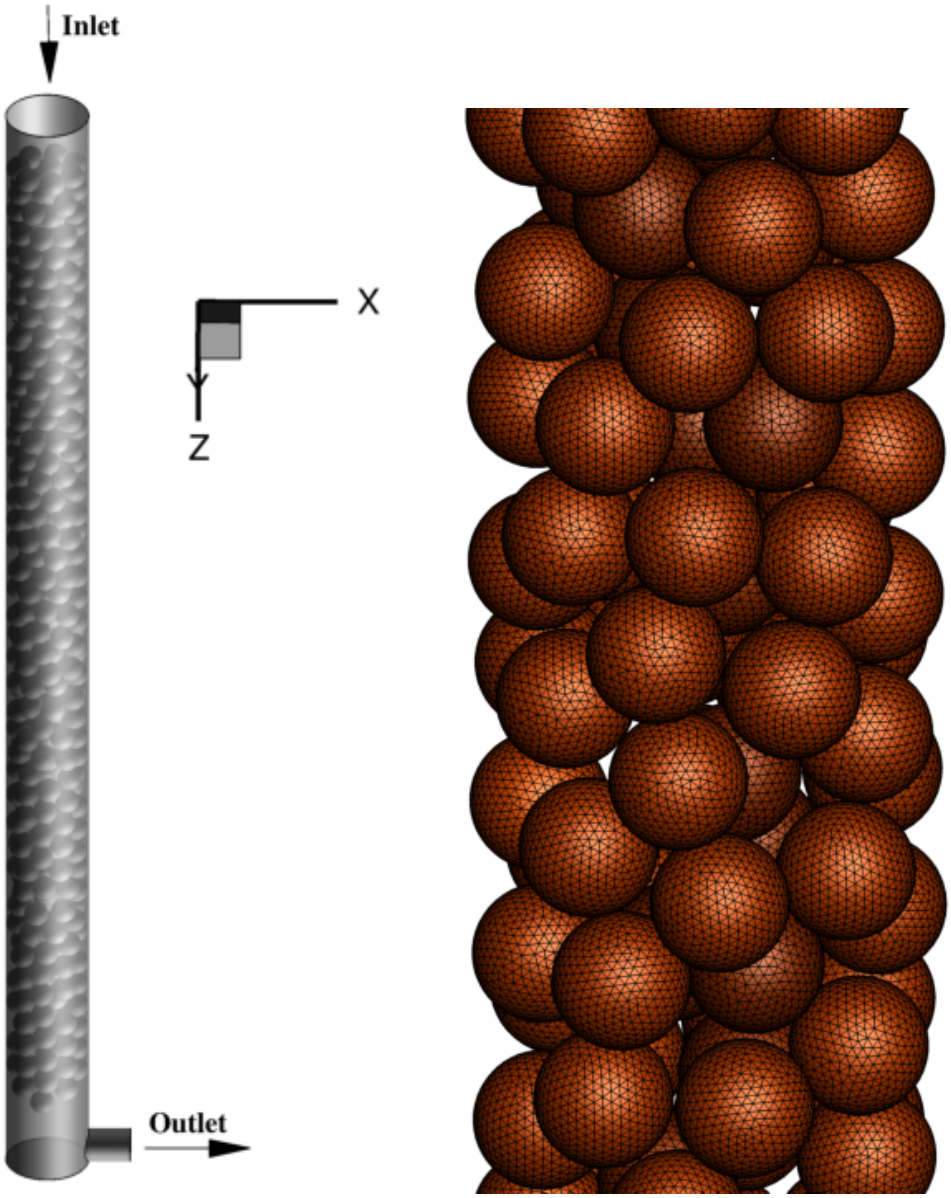

(A) (B)

FIGURE 3.1: The three dimensional (3D) domain representative of the experimental set-up of the fixed bed with 374 particles of diameter, d_p, 3 mm and grid 8×10^6 cells showing (a) the particle packing in the fixed bed and (b) the mesh grid of particle in the bed

TABLE 3.4: Governing equations used for 3D CFD Simulation

	Equations	Ref.
Conservation of mass	$\frac{\partial(\rho v_i)}{\partial x_i} = 0$	
Conservation of momentum	$\frac{\partial\left(\rho v_i v_j\right)}{\partial x_j} + \frac{\partial p}{\partial x_i} + \frac{\partial \tau_{ij}}{\partial x_j} = \rho g_i$	
Stress tensor	$\tau_{ij} = -\mu\left(\frac{\partial v_i}{\partial x_j} + \frac{\partial v_j}{\partial x_i}\right) + \left(\frac{2}{3}\mu\right)\delta_{ij}\frac{\partial v_k}{\partial x_k}$	
Conservation of energy	$\nabla \cdot \left(\overrightarrow{v}\left(\rho E + p\right)\right) + \nabla \cdot j_{q,j} = \nabla \cdot \left(\overline{\overline{\tau}}_{eff} \cdot \overrightarrow{v}\right) + S_h$	[166, 167]
	$E = h - \frac{p}{\rho} + \frac{v^2}{2}$	
Diffusive heat transport $j_{q,j}$	$j_{q,j} = -\lambda\frac{\partial T}{\partial x_j} + \sum_{i=1}^{N_g} h_i j_{i,j}$	
Specific enthalpy, h	$h = \sum_{i=1}^{N_g} Y_i h_i\left(T\right)$	

- Also, the Joule heating was modeled using source term.
- Also, wall thickness not considered

3.2.2 Results

From the simulation results carried out for the three electrical power used for the experiments, simulations were carried out for two gas mass flow rate, that is, the slowest and fastest flow rate used during the experiment. The results were then processed and temperature and velocity in the axial direction and radial direction inside the fixed bed were then compared with each other for the three experimental electrical powers simulated. Also, the temperature at the wall of the fixed bed and the particle temperature inside the bed were also compared.

3.2.2.1 Velocity in the fixed bed

The velocity of the gas flowing through the fixed bed was observed to increase with increase in electrical energy used to heat the fixed bed. The increase in electrical power through the bed increases the kinetic energy of the gas and therefore the velocity. Also as the mass flow rate of the gas is increased, the gas flows more through the center of the bed. This is as seen in figures 3.2, 3.3, 3.4 and 3.5. The

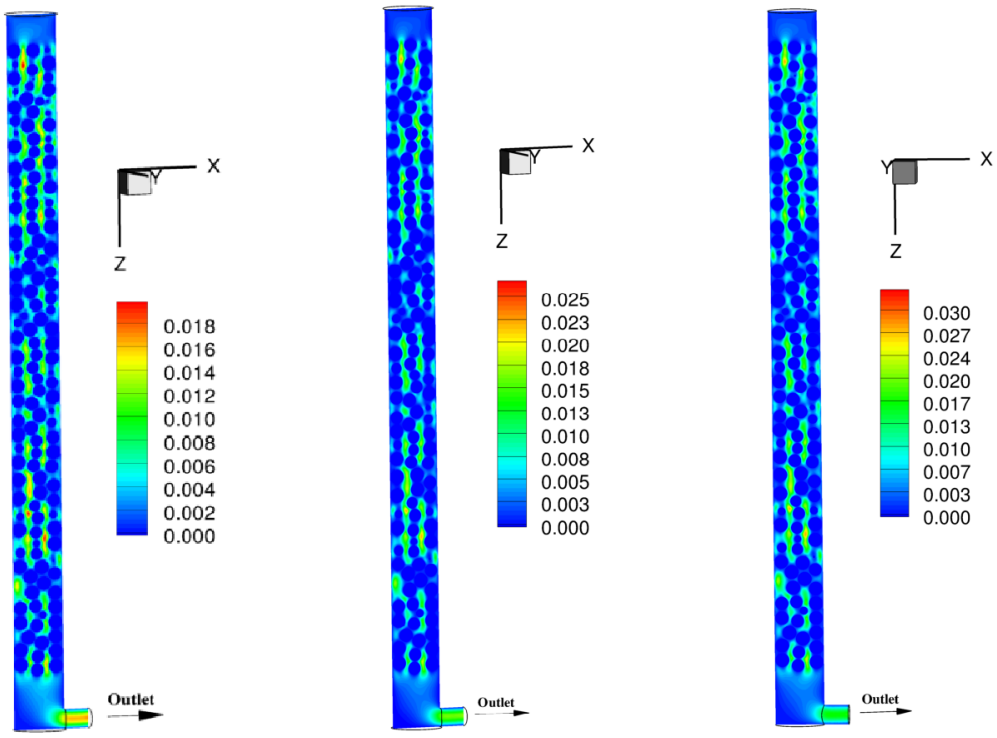

(A) (B) (C)

FIGURE 3.2: Velocity profile across the bed of gas flow for the three energy applied across the bed with flow rate of 1.27×10^{-7} kg/s: (a) at 15 W power, (b) at 22.5 W power, and (c) at 42 W power

increase in kinetic energy and in turn increase in velocity of the gas (air) moving through the fixed caused the gas to move more through the center of the bed rather than creeping by the wall from the inlet to the outlet. This was also observed for higher flow rate with the same electrical power been passed through the fixed bed. This therefore results in higher gas temperature for higher flow rate and also for higher electrical power passed through the fixed bed when compared to the same flow rate of gas passing through the fixed bed but with lower electrical power.

3.2.2.2 Temperature in the fixed bed

From the axial temperature profile, it was seen that inside the bed, the temperature at the wall is lower than that at the center of the tube. Also, the temperatures at the inlet and outlet position of the bed were found to be much lower than the temperature both at the wall and at the center. This was also buttressed by the

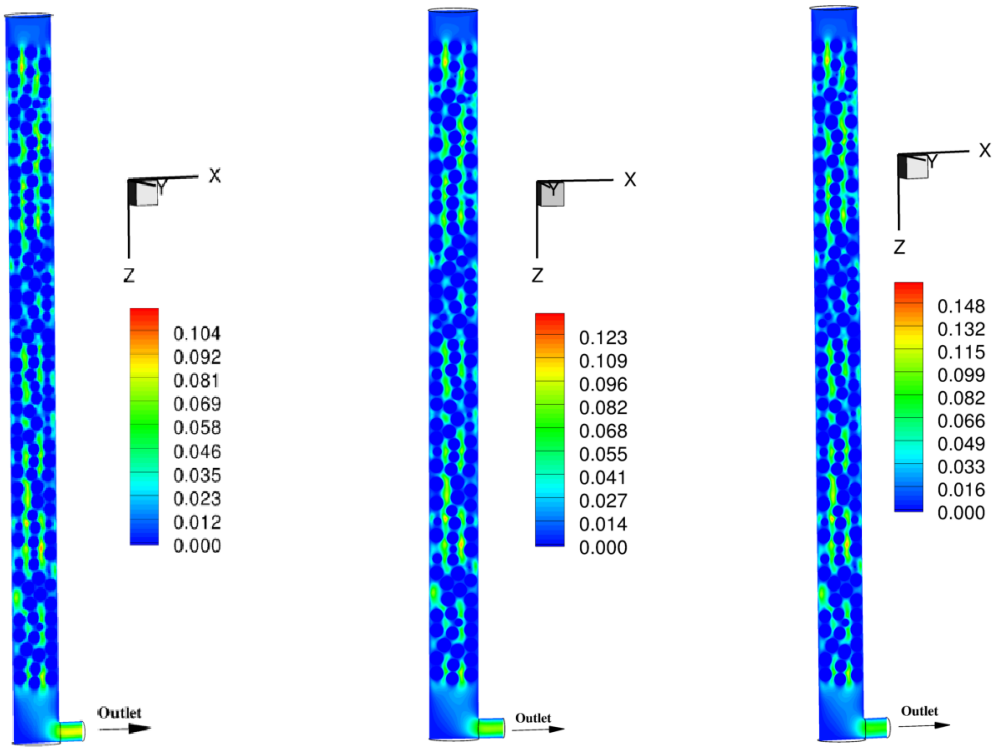

(A) (B) (C)

FIGURE 3.3: Velocity profile across the bed of gas flow for the three energy applied across the bed with flow rate of 6.13× 10^{-7} kg/s: (a) at 15 W power, (b) at 22.5 W power, and (c) at 42 W power

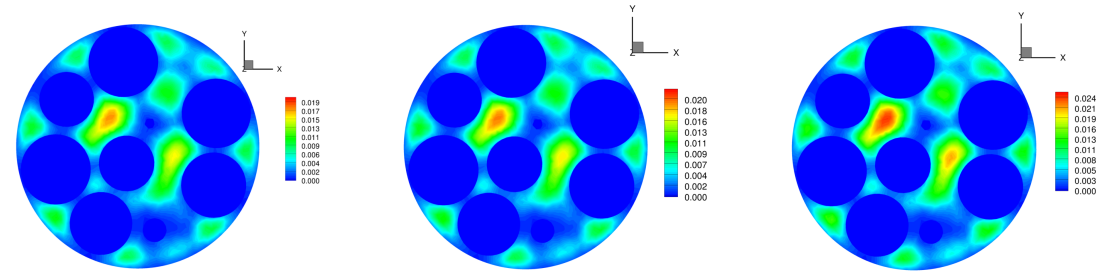

(A) (B) (C)

FIGURE 3.4: Radial Velocity profile across the bed of gas flow for the three energy applied across the bed with flow rate of 1.27× 10^{-7} kg/s: (a) at 15 W power, (b) at 22.5 W power, and (c) at 42 W power

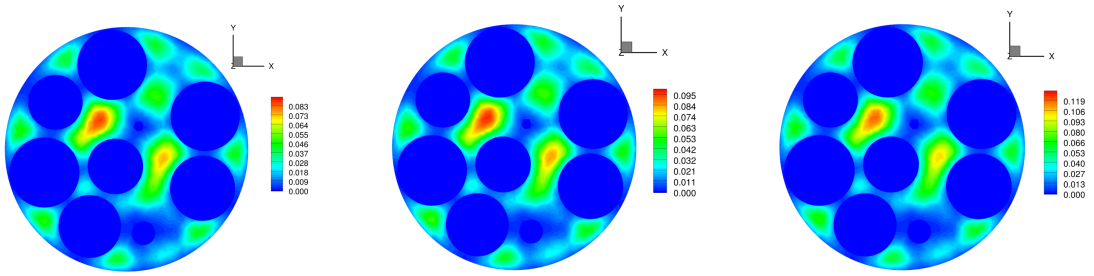

(A) (B) (C)

FIGURE 3.5: Radial Velocity profile across the bed of gas flow for the three energy applied across the bed with flow rate of 6.13× 10^{-7} kg/s: (a) at 15 W power, (b) at 22.5 W power, and (c) at 42 W power

radial temperature profile which shows a lower temperature at the wall of the bed. This difference in temperature was attributed to the fact that the bed is not adiabatic and therefore heat is been lost at the wall of the bed due to radiation and convection at the wall which cools down the wall. Also, the temperature of the gas can also be seen that to increase with increase in the electrical power passed through the fixed bed and also with increase in mass flow rate. The simulation shows that the temperature of the gas at the outlet is much less than that at the center. This was attributed to the fact that the gas flows near the wall which is been cooled down and therefore results in the gas been less heated and for the lower flow rate and also as the input electrical power is increased, the flow is more at the center and therefore more heated up. This is as shown in figures 3.6, 3.7, 3.8 and 3.9.

3.2.2.3 Temperature of the fixed bed wall

The temperature at the wall of the fixed bed is lower than than that at the center of the bed. This is because heat is been lost at the wall both by radiation and convection at the wall to the surrounding air. Results are as shown in figures 3.10 and 3.11. The wall of the fixed bed is been cooled down by the free convection of the surrounding air around the fixed bed. This is so because there is a temperature gradient between the surrounding of the fixed bed and the enclosure of the fixed bed. Therefore, heat is been lost to the surrounding air.

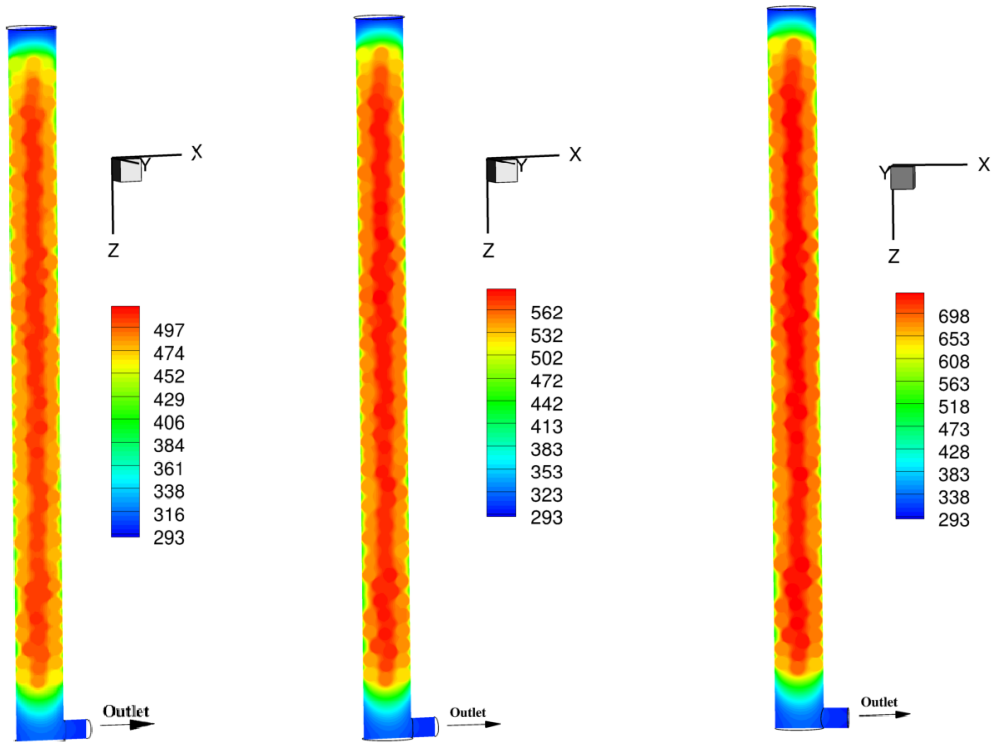

(A) (B) (C)

FIGURE 3.6: Temperature profile across the bed with gas flow for the three energy applied across the bed with flow rate of 1.27×10^{-7} kg/s: (a) at 15 W power, (b) at 22.5 W power, and (c) at 42 W power

3.2.2.4 Particle (nickel spheres) temperature

Also, the temperature of the particle in the bed is as shown in figures 3.12 and 3.13 for both mass flow rate simulated. It can be seen that the temperature is higher at the center than that at close to the wall and those at the inlet and outlet of the fixed bed. This is so because the electric current passed through the fixed bed is concentrated more at the center and therefore, the particle at the center of the bed is heated more than those at the inlet and outlet position of the bed which are heated up more by conduction and convection. The results obtained from the simulation is the same as those observed for the experiment and it also correlates with the results obtained from the numerical model developed.

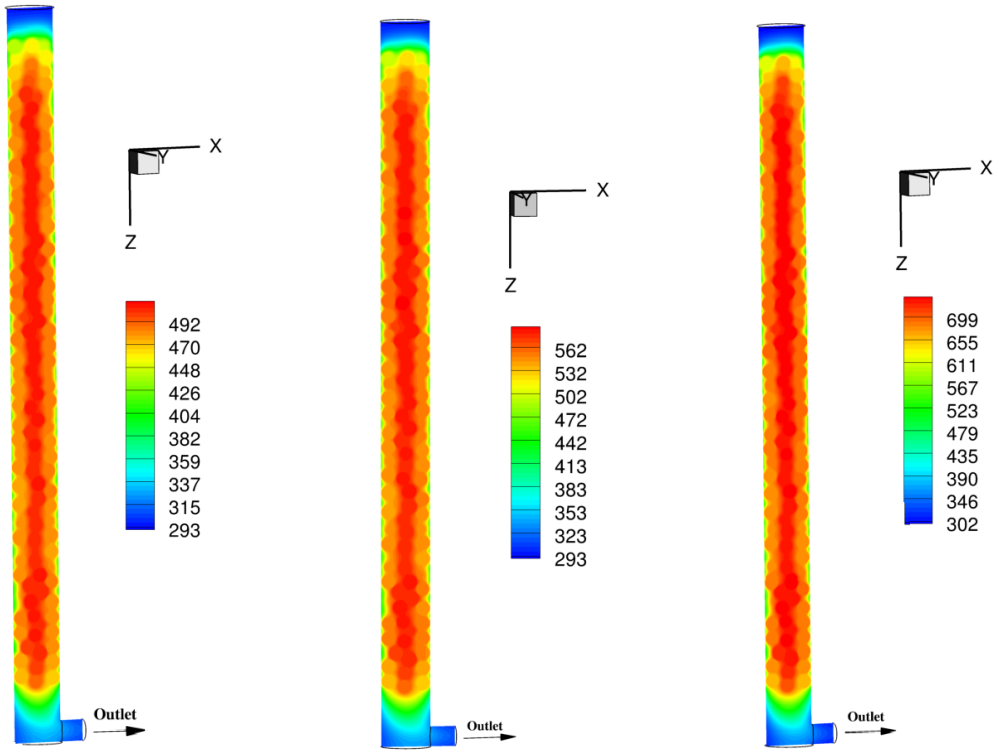

(A) (B) (C)

FIGURE 3.7: Temperature profile across the bed with gas flow for the three energy applied across the bed with flow rate of 6.13× 10^{-7} kg/s: (a) at 15 W power, (b) at 22.5 W power, and (c) at 42 W power

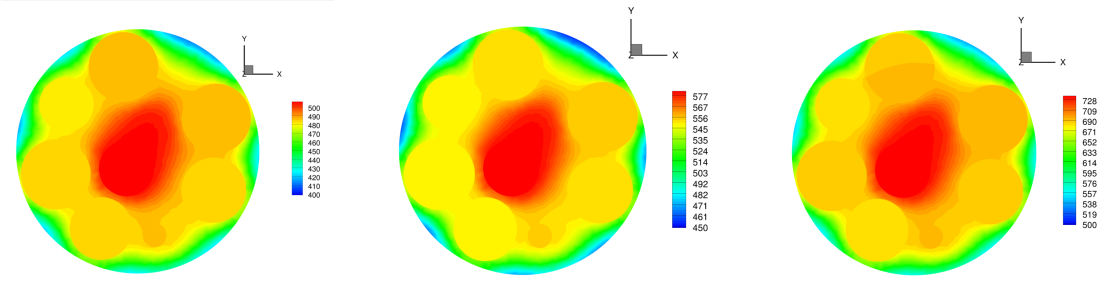

(A) (B) (C)

FIGURE 3.8: Radial Temperature profile across the bed with gas flow for the three energy applied across the bed with flow rate of 1.27× 10^{-7} kg/s: (a) at 15 W power, (b) at 22.5 W power, and (c) at 42 W power

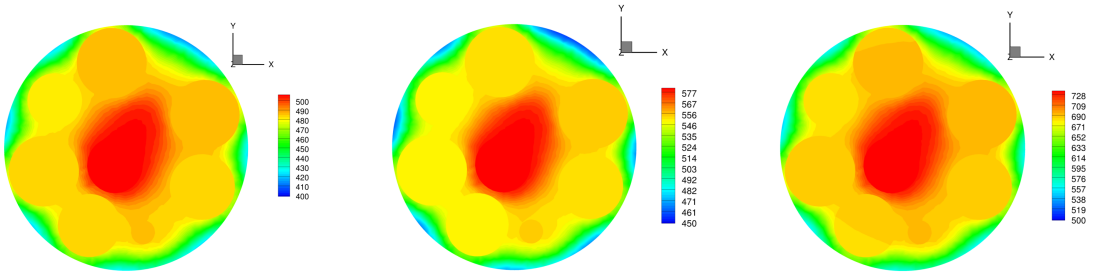

(A) (B) (C)

FIGURE 3.9: Radial Temperature profile across the bed with gas flow for the three energy applied across the bed with flow rate of 6.13× 10^{-7} kg/s: (a) at 15 W power, (b) at 22.5 W power, and (c) at 42 W power

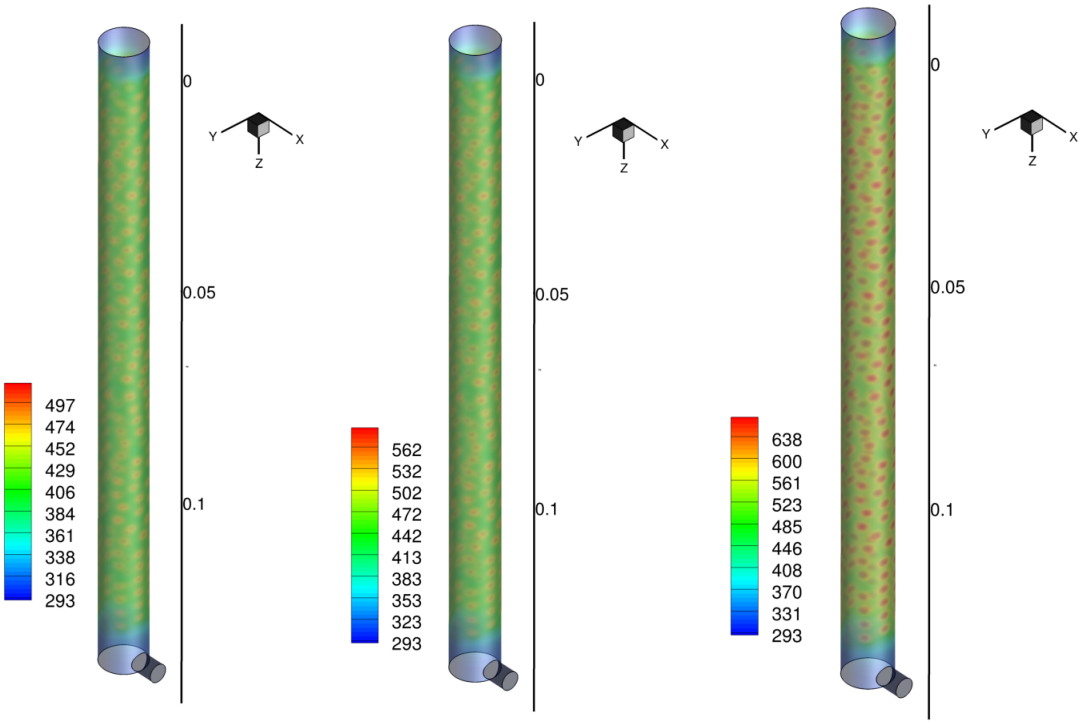

(A) (B) (C)

FIGURE 3.10: Temperature profile at the wall of the bed for the three energy applied across the bed with flow rate of 1.27× 10^{-7} kg/s: (a) at 15 W power, (b) at 22.5 W power, and (c) at 42 W power

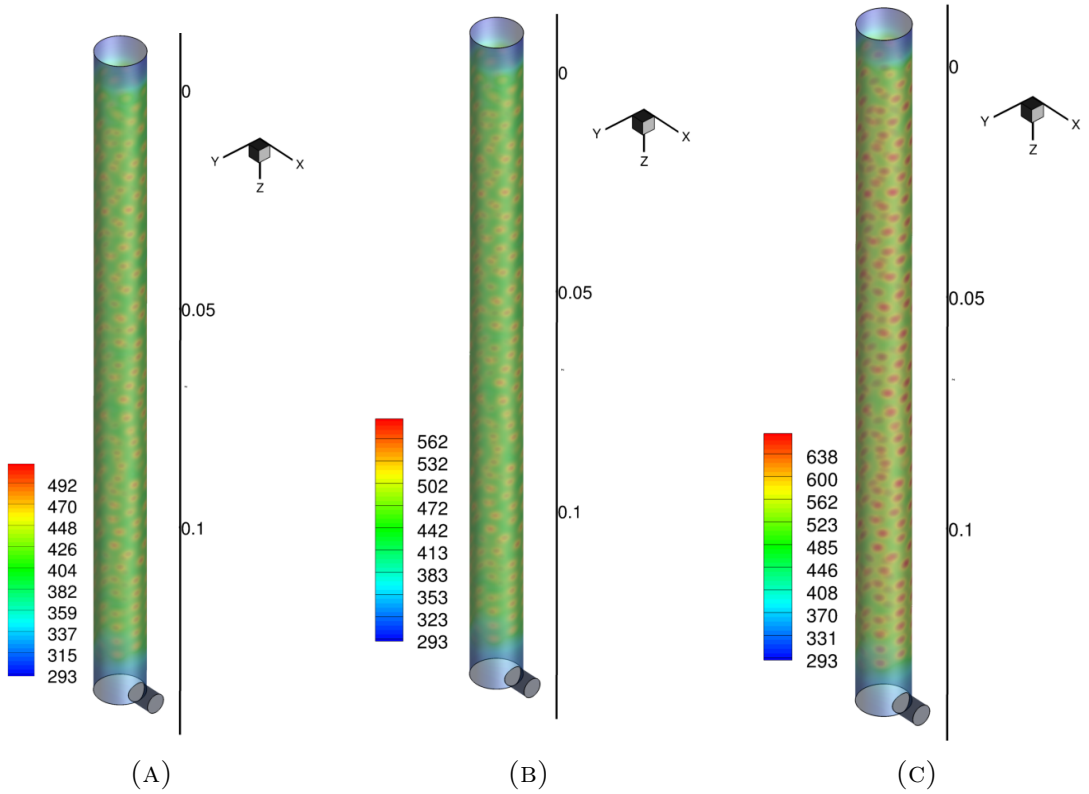

(A) (B) (C)

FIGURE 3.11: Temperature profile at the wall of the bed for the three energy applied across the bed with flow rate of 6.13× 10^{-7} kg/s: (a) at 15 W power, (b) at 22.5 W power, and (c) at 42 W power

3.3 CFD-Simulation and Experimental results

The results from the simulation and that from the steady state approximation of experimental results were then compared. This shows a very good correlation for both the temperature inside the tube and that at the outlet of the fixed bed. The results are shown in figure 3.14. From the figures showing the steady state temperature as obtained from the CFD-Simulation, it can be seen that the temperature inside the tube reduces as the mass flow rate of the gas increases and also the temperature of the gas at the outlet of the bed increases with increase in gas mass flow rate. This correlates with the trend observed from the experimental results. To quantify the difference between the results obtained from the experiments and that from the CFD-Simulation, the absolute percentage relative error has been evaluated as:

$$|\%\ Error| = \left| \frac{T_{exp} - T_{cfd}}{T_{exp}} \times 100 \right| \tag{3.7}$$

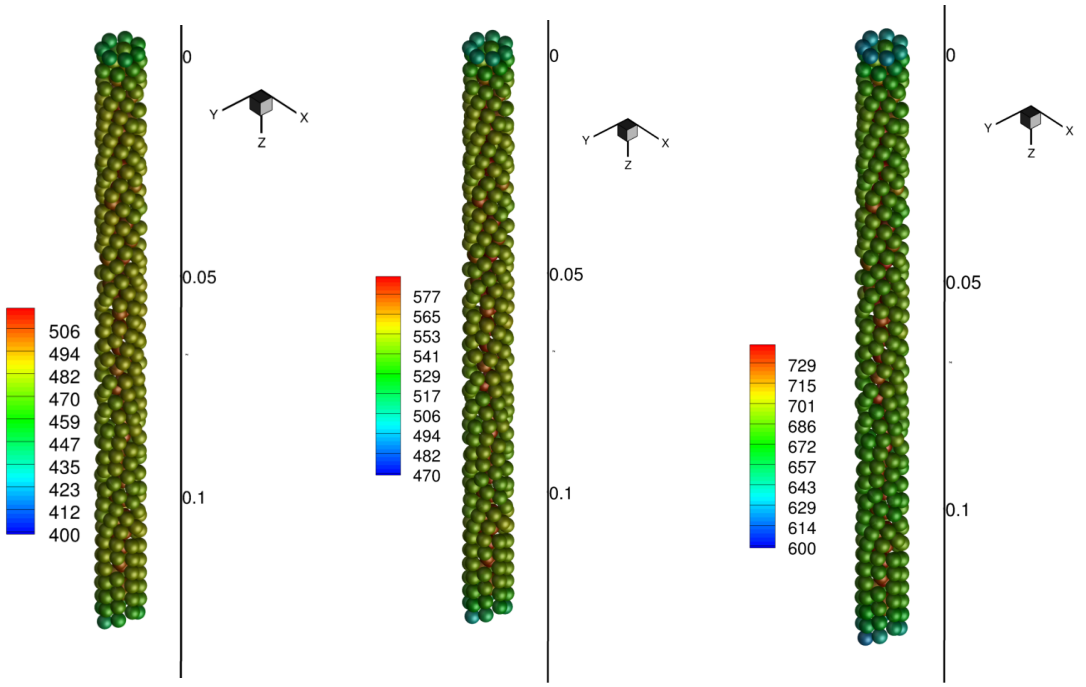

(A) (B) (C)

FIGURE 3.12: Particle Temperature profile across the bed for the three energy applied across the bed with flow rate of 1.27× 10^{-7} kg/s: (a) at 15 W power, (b) at 22.5 W power, and (c) at 42 W power

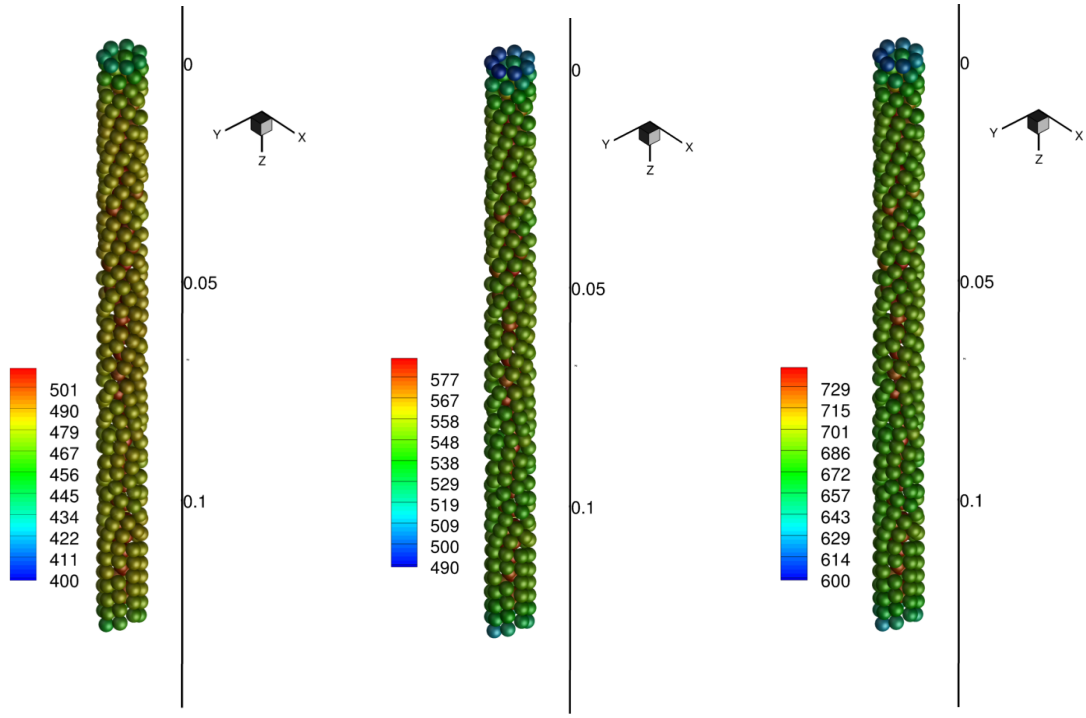

(A) (B) (C)

FIGURE 3.13: Temperature profile across the bed of gas flow for the three energy applied across the bed with flow rate of 6.13× 10^{-7} kg/s: (a) at 15 W power, (b) at 22.5 W power, and (c) at 42 W power

The absolute error between the steady state experimental and CFD-Simulation values for the both temperature inside the bed and that of the gas at the outlet is as shown in tables 3.6 and 3.7 respectively. This shows that the CFD-Simulation gives a very good approximation of the experiment. The large difference observed between the simulation results and experimental results for some of the simulation carried out can be explained as due to error observed during the experiment where the current been passed through the bed is not stable and sometimes fluctuates. This therefore sometimes does not give the accurate temperature reading for the specific flow rate of gas and electric power been passed through the fixed bed. This was observed during the experiment as the bed has to be cooled down after each temperature reading for the each flow rate of gas and electric power passed through the fixed bed.

TABLE 3.5: Experimental variables

RUN	I, A	U, V	$\dot{q}$, W/m^3	$\dot{m}$, kg/s	Velocity, m/s
1	5	3	2836986.508	1.27E-07	0.0013
				2.53E-07	0.0026
				4.33E-07	0.0045
				6.13E-07	0.0064
2	7.5	3	4255479.762	1.27E-07	0.0013
				2.53E-07	0.0026
				4.33E-07	0.0045
				6.13E-07	0.0064
3	10	4.2	7943562.222	1.27E-07	0.0013
				2.53E-07	0.0026
				4.33E-07	0.0045
				6.13E-07	0.0064

TABLE 3.6: Temperature inside the bed

RUN	Velocity, m/s	Experimental, K ±0.3 K	CFD-Simulation, K	% Error
1	0.0013	521.9	505.8	3.09
	0.0064	454.4	505.7	11.30
2	0.0013	585.5	581.1	0.75
	0.0064	560.2	581.1	3.73
3	0.0013	617.1	735.0	19.11
	0.0064	596.0	735.0	23.32

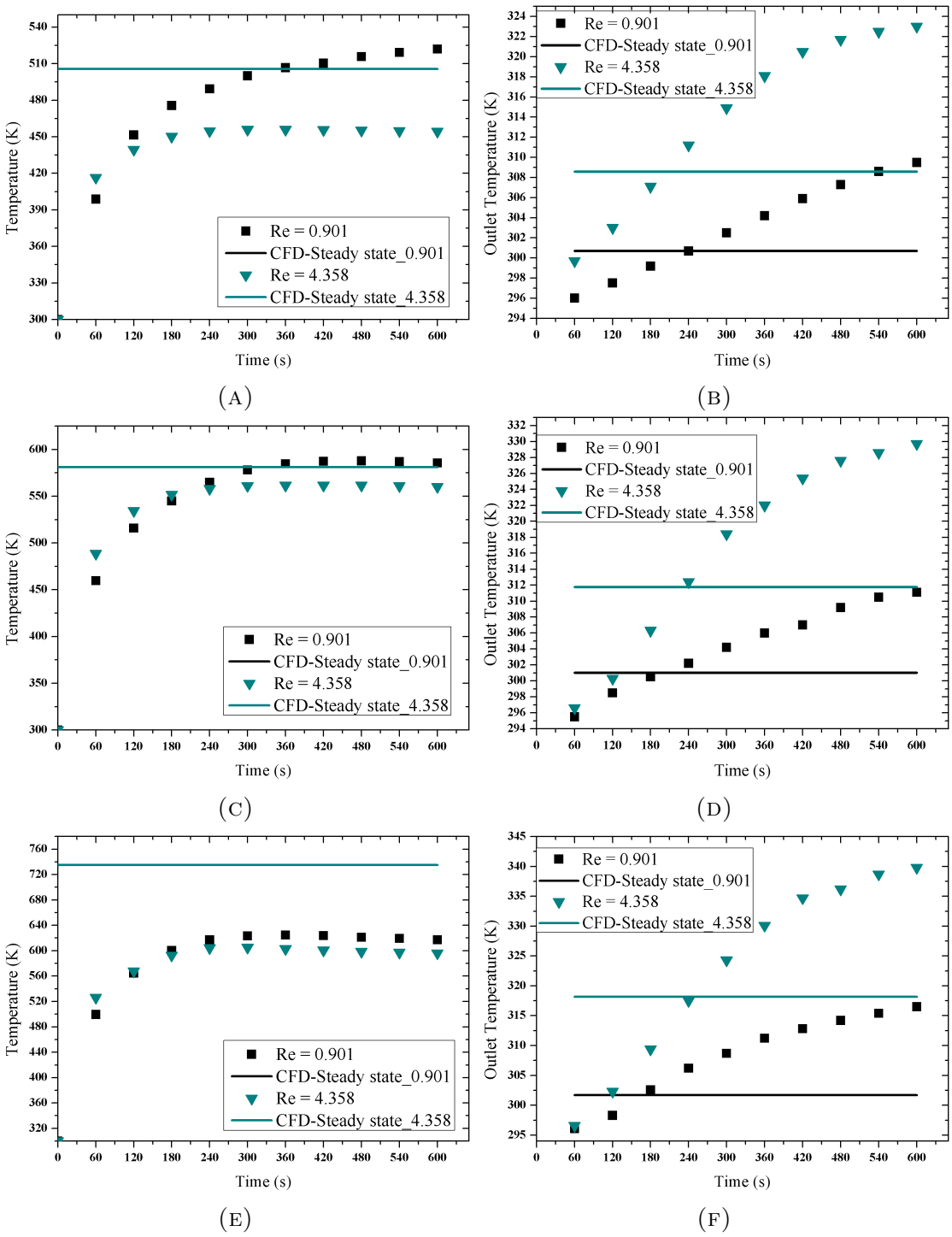

FIGURE 3.14: Experimental (symbols) and CFD-Simulation temperature measurement inside the tube and the outlet air temperature respectively: (a) and (b) at 15 W power, (c) and (d) at 22.5 W power, (e) and (f) at 42 W power

TABLE 3.7: Outlet temperature

RUN	Velocity, m/s	Experimental, K ±0.3 K	CFD-Simulation, K	% Error
1	0.0013	309.5	300.7	2.84
	0.0064	323.0	308.6	4.46
2	0.0013	311.1	301.0	3.24
	0.0064	329.7	311.8	5.44
3	0.0013	316.5	301.7	4.67
	0.0064	339.8	318.2	6.36

Chapter 4

CFD-based study of heat and mass transfer in fixed bed heated by the Joule heating effect

Over the past few decades, fossil fuels have been a major source of energy production and this is accompanied by very large amounts of greenhouse gases such as carbon dioxide (CO_2), nitrous oxide (NO), methane (CH_4) and chlorofluorocarbons (CFCs), been emitted into the atmosphere [168, 169]. These greenhouse gases have very severe effect on the climatic conditions in the world as they contribute to global warming. Therefore, the need to find alternative source of energy production is arises. One of such alternative is through reforming of natural gas. An example of such natural gas used extensively in the industry is methane. The reforming process can either be done as dry reforming (DRM) or steam reforming (SRM) of methane.

Dry reforming of methane (DRM) is the process where methane reacts with carbon dioxide to produce a mixture of hydrogen and carbon monoxide which is called syngas. It is highly endothermic and is usually carried out at high temperatures [168]. One problem associated with DRM is that the catalysts used during the

reforming process are easily deactivated due to the formation of coke [168, 170–172]. It is represented by the chemical equation as shown below:

$$CH_4 + CO_2 \rightleftharpoons 2H_2 + 2CO \qquad \Delta H \approx +260 kJ/mol \qquad \text{(R4.1)}$$

On the other hand, steam reforming of methane (SRM) involves the reaction between methane and steam called the steam reforming (SRM) reaction and the reaction between carbon monoxide and steam called the water gas shift (WGS) reaction. The SRM reaction is an endothermic reaction while the WGS reaction is an exothermic one.

Hydrogen production can be achieved by either the dry reforming or steam reforming of methane. Each method has its pros and cons. Dry reforming of methane (DRM) could be seen as better way to further reduce greenhouse gases since both reactants are greenhouse gas but it requires more energy to produce hydrogen when compared to the energy required to produce the same amount of hydrogen from SRM due to its higher endothermicity [173]. Therefore, due to the lower energy required for hydrogen production and thereby cost effectiveness, steam reforming of methane (SRM) still remains the main process of hydrogen production on a commercial scale [174, 175]. It also has its limitations such as reversibility of the reaction [176, 177], diffusion limitations, and catalyst deactivation [178, 179].

As an alternative source of energy that can be used to replace fossil fuels is hydrogen [180]. This is so because it has some advantages over the fossil fuel, one of which is clean and more efficient combustion. It can be used for highly efficient and environmentally friendly electricity generation using fuel cells [174, 180, 181]. *Hydrogen is also an important chemical feedstock with applications ranging from desulfurization, hydro treating, petroleum refining and production of chemicals*[175]. It can also be used for processes such as oil refining, methanol, metallurgy, ammonia, and space transportation [180, 182]. In addition, hydrogen is used in the green cars industry [180]. Hydrogen can be used as an energy storage medium as it burns in a less polluting way than fossil fuels [183] and it also has a higher heating value [184].

For the purpose of this study, steam reforming of methane (SRM) over nickel catalyst in a fixed bed using Joule heating has been simulated and this has been done for different electrical power passing through the fixed bed. This was then compared to the same simulation but with the heat for the reaction been provided through the heated wall of the fixed bed.

4.0.1 Reactions and Governing equations

Steam reforming of methane (SRM) involves several elementary reactions. This is usually reduced to the following two semi-global main reactions [185]

Homogeneous reactions:

$$CH_4 + H_2O \longrightarrow CO + 3H_2 \qquad \Delta H^0_{298} \approx +206 kJ/mol \qquad \text{(R4.2)}$$

$$CO + H_2O \longleftrightarrow CO_2 + H_2 \qquad \Delta H^0_{298} \approx -41 kJ/mol \qquad \text{(R4.3)}$$

Heterogeneous reaction:

$$CH_4 + H_2O \xrightarrow{Ni} CO + 3H_2 \qquad \text{(R4.4)}$$

The first i.e. steam reforming of methane (SRM) and second i.e. water-gas shift(WGS) reactions above are homogeneous reactions are endothermic and exothermic respectively. The third reaction is the SRM reaction which occurs on the surface of the catalyst i.e. heterogeneous.

To solve for the mass, momentum, species concentration, and energy, the governing equations include the continuity equation and mass conservation, momentum balance, and energy and species transport equation[168, 174, 180, 186]. The mass conservation and momentum balance equation are expressed in the x-, y-, z- directions. The governing equations are as shown in table 4.1 [168].[1,2]

[1]The binary diffusion coefficients D_i are obtained through polynomial fits.

[2]With thermal conductivity of the mixture λ and mixture specific enthalpy h is expressed as a function of temperature

TABLE 4.1: Governing equations

	Equations	Ref.
Conservation of mass	$\frac{\partial(\rho v_i)}{\partial x_i} = 0$	
Conservation of momentum	$\frac{\partial\left(\rho v_i v_j\right)}{\partial x_j} + \frac{\partial p}{\partial x_i} + \frac{\partial \tau_{ij}}{\partial x_j} = \rho g_i$	
Stress tensor	$\tau_{ij} = -\mu\left(\frac{\partial v_i}{\partial x_j} + \frac{\partial v_j}{\partial x_i}\right) + \left(\frac{2}{3}\mu\right)\delta_{ij}\frac{\partial v_k}{\partial x_k}$	
Conservation of species i	$\frac{\partial\left(\rho v_j Y_i\right)}{\partial x_j} + \frac{\partial\left(j_{i,j}\right)}{\partial x_j} = R_i + S_i \quad i = 1, \ldots, N_g$	[166, 167]
Diffusion mass flux, $j_{i,j}$	$j_{i,j} = -\rho\frac{Y_i}{X_i}D_i^M\frac{\partial X_i}{\partial x_j} - \frac{D_i^T}{T}\frac{\partial T}{\partial x_j}$	
Molar fraction	$X_i = \frac{1}{\sum_{j=1}^{N_g}\frac{Y_j}{M_j}}\frac{Y_i}{M_i}$	
Conservation of energy	$\nabla\cdot\left(\overrightarrow{v}\left(\rho E + p\right)\right) + \nabla\cdot j_{q,j} = \nabla\cdot\left(\overline{\overline{\tau}}_{eff}\cdot\overrightarrow{v}\right) + S_h$	
	$E = h - \frac{p}{\rho} + \frac{v^2}{2}$	
Diffusive heat transport $j_{q,j}$	$j_{q,j} = -\lambda\frac{\partial T}{\partial x_j} + \sum_{i=1}^{N_g} h_i j_{i,j}$	
Specific enthalpy, h	$h = \sum_{i=1}^{N_g} Y_i h_i\left(T\right)$	

4.1 CFD-Simulation of SRM

Development of new technologies in renewable energy sector in recent times have led to a new problem which is the storage of energy. One way to do this is through the transfer of electrical energy to chemical energy (**E2C**) using gasification or reformer technologies. Using this technologies allows for usage of carbon dioxide, which can invariably help in reducing greenhouse gas emissions. For the purpose of this study, the Computational Fluid dynamics (CFD) simulation of methane reforming with steam has been carried out. Steam reforming of methane (SRM) represents the way to go about hydrogen production on an commercial scale in industries. The CFD simulation was carried out in a fixed bed with nickel particles serving as the catalyst. One issue with steam reforming of methane is how to achieve the desired heat required for the reaction as it is highly endothermic. The heat required is usually around 600-700 C.

Instead of the traditional combustion, we have studied how the heat required for the reforming process can be generated from Joule heating effect utilizing electrical current which can be produced from renewable energy sources. This has been done by heating a fixed bed filled with nickel particles of 3 mm diameter serving as the

catalyst using the Joule heating effect by passing electrical current through the bed through electrodes connected on both ends of the fixed bed. Methane, steam and carbon dioxide is then introduced into the fixed bed of 1 cm diameter and the simulation carried out under the steady state condition.

4.1.1 CFD-Simulation of SRM and Results

The main idea of this part of the study is the parametric study of processes through which energy storage can be achieved and for this particular case we are considering the steam reforming process. Drawing from the knowledge of heat transfer in a fixed bed as determined from the previous studies, Compuational fluid dynamics (CFD) simulations were carried out for Steam reforming of methane using DC discharge. This is based on using the Joule heating effect to heat up the catalyst bed which is made up of Nickel particles. The number of particles in the fixed bed was reduced to 50 particles so as to reduce the computational cost and time. The domain used for the simulation is represented as a three-dimensional geometry to give a more accurate representation of the fixed bed and it is as seen in figure 4.1 consists of 2057616 cells, 4288960 faces and 430065 nodes. The model used here and solution method is as shown in table 4.7 below. This was carried out on a 4 core computer with 3.5 GHz, 32 Gb RAM.

The simulation was then carried out using Ansys commercial software 14.0 for different reaction kinetic and source term. A total of 10 equations were coupled together and solved. This include the momentum equation in the x-, y- and z- direction (U_x, U_y, U_z), pressure, temperature and mass fraction for all the components (Y_{CH_4}, Y_{H_2O}, Y_{CO}, Y_{H_2}, Y_{CO_2}). For comparison simulations were carried out for different surface kinetic and different source term as shown in table 4.3. Also, for a specified wall temperature, simulations were carried out and the results compared to that of the Joule heating effect. Also, for each electrical power used, simulations were carried out for the slowest and fastest mass flow rate as used during the experiment for comparison with the experimental results. The simulations were carried out for the steady state case and this was because

an unsteady state simulation requires more computational cost and time. For the purpose of this study, we have used the simplified form of the reaction rate expression, given as:

$$k = A_k T^{\beta} exp\left(\frac{-E_a}{RT}\right) \tag{4.1}$$

TABLE 4.2: Kinetic used for the CFD simulation in equation (4.1)

Reactions	Reaction type	RUN	A_k, m^3/mol.s	E_a, J/kg.mol	β	Ref.
$CO + H_2O$ ↓ $CO_2 + H_2$	Volumetric	1 - 6	2.74×10^6	8.368×10^4	0	[167, 187]
$CO_2 + H_2$ ↓ $CO + H_2O$	Volumetric	1 - 6	9.98×10^7	1.205×10^5	0	[167, 187]
$CH_4 + H_2O$ ↓ $CO + 3H_2$	Volumetric	1 - 6	3×10^5	1.255×10^5	0	[167, 187]
$CH_4 + H_2O$ ↓ $CO + 3H_2$	Wall Surface	1 - 6	see table 4.3		0	***calculated & varied***

TABLE 4.3: Surface kinetics and Source term for fixed bed of 50 Nickel particles

RUN	A_k, m^2/kmol.s	E_a, J/kg.mol	Source term, W/m^3	Power, W
1	3×10^{10}	1.255×10^5	1×10^9	706.86
2	1.5×10^6	1.255×10^5	1×10^9	706.86
3	1.5×10^6	1.255×10^8	1×10^8	70.69
4	1.5×10^6	1.255×10^5	5×10^8	353.43
5	1.5×10^7	1.255×10^5	5×10^8	353.43
6	1.5×10^6	1.255×10^5	$T_w = 1200$ K	–

TABLE 4.4: Inlet and Outlet Conditions for the CFD simulations

RUN	Inlet	Outlet						
		T, K	Y_{CH_4}	Y_{CO_2}	Y_{H_2}	Y_{CO}	Y_{H_2O}	U_V, m/s
1	$T_{in} = 400$ K	937.00	0.00013	0.1598	0.06001	0.49638	0.04256	0.454
2	$Y_{CH_4} = 0.3$	957.01	0.07220	0.1796	0.09216	0.35042	0.11385	0.602
3	$Y_{CO_2} = 0.1$	868.49	0.23972	0.2125	0.02885	0.03368	0.28623	0.386
4	$Y_{H_2} = 0$	890.74	0.20096	0.2497	0.04052	0.07918	0.22892	0.418
5	$Y_{CO} = 0$	887.67	0.06508	0.2061	0.08952	0.34521	0.09375	0.531
6	$Y_{H_2O} = 0.4$	1164.16	0.20038	0.1727	0.04182	0.12998	0.25666	0.530

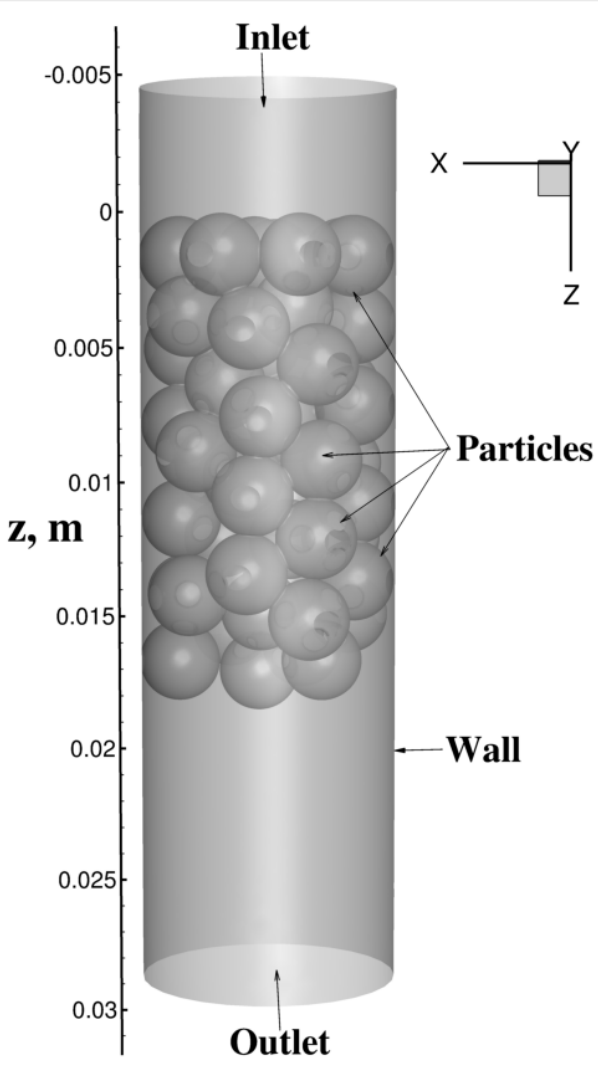

FIGURE 4.1: Geometry of fixed bed of 1 cm diameter for CFD simulation consisting of 50 Nickel particles of 3 mm diameter

4.1.1.1 Results

For the purpose of discussion, we have selected four runs from six runs for which simulations were carried out. The runs selected for discussion are run 2 - 5. This is because this runs can be used for comparison as the input parameters differ from each other. The kinetic used for the homogeneous reactions are the same for all the runs [see 167, pg. 210, 281]. The kinetic used for the heterogeneous reactions were obtained from the volumetric kinetic obtained in literature. This was done by converting the volumetric kinetic to surface kinetic. To do this, we obtained the ratio of volume to surface area of a sphere as shown below:

$$\frac{Volume}{Surface\ area} = \frac{\frac{4}{3}\pi r_p^3}{4\pi r_p^2} = \frac{r_p}{3} = \frac{d_p}{6}$$

$$Volumetric\ kinetic, k_v = A_k \cdot exp\left(\frac{E_a}{R \cdot T}\right)$$

$$Surface\ kinetic, k_s = \frac{d_p}{6} \cdot k_v$$

This was then scaled up by a factor of 10, 100, and $2{\times}10^5$.

Runs with the same kinetic but different source term

For Run 2, 3 and 4, the same reaction kinetic has been used. The difference in the input parameters is the energy input, that is , the source term as can be seen from table 4.3 which has been increased by a factor of 10, 5 and 2.

Runs 2 and 3

The source term for Run 2 is a factor of 10 more than that of Run 3. This increase in source term increases the temperature in the bed which in turn leads to an increase in methane and steam conversion, thereby leading to an increase in yield of carbon monoxide and hydrogen. At the outlet as seen in table 4.4, the methane and steam conversion has increased from 20.1% to 75.6% and 28.4% to 71.5% respectively. The yield of carbon monoxide and hydrogen increased significantly with an increase in source term by a factor of 10.

Runs 3 and 4

The source term for Run 4 is a factor of 5 more than that of Run 3. This increase in source term increases the temperature in the bed slightly and this results in an increase in methane and steam conversion, thereby leading to an increase in yield of carbon monoxide and hydrogen. At the outlet as seen in table 4.4, the methane and steam conversion has increased from 20.1% to 33.0% and 28.4% to 42.8% respectively. The yield of carbon monoxide and hydrogen increased 135.1% and 40.5% respectively for an increase in source term by a factor of 5.

Runs 2 and 4

The source term for Run 2 is a factor of 2 more than that of Run 4. This increase in source term increases the temperature in the bed which in turn leads to an increase in methane and steam conversion, thereby leading to an increase in yield of carbon monoxide and hydrogen. At the outlet as seen in table 4.4, the methane and steam conversion has increased from 33.0% to 75.6% and 42.8% to 71.5% respectively. The yield of carbon monoxide and hydrogen increased significantly with an increase in source term by a factor of 2.

Runs with different kinetic but the same source term

Run 4 and 5 fall under this category and have the same source term of $5\times10^8 \mathrm{W/m^3}$ but different pre-eponential factor.

Runs 4 and 5

The difference in kinetic leads to difference in the reaction for Run 4 and 5. The pre-exponential factor is increased by a factor of 10 for Run 5. Since the source term for both run is the same, the temperature in the fixed bed is about the same. Increasing the kinetic for Run 5 increases the reaction rate and this therefore means that the conversion rate of methane and steam increases and the yield of hydrogen and carbon

monoxide increases as a result. The conversion rate of methane and steam increased from 33.0% to 78.3% and 48.2% to 76.6% respectively.

Runs with different kinetic and source term

Runs 2 and 5

Here, both the kinetic and the source term differ. The kinetic for Run 2 is a factor of 10 less than that of Run 5 while the source term for Run 2 is a factor of 2 higher than that of Run 5. The higher kinetic increases the reaction rate while the increased the sourced term increases the temperature which in turn increases the reaction rate. This therefore leads to about the same reaction rate for both Run 2 and 5. This shows that both the source term and reaction kinetic plays an important role in the rate of the reaction. As can be seen in table 4.4, at the outlet the conversion rate of methane and steam increases from 75.6% and 71.5% for Run 2 to 78.3% and 76.6% for Run 5 respectively. This also shows that reaction kinetic increases the reaction rate slightly more than the source term does.

Particle Temperature Profile

From figure 4.6, it can be seen that for run except run 6 where the particles are heated on the surface when compared to the other runs where the particles are heated to the core. Also, the temperature profile for the particle is the same for run 6 from inlet to the outlet whereas temperature increases from the inlet to the outlet for the other runs.

4.1.1.2 Heat transfer Rate

The heat transfer rate in the bed can be calculated by using the equation below:

$$\dot{m}\left(C_{p_{out}}T_{out} - C_{p_{in}}T_{in}\right) = Q_{gas} \tag{4.2}$$

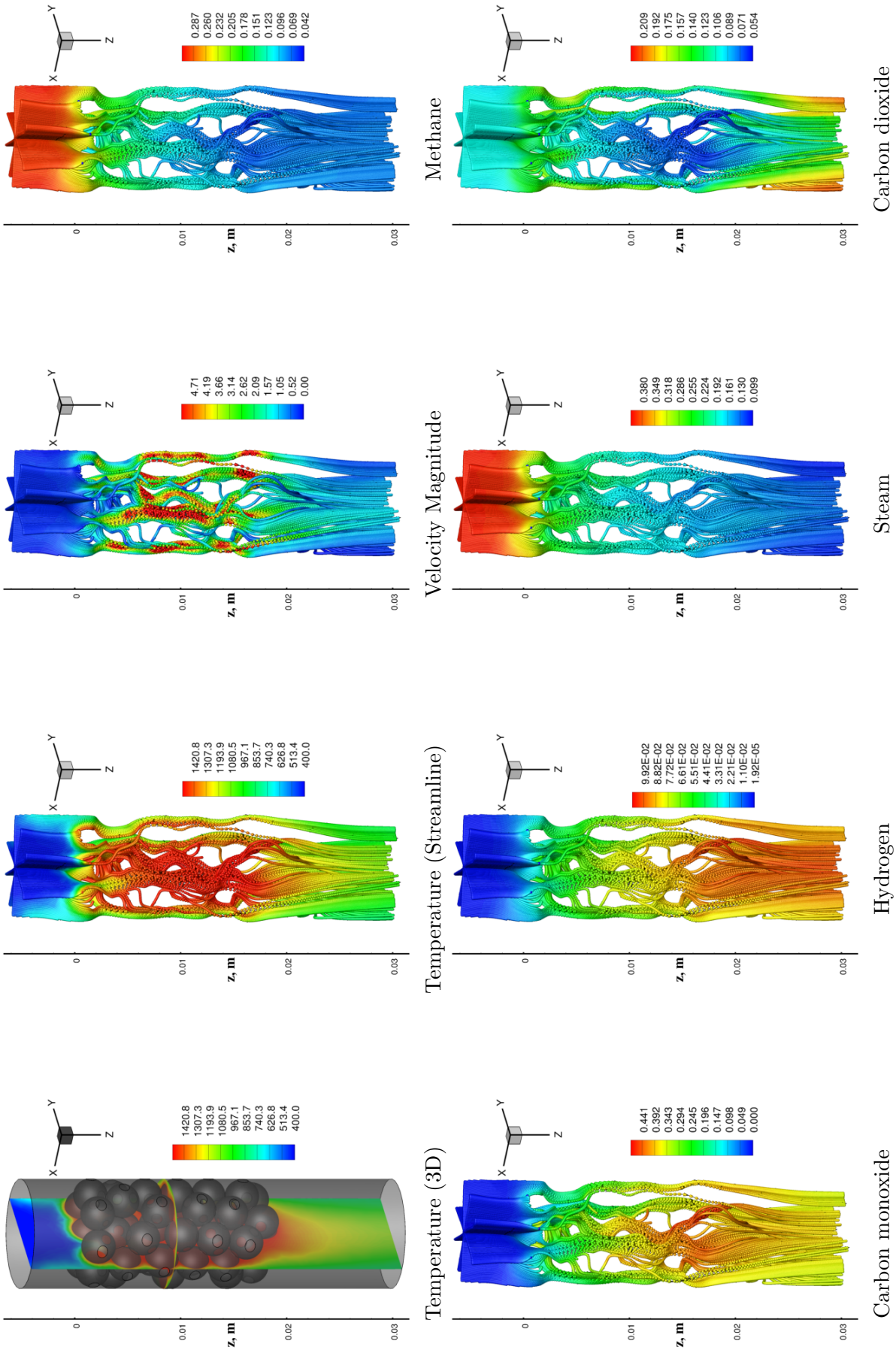

FIGURE 4.2: Results from Run 2 in table 4.3

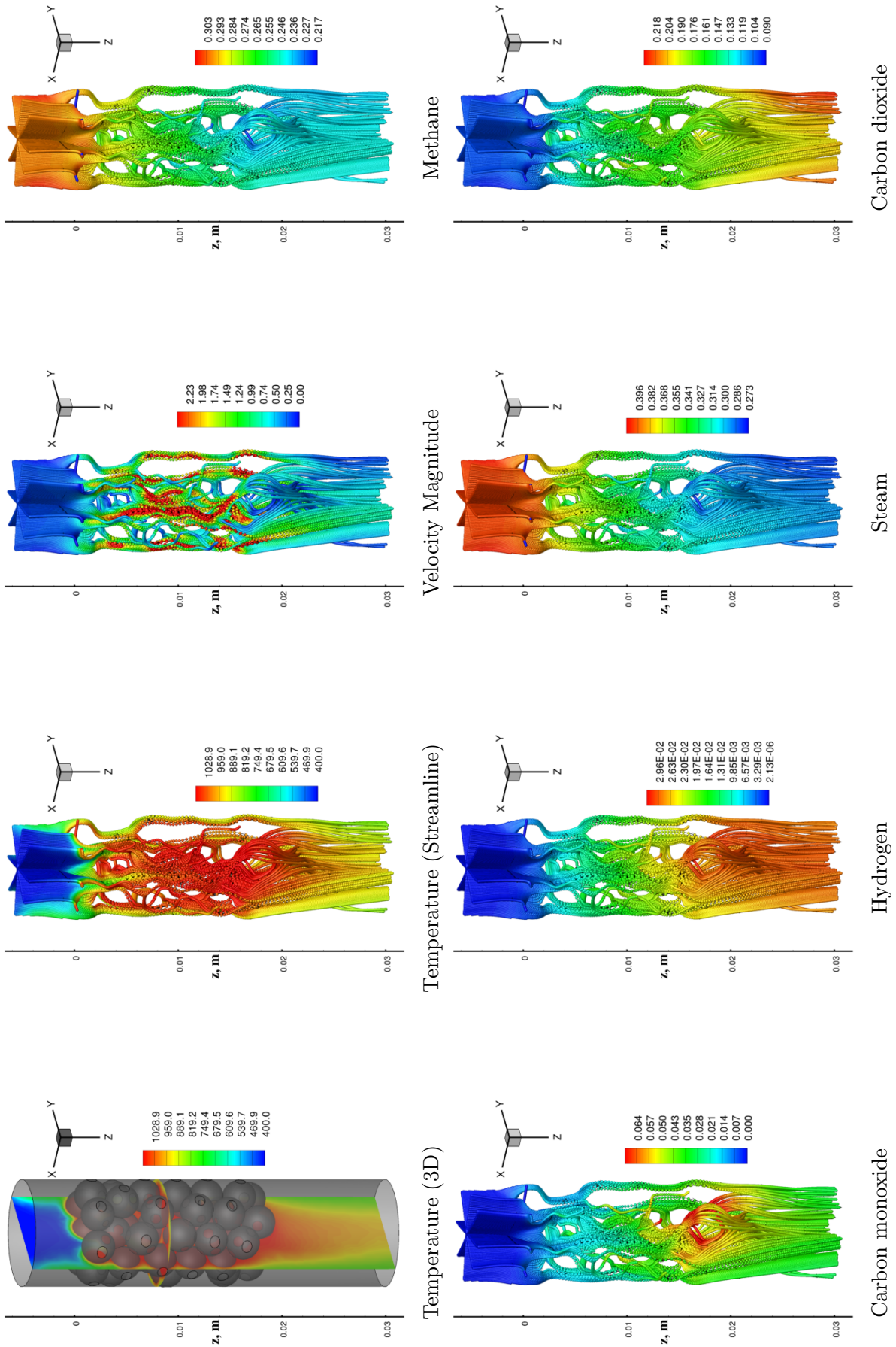

FIGURE 4.3: Results from Run 3 in table 4.3

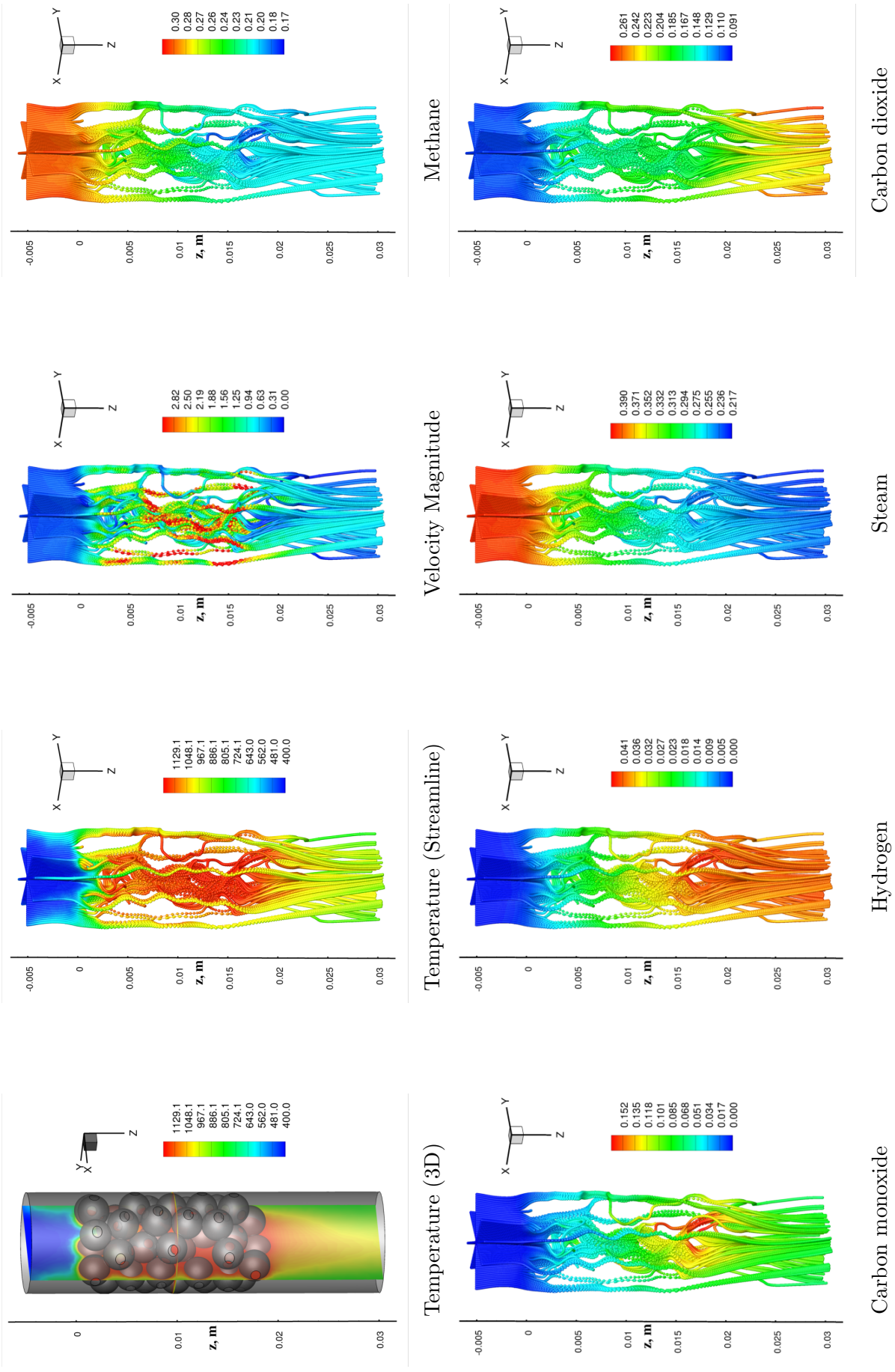

FIGURE 4.4: Results from Run 4 in table 4.3

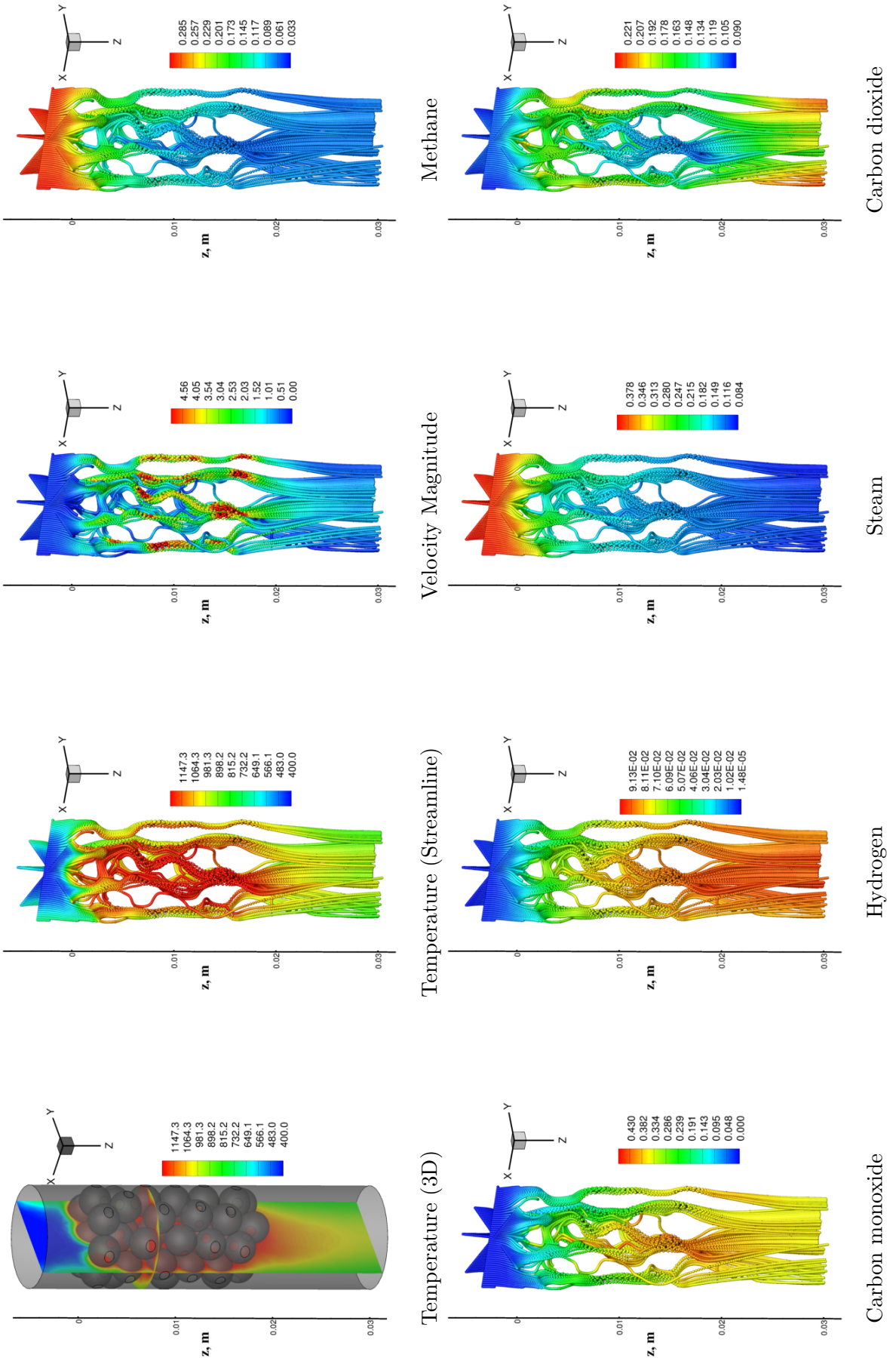

FIGURE 4.5: Results from Run 5 in table 4.3

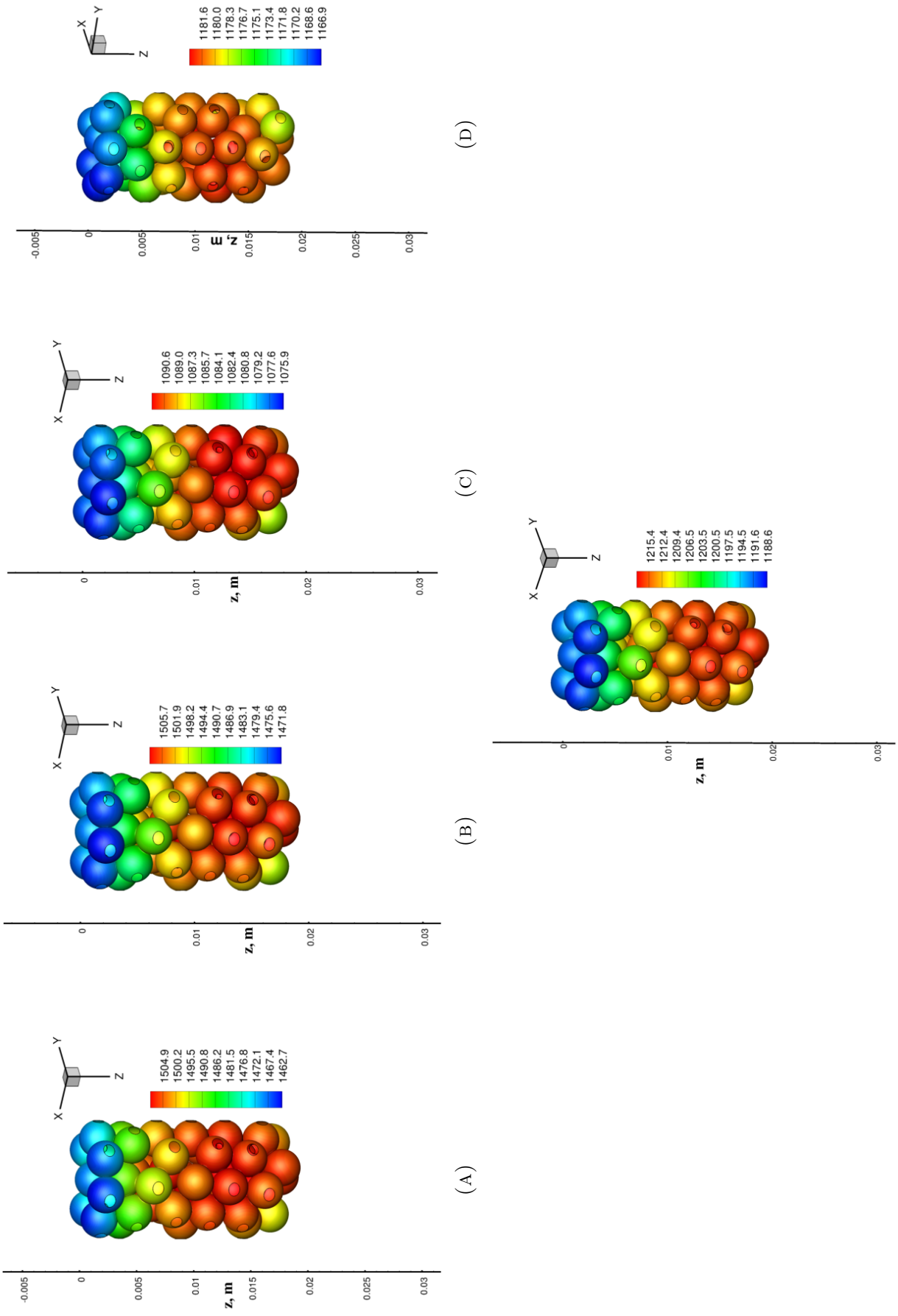

FIGURE 4.6: Particle temperature profile for fixed bed of 50 particles of Nickel: (a) and (b) for Run 1 & 2, (c) for Run 3 and (d) and (e) for Run 4 & 5 in table 4.3

From the CFD-simulations carried out, the mass flow rate, $\dot{m}$, the specific heat, C_p, at the inlet and outlet and the inlet and outlet temperature are computed for each run of simulations. The mass flow rate is constant for all runs. This is as shown in table 4.5.

TABLE 4.5: Heat transfer rate for CFD-simulations in ANSYS FLUENT 14.0

RUN	$\dot{m} \times 10^{-6}$, kg/s	T_{in}, K	$C_{p_{in}}$, J/kg.K	T_{out}, K	$C_{p_{out}}$, J/kg.K	Q_{gas}, W
1	7.082	400	1863.127	937	2084.738	8.556
2	7.082	400	1862.050	957	2873.739	14.201
3	7.082	400	1862.033	868	2606.126	10.754
4	7.082	400	1862.132	891	2619.969	11.252
5	7.082	400	1862.851	888	2729.904	11.884
6	7.082	400	1914.439	1164	2834.952	17.949

Comparing the heat transfer rate from the CFD-simulations with the energy input used for the simulations for the first five runs for which Joule heating effect is applied to, we observed that the heat transfer rate is far less than the energy input provided for the simulation. This disparity between the heat transfer rate and the energy input is as a results of the chemical reaction occurring which requires heat for the reaction to occur since steam reforming of methane is an endothermic reaction. The percentage difference between the heat transfer rate and the energy rate input is given by:

$$Q = I \cdot U = Q_{heat}$$
$$\%DIFF = \left[1 - \frac{Q_{heat} - Q_{gas}}{Q_{heat}}\right] \times 100 \tag{4.3}$$

The comparison is as shown in table 4.6.

TABLE 4.6: Comparison between heat rate from simulation and the input energy

RUN	Q_{heat}, W	Q_{gas}, W	$\%DIFF$
1	706.86	8.556	1.21
2	706.86	14.201	2.01
3	70.69	10.754	15.21
4	353.43	11.252	3.18
5	353.43	11.884	3.36

The overall energy required to heat up the system and also enable the chemical reactions to occur includes the heat for the gas , solid particles and that needed for reaction, i.e.

$$Q_{heat} = Q_{gas} + Q_{solid} + Q_{reaction} \tag{4.4}$$

Therefore, knowing the energy required to heat up the gas and solid can give us insight into how much more energy is needed for the reaction to proceed.

TABLE 4.7: Models and Scheme used for the CFD simulations in ANSYS FLUENT 14.0

Model	Energy		
	Viscous:	Laminar	
	Radiation:	P1	
	Species:	Species transport	
		Reactions:	Volumetric
			Wall Surface
			Wall surface reactions options: Heat of surface reactions
		Options:	Inlet diffusion
			Diffusion energy source
			Full multicomponent diffusion
			Thermal diffusion
Scheme used	Pressure-Velocity Coupling:	Coupled Scheme	
	Spatial discertization:		
		Gradients:	Least Squares cell based
		Pressure:	Standard
		Momentum:	Third-Order MUSCL
		Species:	Third-Order MUSCL
		Energy:	Third-Order MUSCL

TABLE 4.8: Bed condition for the different runs

Inlet		RUN					
		1	2	3	4	5	6
$T_{in} = 400$ K	T, K	400 - 1530	400 - 1520	400 - 1090	400 - 1180	400 - 1220	400 - 1200
$Y_{CH_4} = 0.3$	Y_{CH_4}	0.00 - 0.30	0.04 - 0.30	0.22 - 0.30	0.17 - 0.30	0.03 - 0.30	0.19 - 0.30
$Y_{CO_2} = 0.1$	Y_{CO_2}	0.04 - 0.19	0.05 - 0.22	0.09 - 0.23	0.09 - 0.28	0.09 - 0.23	0.08 - 0.20
$Y_{H_2} = 0$	Y_{H_2}	0 - 0.12	0 - 0.11	0 - 0.03	0 - 0.04	0 - 0.10	0 - 0.04
$Y_{CO} = 0$	Y_{CO}	0 - 0.581	0 - 0.483	0 - 0.090	0 - 0.179	0 - 0.471	0 - 0.150
$Y_{H_2O} = 0.4$	Y_{H_2O}	0.035 - 0.406	0.099 - 0.406	0.273 - 0.407	0.127 - 0.407	0.084 - 0.407	0.239 - 0.413
	U_V, m/s	0 - 5.20	0 - 5.17	0 - 2.45	0 - 5.56	0 - 5.19	0 - 3.71

Chapter 5

Conclusions and Future Work

5.1 Conclusions

In this work, heat and mass transfer in a fixed bed with Joule heating was studied. This was done in a fixed bed with and without gas flowing through the bed. For both sets of experiments, three electrical power was used i.e. 15 W, 22.5 W and 42 W power. Also, for experiments involving gas flow, four mass flow rates ranging from 1.27 $\times 10^{-7}$ to 6.13 $\times 10^{-7}$ kg/s were studied. From the experiments, it was observed that the solid temperature measured at the center of the bed increases with time and electrical power passed through the bed. The gas temperature measurements were made at the outlet of the bed, and this were found to increase with mass flow rate. Also, it was observed that the gas was not heated efficiently as the gas temperature at the outlet was much lower that the solid temperature. To better understand and explain this, numerical models and CFD simulations were then developed and the experiments validated against them. From the models developed, we found heat was lost at the wall of the bed because its not insulated. Also, it was observed that the gas flows closer to the wall of the bed and so this causes the gas heating to be non efficient. This was explained due to the convection and radiation effect through which heat is been lost at the wall and which therefore cools down the gas as it exits from the bed. Although, the gas

temperature increases with mass flow rate, this was still not efficient enough due to the low mass flow rates used. This increase in gas temperature was explained as due the fact that the gas tends to move closer to the center of the bed as the mass flow rate increases. Based on the knowledge of heat and mass transfer in fixed beds with Joule heating, a preliminary parametric study of energy storage, in particular by steam reforming of methane, was then carried out. The water gas shift reaction and the steam reforming reaction were simulated in three dimensional (3D) geometry created. The surface kinetic for the methane reforming reaction was calculated varied from the kinetic for the homogeneous reaction of methane reforming. It was observed that increasing the input power with the same reaction kinetic increased the conversion of methane and therefore yield of syngas. This was also observed for the case where the same input power was used but different reaction kinetic. Also, we found out that the simulation results carried out with the appropriate kinetics can help determine the amount of energy required for either a gasification or reforming process.

5.2 Future Work

Based on the experiments, modeling and simulations carried out for this study and the observations made from the results obtained, the following suggestions have been reached to further improve this future research into this study:

- For the experiments carried out, the wall of the fixed bed should be insulated. This is to reduce the heat lost to the surrounding which in turn affects the results.
- Further study of this work should be carried out with high Reynolds number from about 100 ($\mathrm{Re}_{in} \geqslant 100$). This is because for low Reynolds number i.e. ($\mathrm{Re}_{in} < 5$), the gas is been cooled at the outlet causing the low gas temperature.

- Also, to reduce the wall channelling effect which also contributes to lower gas temperature, then increasing the number of particles in the cross section of the fixed bed.

- Further study into the chemistry and therefore, semi-global kinetics of methane-steam reaction at the surface of the catalyst has to been looked into more in-depth.

Appendix A

MATLAB Code

A.1 Matlab Code for solving for temperature in a fixed bed without gas flow

A.1.1 Matlab code for the ODE

```
%%%%%%%%%%%%%%%%%%%%%%%%%%%%%%%%%%%%%%%%%%%%%%%%%%%%%%%%%%%%%%%%%%%%%%%%%%%%%%%%
%%%%%%%%%%%%%%%%%%%%%%%%%%%%%%%%%%%%%%%%%%%%%%%%%%%%%%%%%%%%%%%%%%%%%%%%%%%%%%%%

function dTdt = TempRate(t, T, Vol, As, Tamb)

%%%%%%%%%%%%%%%%%%%%%%%%%%%%%%%%%%%%%%%%%%%%%%%%%%%%%%%%%%%%%%%%%%%%%%%%%%%%%%%%
%%%%%%%%%%%%%%%%%%%%%%%%%%%%%%%%%%%%%%%%%%%%%%%%%%%%%%%%%%%%%%%%%%%%%%%%%%%%%%%%
Tamb = 300;                 % Ambient temperature

%%%%%%%%%%%%%%%%%%%%%%%%%%%%%%%%%%%%%%%%%%%%%%%%%%%%%%%%%%%%%%%%%%%%%%%%%%%%%%%%
%%%%%%%%%%%%%%%%%%%%%%%%%%%%%%%%%%%%%%%%%%%%%%%%%%%%%%%%%%%%%%%%%%%%%%%%%%%%%%%%
%% Properties of the bed
eps = 0.6732;               % Void fraction of bed

%%%%%%%%%%%%%%%%%%%%%%%%%%%%%%%%%%%%%%%%%%%%%%%%%%%%%%%%%%%%%%%%%%%%%%%%%%%%%%%%
%%%%%%%%%%%%%%%%%%%%%%%%%%%%%%%%%%%%%%%%%%%%%%%%%%%%%%%%%%%%%%%%%%%%%%%%%%%%%%%%
%% Density and specific heat of particle (Nickel)
Rho_Ni = 8900;              % Density of Nickel particle
c_Ni = 460.6;               % Specific heat of Nickel particle

%%%%%%%%%%%%%%%%%%%%%%%%%%%%%%%%%%%%%%%%%%%%%%%%%%%%%%%%%%%%%%%%%%%%%%%%%%%%%%%%
%%%%%%%%%%%%%%%%%%%%%%%%%%%%%%%%%%%%%%%%%%%%%%%%%%%%%%%%%%%%%%%%%%%%%%%%%%%%%%%%
```

```
23 %% Density and specific heat of fluid (Air)
24 Rho_air = 1.225;              % Density of Nickel particle
25 % c_air = 1006.43;            % Specific heat of Nickel particle
26
27 %%%%%%%%%%%%%%%%%%%%%%%%%%%%%%%%%%%%%%%%%%%%%%%%%%%%%%%%%%%%%%%%%%%%%%%%%%%%%%%%
28 %%%%%%%%%%%%%%%%%%%%%%%%%%%%%%%%%%%%%%%%%%%%%%%%%%%%%%%%%%%%%%%%%%%%%%%%%%%%%%%%
29 %% Total density and specific heat of the bed (Nickel and Air)
30 % Total density of bed
31 Rho = (eps*Rho_Ni) + ((1-eps)*Rho_air);
32
33 % Total specific heat of bed
34 c = (eps*c_Ni); %+ (0.4*c_air);
35
36 %%%%%%%%%%%%%%%%%%%%%%%%%%%%%%%%%%%%%%%%%%%%%%%%%%%%%%%%%%%%%%%%%%%%%%%%%%%%%%%%
37 %%%%%%%%%%%%%%%%%%%%%%%%%%%%%%%%%%%%%%%%%%%%%%%%%%%%%%%%%%%%%%%%%%%%%%%%%%%%%%%%
38 %% Heat transfer coefficient of bed to outer surrounding
39 % h = 11.44;
40 % h = 11.87;
41 % h = 12.26;
42 % h = 12.4;
43 % h = 12.62;
44 % h = 13;
45 % h = 13.26;
46 h = 13.4;
47 % h = 13.62;
48 % h = 14;
49 % h = 15;
50 % h = 16.4;
51 % h = 17;
52 % h = 18;
53
54 %%%%%%%%%%%%%%%%%%%%%%%%%%%%%%%%%%%%%%%%%%%%%%%%%%%%%%%%%%%%%%%%%%%%%%%%%%%%%%%%
55 %%%%%%%%%%%%%%%%%%%%%%%%%%%%%%%%%%%%%%%%%%%%%%%%%%%%%%%%%%%%%%%%%%%%%%%%%%%%%%%%
56 %% Dimensions of the bed
57 D = 0.01;                     % Diameter of tube
58 L = 0.1;                      % Length of tube
59
60 %%%%%%%%%%%%%%%%%%%%%%%%%%%%%%%%%%%%%%%%%%%%%%%%%%%%%%%%%%%%%%%%%%%%%%%%%%%%%%%%
61 %%%%%%%%%%%%%%%%%%%%%%%%%%%%%%%%%%%%%%%%%%%%%%%%%%%%%%%%%%%%%%%%%%%%%%%%%%%%%%%%
62 %% Boltzmann constant and emissivity of the bed
63 Sig = 5.67e-08;               % Stefan Boltzmann constant
64 % Eps = 0.97;
65 % Eps = 0.98;
66 Eps = 0.99;                   % Emissivity of bed
67
68 %%%%%%%%%%%%%%%%%%%%%%%%%%%%%%%%%%%%%%%%%%%%%%%%%%%%%%%%%%%%%%%%%%%%%%%%%%%%%%%%
69 %%%%%%%%%%%%%%%%%%%%%%%%%%%%%%%%%%%%%%%%%%%%%%%%%%%%%%%%%%%%%%%%%%%%%%%%%%%%%%%%
70 %%  Current and voltage been passed through the bed
```

```
% For 15W power through the fixed bed
% I = 5;                    % Current passing through the bed
% U = 3;                    % Voltage passing through the bed

%%%%%%%%%%%%%%%%%%%%%%%%%%%%%%%%%%%%%%%%%%%%%%%%%%%%%%%%%%%%%%%%%%%%%%%%%%%%%%%
%%%%%%%%%%%%%%%%%%%%%%%%%%%%%%%%%%%%%%%%%%%%%%%%%%%%%%%%%%%%%%%%%%%%%%%%%%%%%%%
% For 22.5W power through the fixed bed
% I = 7.5;                  % Current passing through the bed
% U = 3;                    % Voltage passing through the bed

%%%%%%%%%%%%%%%%%%%%%%%%%%%%%%%%%%%%%%%%%%%%%%%%%%%%%%%%%%%%%%%%%%%%%%%%%%%%%%%
%%%%%%%%%%%%%%%%%%%%%%%%%%%%%%%%%%%%%%%%%%%%%%%%%%%%%%%%%%%%%%%%%%%%%%%%%%%%%%%
% For 42W power through the fixed bed
I = 10;                     % Current passing through the bed
U = 4.2;                    % Voltage passing through the bed

%%%%%%%%%%%%%%%%%%%%%%%%%%%%%%%%%%%%%%%%%%%%%%%%%%%%%%%%%%%%%%%%%%%%%%%%%%%%%%%
%%%%%%%%%%%%%%%%%%%%%%%%%%%%%%%%%%%%%%%%%%%%%%%%%%%%%%%%%%%%%%%%%%%%%%%%%%%%%%%
%% Calculating the volume and area of bed
Vol = ((pi*D^2*L)/4);       % Volume of the bed
Area = pi*D*L;              % Surface area of the bed

%%%%%%%%%%%%%%%%%%%%%%%%%%%%%%%%%%%%%%%%%%%%%%%%%%%%%%%%%%%%%%%%%%%%%%%%%%%%%%%
%%%%%%%%%%%%%%%%%%%%%%%%%%%%%%%%%%%%%%%%%%%%%%%%%%%%%%%%%%%%%%%%%%%%%%%%%%%%%%%
%% Estimating the coefficients in the ODE
Is = (I*U)/(Rho*Vol*c);
As = (h*Area)/(Rho*Vol*c);
Es = (Sig*Eps*Area)/(Rho*Vol*c);

%%%%%%%%%%%%%%%%%%%%%%%%%%%%%%%%%%%%%%%%%%%%%%%%%%%%%%%%%%%%%%%%%%%%%%%%%%%%%%%
%%%%%%%%%%%%%%%%%%%%%%%%%%%%%%%%%%%%%%%%%%%%%%%%%%%%%%%%%%%%%%%%%%%%%%%%%%%%%%%
% The first order ODE in time as a function
dTdt = Is - As*(T - Tamb) - Es*(T^4 - Tamb^4);
```

A.1.2 Matlab function code to solve the ODE

```
%%%%%%%%%%%%%%%%%%%%%%%%%%%%%%%%%%%%%%%%%%%%%%%%%%%%%%%%%%%%%%%%%%%%%%%%%%%%%%%
%%%%%%%%%%%%%%%%%%%%%%%%%%%%%%%%%%%%%%%%%%%%%%%%%%%%%%%%%%%%%%%%%%%%%%%%%%%%%%%

function PlateTemp (T1, Vol, Area, Tamb)
% The function PlateTemp calculates the temperature in a tube
% Input variables:
% T1    The initial temperature in degrees K
% Vol   Volume of the tube in cubic meter
% Area  Area of the tube in square meter
```

```
% Tamb  The ambient temperature in degrees K

%%%%%%%%%%%%%%%%%%%%%%%%%%%%%%%%%%%%%%%%%%%%%%%%%%%%%%%%%%%%%%%%%%%%%%%%%%%%%%%
%%%%%%%%%%%%%%%%%%%%%%%%%%%%%%%%%%%%%%%%%%%%%%%%%%%%%%%%%%%%%%%%%%%%%%%%%%%%%%%
% Output:
% A plot of temperature versus time.

%%%%%%%%%%%%%%%%%%%%%%%%%%%%%%%%%%%%%%%%%%%%%%%%%%%%%%%%%%%%%%%%%%%%%%%%%%%%%%%
%%%%%%%%%%%%%%%%%%%%%%%%%%%%%%%%%%%%%%%%%%%%%%%%%%%%%%%%%%%%%%%%%%%%%%%%%%%%%%%
tspan = [0  600];     % time range for which the tempertaure is calculated
                      % in seconds

%%%%%%%%%%%%%%%%%%%%%%%%%%%%%%%%%%%%%%%%%%%%%%%%%%%%%%%%%%%%%%%%%%%%%%%%%%%%%%%
%%%%%%%%%%%%%%%%%%%%%%%%%%%%%%%%%%%%%%%%%%%%%%%%%%%%%%%%%%%%%%%%%%%%%%%%%%%%%%%
T1 = 300;             % Initial temperature in degree K

%%%%%%%%%%%%%%%%%%%%%%%%%%%%%%%%%%%%%%%%%%%%%%%%%%%%%%%%%%%%%%%%%%%%%%%%%%%%%%%
%%%%%%%%%%%%%%%%%%%%%%%%%%%%%%%%%%%%%%%%%%%%%%%%%%%%%%%%%%%%%%%%%%%%%%%%%%%%%%%
% Time at which temperature was measured during experiment
Tim = 0:60:600;       % in seconds

%%%%%%%%%%%%%%%%%%%%%%%%%%%%%%%%%%%%%%%%%%%%%%%%%%%%%%%%%%%%%%%%%%%%%%%%%%%%%%%
%%%%%%%%%%%%%%%%%%%%%%%%%%%%%%%%%%%%%%%%%%%%%%%%%%%%%%%%%%%%%%%%%%%%%%%%%%%%%%%
% Experimental results of temperature for 15W power of electricity
% for 600 seconds
% Tepp = [300  367.8  403.9  424.3  445.5  456.8  464.9  469  471.5  473.2  474.6];

%%%%%%%%%%%%%%%%%%%%%%%%%%%%%%%%%%%%%%%%%%%%%%%%%%%%%%%%%%%%%%%%%%%%%%%%%%%%%%%
%%%%%%%%%%%%%%%%%%%%%%%%%%%%%%%%%%%%%%%%%%%%%%%%%%%%%%%%%%%%%%%%%%%%%%%%%%%%%%%
% Experimental results of temperature for 22.5W power of electricity
% for 600 seconds
% Tepp = [300  399.9  436.5  475.1  496.3  510.9  520.8  525.3  526.5  527  526.3];

%%%%%%%%%%%%%%%%%%%%%%%%%%%%%%%%%%%%%%%%%%%%%%%%%%%%%%%%%%%%%%%%%%%%%%%%%%%%%%%
%%%%%%%%%%%%%%%%%%%%%%%%%%%%%%%%%%%%%%%%%%%%%%%%%%%%%%%%%%%%%%%%%%%%%%%%%%%%%%%
% Experimental results of temperature for 42W power of electricity
% for 600 seconds
Tepp = [300  436.5  523  570.9  609.9  623.5  633.3  638.6  641.1  643.1  643.7];

%%%%%%%%%%%%%%%%%%%%%%%%%%%%%%%%%%%%%%%%%%%%%%%%%%%%%%%%%%%%%%%%%%%%%%%%%%%%%%%
%%%%%%%%%%%%%%%%%%%%%%%%%%%%%%%%%%%%%%%%%%%%%%%%%%%%%%%%%%%%%%%%%%%%%%%%%%%%%%%
% Numerical solution of the ODE with time
[Time  Temp] = ode45(@TempRate, tspan, T1, [], Vol, Area, Tamb);
plot (Time, Temp,'b-o', Tim, Tepp, 'r-d')
xlabel('Time (s)')
ylabel('Temperature (K)')
legend ('Numerical Solution', 'Experimental', 'Location', 'southeast');
title ('Temperature variation with time, for current = 5 A')
```

```
58 % title ('Temperature variation with time, for current = 7.5 A')
59 % title ('Temperature variation with time, for current = 10 A')
```

Once both functions has been written, the Ordinary differential equation is then solved by writing the following command in the command window of MATLAB.

PlateTemp(673, Vol, Area, Tamb)

Appendix B

Numerical method and Matlab code

B.1 Solution Algorithm and Final Matrix

The steady-state temperature inside a cylindrical fixed bed is can be calculated from the solution of the equation:

$$\frac{1}{r}\frac{\partial}{\partial r}\left(r\varepsilon k_s\frac{\partial T}{\partial r}\right)+\dot{q}-\dot{A}_{\Sigma}h\left(T-T_g\right)=0 \tag{B.1}$$

Equation B.1 can be rewritten as:

$$\frac{\partial}{\partial r}\left(r\varepsilon k_s\frac{\partial T}{\partial r}\right)+r\dot{q}-r\dot{A}_{\Sigma}h\left(T-T_g\right)=0 \tag{B.2}$$

The boundary conditions are:

$$\left.\frac{\partial T}{\partial r}\right|_{(r=0)}=0$$
$$T(r=r_0)=T_s$$

Introducing a new variable $\lambda = r\varepsilon k_s$, equation B.2 can be written as:

$$\frac{\partial}{\partial r}\left(\lambda\frac{\partial T}{\partial r}\right)+r\dot{q}-r\dot{A}_{\Sigma}h\left(T-T_g\right)=0 \tag{B.3}$$

Using the FD discretization, the differential term of the equation can be rewritten as follows:

$$\left(\lambda\tfrac{\partial T}{\partial r}\right)_{i+1}=\lambda_{i+1}\tfrac{T_{i+1}-T_i}{\Delta r},\quad \left(\lambda\tfrac{\partial T}{\partial r}\right)_{i}=\lambda_{i}\tfrac{T_i-T_{i-1}}{\Delta r}$$

$$\tfrac{\partial}{\partial r}\left(\lambda\tfrac{\partial T}{\partial r}\right)\approx\tfrac{\left(\lambda\frac{\partial T}{\partial r}\right)_{i+1}-\left(\lambda\frac{\partial T}{\partial r}\right)_{i}}{\Delta r}\approx\tfrac{\lambda_{i+1}\frac{T_{i+1}-T_i}{\Delta r}-\lambda_i\frac{T_i-T_{i-1}}{\Delta r}}{\Delta r}=\tfrac{\lambda_{i+1}T_{i+1}-\left(\lambda_{i+1}+\lambda_i\right)T_i+\lambda_iT_{i-1}}{\Delta r^2}$$

The final discretization equation has the form:

$$A_{i+1}T_{i+1}+A_iT_i+A_{i-1}T_{i-1}=b_i \tag{B.4}$$

$$\begin{aligned}A_{i+1}&=\tfrac{\lambda_{i+1}}{\Delta r^2}\\ A_i&=-\tfrac{\lambda_{i+1}+\lambda_i}{\Delta r^2}-r_i\dot{A}_{\Sigma}h\\ A_{i-1}&=\tfrac{\lambda_i}{\Delta r^2}\\ b_i&=-r_i\dot{q}-r_i\dot{A}_{\Sigma}hT_g\end{aligned}$$

where

$$\begin{aligned}\lambda_{i+1}&=r_{i+1}\varepsilon k_s\\ \lambda_i&=r_i\varepsilon k_s\end{aligned}$$

Using 3 subintervals, N=3 implies that i =1, 2, 3, 4. Equation B.4 can be rewritten as follows:

$$\frac{\lambda_i}{\Delta r^2}T_{i-1}+\left(-\frac{\lambda_{i+1}+\lambda_i}{\Delta r^2}-r_i\dot{A}_{\Sigma}h\right)T_i+\frac{\lambda_{i+1}}{\Delta r^2}T_{i+1}=-r_i\dot{q}-r_i\dot{A}_{\Sigma}hT_g \tag{B.5}$$

Equation B.5 can then be written for the interior points ($i=2,3$):

$$i = 2 : \frac{\lambda_2}{\Delta r^2} T_1 + \left(-\frac{\lambda_3 + \lambda_2}{\Delta r^2} - r_2 \dot{A}_\Sigma h \right) T_2 + \frac{\lambda_3}{\Delta r^2} T_3 = -r_2 \dot{q} - r_2 \dot{A}_\Sigma h T_g$$
$$i = 3 : \frac{\lambda_3}{\Delta r^2} T_2 + \left(-\frac{\lambda_4 + \lambda_3}{\Delta r^2} - r_3 \dot{A}_\Sigma h \right) T_3 + \frac{\lambda_4}{\Delta r^2} T_4 = -r_3 \dot{q} - r_3 \dot{A}_\Sigma h T_g$$

The terms T_1 and T_4 can be evaluated from the boundary conditions: At r=0, we have Neumann boundary condition which can be evaluated as:

$$\left. \frac{\partial T}{\partial r} \right|_{r=0} = \frac{T_2 - T_1}{\Delta r} = 0$$
$$\Rightarrow T_1 = T_2$$

At r= r_0, at the endpoint, T_4 is known due to Dirichlet boundary condition.

$$T_4 = T_s$$

Substituting the terms T_1 and T_4 into the system of equations gives the following:

$$i = 2 : \left(\frac{\lambda_2}{\Delta r^2} - \frac{\lambda_3 + \lambda_2}{\Delta r^2} - r_2 \dot{A}_\Sigma h \right) T_2 + \frac{\lambda_3}{\Delta r^2} T_3 = -r_2 \dot{q} - r_2 \dot{A}_\Sigma h T_g$$
$$i = 3 : \frac{\lambda_3}{\Delta r^2} T_2 + \left(-\frac{\lambda_4 + \lambda_3}{\Delta r^2} - r_3 \dot{A}_\Sigma h \right) T_3 = -r_3 \dot{q} - r_3 \dot{A}_\Sigma h T_g - \frac{\lambda_4}{\Delta r^2} T_s$$

Therefore, the system of equation can then be written in the matrix form [A][T] = [b] and solved to determine the unknowns T_2 and T_3 .

$$\begin{bmatrix} A_{22} & A_{23} \\ A_{32} & A_{33} \end{bmatrix} \begin{bmatrix} T_2 \\ T_3 \end{bmatrix} = \begin{bmatrix} -r_2 \dot{q} - r_2 \dot{A}_\Sigma h T_g \\ -r_3 \dot{q} - r_3 \dot{A}_\Sigma h T_g - \frac{\lambda_4}{\Delta r^2} T_s \end{bmatrix}$$

where

$$A_{22} = \left(\frac{\lambda_2}{\Delta r^2} - \frac{\lambda_3 + \lambda_2}{\Delta r^2} - r_2 \dot{A}_\Sigma h \right)$$
$$A_{23} = \frac{\lambda_3}{\Delta r^2}$$
$$A_{32} = \frac{\lambda_3}{\Delta r^2}$$
$$A_{33} = \left(-\frac{\lambda_4 + \lambda_3}{\Delta r^2} - r_3 \dot{A}_\Sigma h \right)$$

Therefore, the solid temperature in the radial direction is given as follows:

$$T = \begin{bmatrix} T(1) \\ T(2) \\ T(3) \\ T(4) \end{bmatrix}$$

Gas temperature equation:

$$\rho_g c_p u_g \frac{dT_g}{dz} = \dot{A}_\Sigma h \left(\overline{T} - T_g\right) \tag{B.6}$$

where $\overline{T}$ is the average (over the radius) temperature of the solid phase:

$$\overline{T} = \frac{2}{r_0^2} \int_0^{r_0} T r dr \tag{B.7}$$

The analytical solution for the gas temperature equation above is as follows:

$$\frac{\left(\overline{T} - T_g\right)_{in}}{\left(\overline{T} - T_g\right)_{out}} = e^{\frac{\dot{A}_\Sigma h}{\rho_g c_p u_g}} \tag{B.8}$$

Therefore, the outflow gas temperature can then be estimated as follows by rearranging the above equation:

$$T_{g_{out}} = \overline{T} - \frac{\left(\overline{T} - T_g\right)_{in}}{e^{\frac{\dot{A}_\Sigma h}{\rho_g c_p u_g}}} \tag{B.9}$$

To calculate the surface temperature, T_s of the fixed bed:

$$h_{out}\left(T_s - T_\infty\right) + \varepsilon_\sigma \sigma \left(T_s^4 - T_\infty^4\right) = -k_s \left.\frac{\partial T}{\partial r}\right|_{r=r_0} \tag{B.10}$$

The differential at $r = r_0$ can be evaluated as follows:

$$\left.\frac{\partial T}{\partial r}\right|_{r=r_0} = \frac{T(4) - T(3)}{\Delta r}$$
$$T(4) = T_s$$

Equation B.10 can then be rewritten as follows and solved using the bisection method.

$$h_{out}\left(T_s - T_\infty\right) + \varepsilon_\sigma \sigma \left(T_s^4 - T_\infty^4\right) + k_s \frac{T(4)-T(3)}{\Delta r} = 0$$
$$h_{out}\left(T_s - T_\infty\right) + \varepsilon_\sigma \sigma \left(T_s^4 - T_\infty^4\right) + k_s \frac{T_s-T(3)}{\Delta r} = 0$$

B.2 Matlab Code for solving for temperature in a fixed bed with gas flow

B.2.1 Matlab code for the heterogeneous model

```
%% Computing the tridiagonal matrix
% number of subintervals
clear all;
close all;
M = 3;
% The constants
% void fraction in the enclosure
epsilon = 0.77;
epsilon_s = 1 - epsilon;
% emissivity
E = 0.8;
% Stefan-Boltzmann constant
sig = 5.67e-08;
% ambient gas temperature
Tinf = 273+18;
% thermal conductivity of solids
ks = 91.74;
% thermal conductivity of gas
kg = 0.024;
% number of particles
Np = 374;
% electrical current and el. field potential dif.
I = 5;
U = 3;

% I = 7.5;
% U = 3;

% I = 10;
% U = 3;
```

```
% U = 4.2;
% length of the tube
L = 0.1;
% diameter of tube
d_p=0.003;
% heat transfer between solid and gas
Nu=2.5;
hp = Nu*kg/d_p;
% heat tranf coef between air and wall enclosure
hsurf = 15;

% radius of the particle
rp = d_p/2;
% radius of bed
ro = 0.005;

% Inlet gas temperature
Tg1 = 273+15;
% axial position in bed
% dz = d_p*0.1;
dz = L/N;
z(1) = 0;
% total surface area of particles
Ae = 1.5*Np*4*pi*rp^2;
% specific surface
Aed = Ae/(epsilon_s*L*pi*ro^2);
% source term
qd = (I*U)/(epsilon_s*L*pi*ro^2);
qd;
% density of gas
rhog = 1.;
%specific heat capacity of gas
cpg = 1006.43;
% cros section of the tube
AA = pi*ro^2;
% Flow rate and velocity
% Uf = 6.2;
% Uf = 12.4;
% Uf = 21.2;
Uf = 30;
ug = (Uf*(10^-3)/(1000*60))/AA;  % velocity calculated from flow rate

% radial points defined
dr = ro/M;
r(1) = 0;

% surface temperature at point "a" in the bisection method
Ts = 1000;
```

```
% Defining the radial positions
for i = 1:M
    r(i+1) = r(i) + dr;
    ljam(i) = r(i)*ks*epsilon_s;
end
ljam(M+1) = r(M+1)*ks*epsilon_s;
dr2 = dr^2;
% coefficient of the matrix
%i=2
A1 = 0.5*(ljam(1)+ljam(2))/dr2;
A2 = - (ljam(2)+0.5*ljam(3)+0.5*ljam(1))/dr2 -r(2)*Aed*hp;
A3 = 0.5*(ljam(2)+ljam(3))/dr2;
b1 = -r(2)*qd - r(2)*Aed*hp*Tg1;
%
A11 = A1+A2;
A12 = A3;
% i=3
A2 = 0.5*(ljam(3)+ljam(2))/dr2;
A3 =  - (ljam(3)+0.5*ljam(4)+0.5*ljam(2))/dr2 -r(3)*Aed*hp;
A4 = 0.5*(ljam(3)+ljam(4))/dr2;
b2 = -r(3)*qd - r(3)*Aed*hp*Tg1 - A4*Ts;
A21= A2;
A22= A3;
% matrix and source term vector
AN = [A11 A12; A21 A22;];
b = [b1; b2];

AN;
b;
% solve matrix equation
TN = AN\b;
T(1) = TN(1);
T(2) = TN(1);
T(3) = TN(2);
T(4) = Ts;
T;

figure;
plot(r,T)
% surface balance equation
Tsa=Ts;
fa = hsurf*(Ts - Tinf) + E*sig*(Ts^4 - Tinf^4) + ks*(T(4) - T(3))/dr;
% new Ts
% surface temperature at point "b" in the bisection method
Ts=300;
b2 = -r(3)*qd - r(3)*Aed*hp*Tg1 - A4*Ts;
b = [b1; b2];

```

```
127 TN = AN\b;
128
129 T(1) = TN(1);
130 T(2) = TN(1);
131 T(3) = TN(2);
132 T(4) = Ts;
133 T;
134
135 figure;
136 plot(r,T)
137 Tsb=Ts;
138 fb = hsurf*(Ts - Tinf) + E*sig*(Ts^4 - Tinf^4) + ks*(T(4) - T(3))/dr;
139 imax=50;  % number of iterations used for bisection method
140 if fa*fb > 0
141     disp('Error: the function has the same sign at points a nad b')
142 else
143     disp('iterations')
144     for i =1:imax
145         Ts=0.5*(Tsa+Tsb);
146         toli = abs(Tsa-Tsb)/Tsa;
147         b2 = -r(3)*qd - r(3)*Aed*hp*Tg1 - A4*Ts;
148         b = [b1; b2];
149
150         TN = AN\b;
151         T(1) = TN(1); T(2) = TN(1); T(3) = TN(2); T(4) = Ts;
152         fx = hsurf*(Ts - Tinf) + E*sig*(Ts^4 - Tinf^4) + ks*(T(4) - T(3))/dr;
153         if fx*fa < 0
154             Tsb=Ts; fb = fx;
155         else
156             Tsa=Ts; fa = fx;
157         end
158         fprintf('%3i  %11.6f  %11.6f  %11.6f  %11.6f  %11.6f  %11.6f  %11.6f\n',
    i, Tsa, Tsb, Ts, fx, fa, fb, toli)
159         if toli < 1e-6
160             fprintf('a solution Ts=%11.6f was found',Ts)
161             break
162         end
163 %         if toli < 1e-6
164 %             break
165 %         end
166
167     end
168 end
169
170
171 % Gas temperature
172 tmp1 = Aed*hp*dz/(rhog*cpg*ug);
173 Taver = (T(1)+T(4))/2;
```

```
174 Tg2 = Taver - (Taver-Tg1)/exp(tmp1);
175 Tg2-273;
176 Ts;
```

Bibliography

[1] Parham Sadooghi and Reinhard Rauch. Pseudo heterogeneous modeling of catalytic methane steam reforming process in a fixed bed reactor. *Journal of Natural Gas Science and Engineering*, 11:46–51, 2013.

[2] M Ertan Taskin, Anthony G Dixon, and E Hugh Stitt. CFD study of fluid flow and heat transfer in a fixed bed of cylinders. *Numerical Heat Transfer, Part A: Applications*, 52(3):203–218, 2007.

[3] Howard F Rase. *Fixed-bed reactor design and diagnostics: gas-phase reactions*. Butterworths Boston, 1990.

[4] Dongsheng Wen and Yulong Ding. Heat transfer of gas flow through a packed bed. *Chemical Engineering Science*, 61(11):3532–3542, 2006.

[5] L Zili and S Ben Nasrallah. Heat and mass transfer during drying in cylindrical packed beds. *Numerical Heat Transfer: Part A: Applications*, 36(2): 201–228, 1999.

[6] K Vafai, CP Desai, and SC Chen. An investigation of heat transfer process in a chemically reacting packed bed. *Numerical Heat Transfer, Part A: Applications*, 24(2):127–142, 1993.

[7] A Carotenuto, G Buonanno. The effective thermal conductivity of packed beds of spheres for a finite contact area. *Numerical Heat Transfer: Part A: Applications*, 37(4):343–357, 2000.

[8] Anthony G Dixon. Heat transfer in fixed beds at very low (< 4) tube-to-particle diameter ratio. *Industrial & Engineering Chemistry Research*, 36 (8):3053–3064, 1997.

[9] Kunii Daizo and Suzuki Motoyuki. Particle-to-fluid heat and mass transfer in packed beds of fine particles. *International Journal of Heat and Mass Transfer*, 10(7):845–852, 1967.

[10] DJ Gunn and JFC De Souza. Heat transfer and axial dispersion in packed beds. *Chemical Engineering Science*, 29(6):1363–1371, 1974.

[11] N Wakao, S Kaguei, and T Funazkri. Effect of fluid dispersion coefficients on particle-to-fluid heat transfer coefficients in packed beds: correlation of nusselt numbers. *Chemical engineering science*, 34(3):325–336, 1979.

[12] Donald E Beasley and John A Clark. Transient response of a packed bed for thermal energy storage. *International Journal of Heat and Mass Transfer*, 27(9):1659–1669, 1984.

[13] Licínio M Ferreira, José AM Castro, and Alírio E Rodrigues. An analytical and experimental study of heat transfer in fixed bed. *International journal of heat and mass transfer*, 45(5):951–961, 2002.

[14] AP Collier, AN Hayhurst, JL Richardson, and SA Scott. The heat transfer coefficient between a particle and a bed (packed or fluidised) of much larger particles. *Chemical Engineering Science*, 59(21):4613–4620, 2004.

[15] AP De Wasch and GF Froment. A two dimensional heterogeneous model for fixed bed catalytic reactors. *Chemical Engineering Science*, 26(5):629–634, 1971.

[16] AP De Wasch and GF Froment. Heat transfer in packed beds. *Chemical Engineering Science*, 27(3):567–576, 1972.

[17] Marvin B Glaser and George Thodos. Heat and momentum transfer in the flow of gases through packed beds. *AIChE Journal*, 4(1):63–68, 1958.

[18] Neal R Amundson. Solid-fluid interactions in fixed and moving beds fixed beds with small particles. *Industrial & Engineering Chemistry*, 48(1):26–35, 1956.

[19] JR Arthur and JW Linnett. The interchange of heat between a gas stream and solid granules. Part I. *J. Chem. Soc.*, pages 416–424, 1947.

[20] Ao Anzelius. Über erwärmung vermittels durchströmender medien. *ZAMM-Journal of Applied Mathematics and Mechanics/Zeitschrift für Angewandte Mathematik und Mechanik*, 6(4):291–294, 1926.

[21] Bernard W Gamson, George Thodos, and OA Hougen. Heat, mass and momentum transfer in the flow of gases through granular solids. *Trans. AIChE*, 39(1):1–35, 1943.

[22] GOG Löf and RW Hawley. Unsteady-state heat transfer between air and loose solids. *Industrial & Engineering Chemistry*, 40(6):1061–1070, 1948.

[23] CN Satterfield, H Resnick, and RL Wentworth. Simultaneous heat and mass transfer in a diffusion-controlled chemical reaction 1. *Chemical Engineering Progress*, 50(9):460–466, 1954.

[24] T.E.W Schumann. Heat transfer: A liquid flowing through a porous prism. *Journal of the Franklin Institute*, 208(3):405–416, 1929.

[25] RG Taecker and OA Hougen. Heat, mass transfer of gas film in flow of gases through commercial tower packings. *Chemical Engineering Progress*, 45(3): 188–193, 1949.

[26] RH Wilhelm, WC Johnson, and F S Acton. Conduction, convection, and heat release in catalytic converters. *Industrial & Engineering Chemistry*, 35 (5):562–575, 1943.

[27] Allan P Colburn. Heat transfer and pressure drop in empty, baffled, and packed tubes1. *Industrial & Engineering Chemistry*, 23(8):910–913, 1931.

[28] Sabri Ergun. Fluid flow through packed columns. *Chem. Eng. Prog.*, 48: 89–94, 1952.

[29] SA Logtenberg, M Nijemeisland, and AG Dixon. Computational fluid dynamics simulations of fluid flow and heat transfer at the wall–particle contact points in a fixed-bed reactor. *Chemical Engineering Science*, 54(13):2433–2439, 1999.

[30] Chi-Hsiung Li and BA Finlayson. Heat transfer in packed beds—a reevaluation. *Chemical Engineering Science*, 32(9):1055–1066, 1977.

[31] E Tsotsas and E-U Schlünder. Heat transfer in packed beds with fluid flow: remarks on the meaning and the calculation of a heat transfer coefficient at the wall. *Chemical engineering science*, 45(4):819–837, 1990.

[32] D Vortmeyer and E Haidegger. Discrimination of three approaches to evaluate heat fluxes for wall-cooled fixed bed chemical reactors. *Chemical engineering science*, 46(10):2651–2660, 1991.

[33] MG Freiwald and WR Paterson. Accuracy of model predictions and reliability of experimental data for heat transfer in packed beds. *Chemical engineering science*, 47(7):1545–1560, 1992.

[34] YE Kutsovsky, LE Scriven, HT Davis, and BE Hammer. NMR imaging of velocity profiles and velocity distributions in bead packs. *Physics of Fluids*, 8:863–871, 1996.

[35] AJ Sederman, ML Johns, AS Bramley, P Alexander, and LF Gladden. Magnetic resonance imaging of liquid flow and pore structure within packed beds. *Chemical Engineering Science*, 52(14):2239–2250, 1997.

[36] KR Jolls and TJ Hanratty. Transition to turbulence for flow through a dumped bed of spheres. *Chemical Engineering Science*, 21(12):1185–1190, 1966.

[37] J Tobiś and D Ziółkowski. Modelling of heat transfer at the wall of a packed-bed apparatus. *Chemical engineering science*, 43(11):3031–3036, 1988.

[38] Simon A Logtenberg and Anthony G Dixon. Computational fluid dynamics studies of fixed bed heat transfer. *Chemical Engineering and Processing: Process Intensification*, 37(1):7–21, 1998.

[39] Simon A Logtenberg and Anthony G Dixon. Computational fluid dynamics studies of the effects of temperature-dependent physical properties on fixed-bed heat transfer. *Industrial & engineering chemistry research*, 37(3):739–747, 1998.

[40] Olaf R Derkx and Anthony G Dixon. Determination of the fixed bed wall heat transfer coefficient using computational fluid dynamics. *Numerical Heat Transfer, Part A Applications*, 29(8):777–794, 1996.

[41] D Bhattacharyya and DCT Pei. Heat transfer in fixed bed gas—solid systems. *Chemical Engineering Science*, 30(3):293–300, 1975.

[42] WB Agro and JM Smith. Heat transfer in gas-solid packed bed systems. *Chem. Eng. Programme*, 49:443–450, 1953.

[43] WE Ranz. Friction and transfer coefficients for single particles and packed beds. *Chemical Engineering Progress*, 48(5):247–253, 1952.

[44] Emanuel Singer and RH Wilhelm. Heat transfer in packed beds-analytical solution and design method-fluid flow, solids flow, and chemical reaction. *Chemical Engineering Progress*, 46(7):343–357, 1950.

[45] H Verschoor and G CA Schuit. Heat transfer to fluids flowing through a bed of granular solids. *Applied Scientific Research*, 2(1):97–119, 1951.

[46] RH Wilhelm, WC Johnson, R Wynkoop, and DW Collier. Reaction rate, heat transfer, and temperature distribution in fixed-bed catalytic converters-solution by electrical network. *Chemical Engineering Progress*, 44(2):105–116, 1948.

[47] Sakae Yagi and Daizo Kunii. Studies on effective thermal conductivities in packed beds. *AIChE Journal*, 3(3):373–381, 1957.

[48] Sakae Yagi, Daizo Kunii, and Noriaki Wakao. Studies on axial effective thermal conductivities in packed beds. *AIChE Journal*, 6(4):543–546, 1960.

[49] Ernest B Baumeister and CO Bennett. Fluid-particle heat transfer in packed beds. *AIChE Journal*, 4(1):69–74, 1958.

[50] Russell Wendt Dayton, SL Fawcett, RE Grimble, and CE Sealander. Improved measurements of surface heat transfer by the method of cyclic temperature variations. Technical report, Battelle Memorial Inst., 1952.

[51] CG Furnas. Heat transfer from a gas stream to bed of broken solids. *Industrial & Engineering Chemistry*, 22(1):26–31, 1930.

[52] Bernard W Gamson, George Thodos, and OA Hougen. Heat, mass and momentum transfer in the flow of gases through granular solids. *Trans. AIChE*, 39(1):1–35, 1943.

[53] Richard B Lancashire, Erwin A Lezberg, and James F Morris. Experimental results of a heat-transfer study from a full-scale pebble-bed heater. Technical report, National Aeronautics and Space Administration. Lewis Research Center, Cleveland, 1960.

[54] A Sen Gupta and George Thodos. Mass and heat transfer through fixed and fluidized beds. *Chem. Eng. Progr.*, 58(7):58, 1962.

[55] A Sen Gupta and George Thodos. Transitional behavior for the simultaneous mass and heat transfer of gases flowing through packed and distended beds of spheres. *Industrial & Engineering Chemistry Fundamentals*, 3(3):218–220, 1964.

[56] Noriaki Wakao and Seiichirō Kagei. *Heat and mass transfer in packed beds*, volume 1. Taylor & Francis, 1982.

[57] William W Schertz and Kenneth B Bischoff. Thermal and material transport in nonisothermal packed beds. *AIChE Journal*, 15(4):597–604, 1969.

[58] J Marivoet, P Teodoroiu, and SJ Wajc. Porosity, velocity and temperature profiles in cylindrical packed beds. *Chemical Engineering Science*, 29(8): 1836–1840, 1974.

[59] JJ Lerou and GF Froment. Velocity, temperature and conversion profiles in fixed bed catalytic reactors. *Chemical Engineering Science*, 32(8):853–861, 1977.

[60] Anthony G Dixon. The length effect on packed bed effective heat transfer parameters. *The Chemical Engineering Journal*, 31(3):163–173, 1985.

[61] I Ziółkowska and D Ziolkowski. Modelling of gas interstitial velocity radial distribution over a cross-section of a tube packed with a granular catalyst bed. *Chemical engineering science*, 48(18):3283–3292, 1993.

[62] Anthony G Dixon and Johan H van Dongeren. The influence of the tube and particle diameters at constant ratio on heat transfer in packed beds. *Chemical Engineering and Processing: Process Intensification*, 37(1):23–32, 1998.

[63] Michiel Nijemeisland and Anthony G Dixon. Comparison of CFD simulations to experiment for convective heat transfer in a gas–solid fixed bed. *Chemical Engineering Journal*, 82(1):231–246, 2001.

[64] YASAR Demirel, RN Sharma, and HH Al-Ali. On the effective heat transfer parameters in a packed bed. *International Journal of Heat and Mass Transfer*, 43(2):327–332, 2000.

[65] N Wakao, S Kaguei, and H Nagai. Effective diffusion coefficients for fluid species reacting with first order kinetics in packed bed reactors and discussion on evaluation of catalyst effectiveness factors. *Chemical Engineering Science*, 33(2):183–187, 1978.

[66] WR Paterson and JJ Carberry. Fixed bed catalytic reactor modelling: the heat transfer problem. *Chemical Engineering Science*, 38(1):175–180, 1983.

[67] Sven Hermansson and Henrik Thunman. CFD modelling of bed shrinkage and channelling in fixed-bed combustion. *Combustion and Flame*, 158(5): 988–999, 2011.

[68] Bernhard Peters. Measurements and application of a discrete particle model (DPM) to simulate combustion of a packed bed of individual fuel particles. *Combustion and Flame*, 131(1):132–146, 2002.

[69] E Simsek, B Brosch, S Wirtz, V Scherer, and F Krüll. Numerical simulation of grate firing systems using a coupled CFD/discrete element method (DEM). *Powder technology*, 193(3):266–273, 2009.

[70] Henrik Thunman and Bo Leckner. Co-current and counter-current fixed bed combustion of biofuel—a comparison. *Fuel*, 82(3):275–283, 2003.

[71] Yao Bin Yang, Vida Nasserzadeh Sharifi, and Jim Swithenbank. Substoichiometric conversion of biomass and solid wastes to energy in packed beds. *AIChE journal*, 52(2):809–817, 2006.

[72] Robert Johansson, Henrik Thunman, and Bo Leckner. Sensitivity analysis of a fixed bed combustion model. *Energy & fuels*, 21(3):1493–1503, 2007.

[73] Robert Johansson, Henrik Thunman, and Bo Leckner. Influence of intraparticle gradients in modeling of fixed bed combustion. *Combustion and Flame*, 149(1):49–62, 2007.

[74] Michael L Hobbs, Predrag T Radulovic, and L Douglas Smoot. Modeling fixed-bed coal gasifiers. *AIChE Journal*, 38(5):681–702, 1992.

[75] M Fatehi and M Kaviany. Role of gas-phase reaction and gas-solid thermal nonequilibrium in reverse combustion. *International journal of heat and mass transfer*, 40(11):2607–2620, 1997.

[76] Donghoon Shin and Sangmin Choi. The combustion of simulated waste particles in a fixed bed. *Combustion and flame*, 121(1):167–180, 2000.

[77] Colomba Di Blasi. Dynamic behaviour of stratified downdraft gasifiers. *Chemical engineering science*, 55(15):2931–2944, 2000.

[78] JJ Saastamoinen, R Taipale, M Horttanainen, and P Sarkomaa. Propagation of the ignition front in beds of wood particles. *Combustion and flame*, 123 (1):214–226, 2000.

[79] J Cooper and WLH Hallett. A numerical model for packed-bed combustion of char particles. *Chemical Engineering Science*, 55(20):4451–4460, 2000.

[80] YB Yang, YR Goh, R Zakaria, V Nasserzadeh, and J Swithenbank. Mathematical modelling of MSW incineration on a travelling bed. *Waste management*, 22(4):369–380, 2002.

[81] Haosheng Zhou, AD Jensen, Peter Glarborg, Peter Arendt Jensen, and Andrius Kavaliauskas. Numerical modeling of straw combustion in a fixed bed. *Fuel*, 84(4):389–403, 2005.

[82] MH Hyman. Simulate methane reformer reactions. *Hydrocarbon processing*, 47(7):131, 1968.

[83] Gilbert F Froment and HPK Hofmann. *Design of fixed-bed gas-solid catalytic reactors*. Marcel Dekker: New York, 1987.

[84] Anthony G Dixon, Michael A DiCostanzo, and Brian A Soucy. Fluid-phase radial transport in packed beds of low tube-to-particle diameter ratio. *International Journal of Heat and Mass Transfer*, 27(10):1701–1713, 1984.

[85] Adam Luckos and John R Bunt. Pressure-drop predictions in a fixed-bed coal gasifier. *Fuel*, 90(3):917–921, 2011.

[86] Robert K Niven. Physical insight into the Ergun and Wen & Yu equations for fluid flow in packed and fluidised beds. *Chemical Engineering Science*, 57(3):527–534, 2002.

[87] LG Gibilaro, R Di Felice, SP Waldram, and PU Foscolo. Generalized friction factor and drag coefficient correlations for fluid-particle interactions. *Chemical Engineering Science*, 40(10):1817–1823, 1985.

[88] LHS Roblee, RM Baird, and JW Tierney. Radial porosity variations in packed beds. *AIChE Journal*, 4(4):460–464, 1958.

[89] J Eastwood, EJP Matzen, MJ Young, and N Epstein. Random loose porosity of packed beds. *British Chemical Engineering*, 14(11):1542, 1969.

[90] RJ Wakeman. Packing densities of particles with log-normal size distributions. *Powder technology*, 11(3):297–299, 1975.

[91] Mark Propster and Julian Szekely. The porosity of systems consisting of layers of different particles. *Powder Technology*, 17(1):123–138, 1977.

[92] Alan S Foust, Leonard A Wenzel, Curtis W Clump, Louis Maus, and L Bryce Andersen. *Principles of unit operations*. John Wiley & Sons, 2008.

[93] Norio Ouchiyama and Tatsuo Tanaka. Porosity of a mass of solid particles having a range of sizes. *Industrial & Engineering Chemistry Fundamentals*, 20(1):66–71, 1981.

[94] Norio Ouchiyama and Tatsuo Tanaka. Porosity estimation for random packings of spherical particles. *Industrial & engineering chemistry fundamentals*, 23(4):490–493, 1984.

[95] N Peronius and TJ Sweeting. On the correlation of minimum porosity with particle size distribution. *Powder technology*, 42(2):113–121, 1985.

[96] AB Yu and N Standish. An analytical—parametric theory of the random packing of particles. *Powder technology*, 55(3):171–186, 1988.

[97] AC Hoffmann and HJ Finkers. A relation for the void fraction of randomly packed particle beds. *Powder Technology*, 82(2):197–203, 1995.

[98] RP Zou and AB Yu. Evaluation of the packing characteristics of mono-sized non-spherical particles. *Powder technology*, 88(1):71–79, 1996.

[99] AB Yu, RP Zou, and N Standish. Modifying the linear packing model for predicting the porosity of nonspherical particle mixtures. *Industrial & engineering chemistry research*, 35(10):3730–3741, 1996.

[100] M Song, Karl T Chuang, and K Nandakumar. A theoretical correction of the Ouchiyama and Tanaka formula for predicting average porosity of packed beds consisting of nonuniform spheres. *Industrial & engineering chemistry research*, 37(8):3490–3496, 1998.

[101] Ricardo P Dias, Jose A Teixeira, Manuel G Mota, and Alexander I Yelshin. Particulate binary mixtures: Dependence of packing porosity on particle size ratio. *Industrial & engineering chemistry research*, 43(24):7912–7919, 2004.

[102] F Benyahia and KE O'Neill. Enhanced voidage correlations for packed beds of various particle shapes and sizes. *Particulate science and technology*, 23 (2):169–177, 2005.

[103] RE Hicks. Pressure drop in packed beds of spheres. *Industrial & Engineering Chemistry Fundamentals*, 9(3):500–502, 1970.

[104] CK Chan and CL Tien. Conductance of packed spheres in vacuum. *Journal of Heat Transfer*, 95(3):302–308, 1973.

[105] CL Tien and GR Cunnington. Cryogenic insulation heat transfer. *Advances in heat transfer.*, 9:349–417, 1973.

[106] Shinobu Masamune and JM Smith. Thermal conductivity of beds of spherical particles. *Industrial & Engineering Chemistry Fundamentals*, 2(2):136–143, 1963.

[107] Noriaki Wakao and Koichi Kato. Effective thermal conductivity of packed beds. *Journal of Chemical Engineering of Japan*, 2(1):24–33, 1969.

[108] N Wakao and D Vortmeyer. Pressure dependency of effective thermal conductivity of packed beds. *Chemical Engineering Science*, 26(10):1753–1765, 1971.

[109] MM Yovanovich. Apparent conductivity of glass microspheres from atmospheric pressure to vacuum. ASME Paper 73-HT-43. *American Society of Mechanical Engineers, New York*, 1973.

[110] George C Lindauer. Heat transfer in packed and fluidized beds by the method of cyclic temperature variations. *AIChE Journal*, 13(6):1181–1187, 1967.

[111] OM Martinez, SI Pereira Duarte, OA Ferretti, and NO Lemcoff. Estimation of the pseudohomogeneous one-dimensional heat transfer coefficient in a fixed bed. *Chemical Engineering and Processing: Process Intensification*, 20(5):245–253, 1986.

[112] V Hlavacek and J Votruba. Chemical reactor theory, a review. *Amundson, NR*, page 314, 1977.

[113] GF Froment and KB Bischoff. Chemical reactor analysis and design. pages 178–179, 1979.

[114] SI Pereira Duarte and NO Lemcoff. Analysis of fixed-bed catalytic reactor models. In *ACS symposium series*, number 237, pages 239–254. Oxford University Press, 1984.

[115] OM Martinez, SI Pereira Duarte, and NO Lemcoff. Modeling of fixed bed catalytic reactors. *Computers & chemical engineering*, 9(5):535–545, 1985.

[116] SI Pereira Duarte, OM Martínez, OA Ferretti, and NO Lemcoff. Coeficientes de transferencia de calor para un modelo heterogéneo unidimensional. In *Proc. 1er. Congreso Latinoamericano de Transferencia de Calor y Materia*, volume 2, page 1011, 1982.

[117] Anthony G Dixon and David L Cresswell. Theoretical prediction of effective heat transfer parameters in packed beds. *AIChE Journal*, 25(4):663–676, 1979.

[118] WE Olbrich. A two-phase diffusional model to describe heat transfer processes in a non-adiabatic packed tubular bed. In *Chemeca*, volume 170, pages 101–119, 1970.

[119] D Vortmeyer and R Berninger. Comments on the paper, theoretical prediction of effective heat transfer parameters in packed beds by Anthony Dixon and DL Cresswell [AIChE J., 25, 663 (1979)]. *AIChE Journal*, 28(3):508–510, 1982.

[120] D Vortmeyer and RJ Schaefer. Equivalence of one-and two-phase models for heat transfer processes in packed beds: one dimensional theory. *Chemical Engineering Science*, 29(2):485–491, 1974.

[121] DL Cresswell and AG Dixon. Reply to comments by Vortmeyer and Berninger on the paper "theoretical prediction of effective heat transfer parameters in packed beds (AIChE J., 25, 663, 1979)". *AIChE Journal*, 28(3): 511–513, 1982.

[122] SI Pereira Duarte, OA Ferretti, and NO Lemcoff. A heterogeneous one-dimensional model for non-adiabatic fixed bed catalytic reactors. *Chemical engineering science*, 39(6):1025–1031, 1984.

[123] Max Leva, Murray Weintraub, Milton Grummer, and EL Clark. Cooling of gases through packed tubes. *Industrial & Engineering Chemistry*, 40(4): 747–752, 1948.

[124] Johann Wurzenberger. *A combined packed bed and single particle model applied to biomass combustion*. na, 2001.

[125] Marcos HJ Pedras and Marcelo JS de Lemos. Macroscopic turbulence modeling for incompressible flow through undeformable porous media. *International Journal of Heat and Mass Transfer*, 44(6):1081–1093, 2001.

[126] Marcos HJ Pedras and Marcelo JS de Lemos. Simulation of turbulent flow in porous media using a spatially periodic array and a low Re two-equation closure. *Numerical Heat Transfer: Part A: Applications*, 39(1):35–59, 2001.

[127] Marcelo JS De Lemos. *Turbulence in porous media: Modeling and Applications*. Elsevier, 2012.

[128] Francisco D Rocamora Jr and Marcelo JS de Lemos. Analysis of convective heat transfer for turbulent flow in saturated porous media. *International communications in heat and mass transfer*, 27(6):825–834, 2000.

[129] M de Lemos and F Rocamora. Turbulent transport modeling for heated flow in rigid porous media. *Heat Transfer*, 2:791–796, 2002.

[130] Edimilson J Braga and Marcelo JS de Lemos. Turbulent natural convection in a porous square cavity computed with a macroscopic κ–ε model. *International journal of heat and mass transfer*, 47(26):5639–5650, 2004.

[131] Edimilson J Braga and Marcelo JS De Lemos. Heat transfer in enclosures having a fixed amount of solid material simulated with heterogeneous and homogeneous models. *International Journal of Heat and Mass Transfer*, 48 (23):4748–4765, 2005.

[132] Edimilson J Braga and Marcelo JS de Lemos. Laminar natural convection in cavities filled with circular and square rods. *International communications in heat and mass transfer*, 32(10):1289–1297, 2005.

[133] Edimilson J Braga and Marcelo J de Lemos. Turbulent heat transfer in an enclosure with a horizontal permeable plate in the middle. *Journal of heat transfer*, 128(11):1122–1129, 2006.

[134] Edimilson J Braga and Marcelo JS de Lemos. Simulation of turbulent natural convection in a porous cylindrical annulus using a macroscopic two-equation model. *International journal of heat and mass transfer*, 49(23):4340–4351, 2006.

[135] Edimilson J Braga and Marcelo JS de Lemos. Computation of turbulent free convection in left and right tilted porous enclosures using a macroscopic κ–ε model. *International Journal of Heat and Mass Transfer*, 51(21):5279–5287, 2008.

[136] Edimilson J Braga and Marcelo JS de Lemos. Laminar and turbulent free convection in a composite enclosure. *International Journal of Heat and Mass Transfer*, 52(3):588–596, 2009.

[137] Marcelo JS de Lemos and Maximillian S Mesquita. Turbulent mass transport in saturated rigid porous media. *International communications in heat and mass transfer*, 30(1):105–113, 2003.

[138] Marcelo JS de Lemos and Luzia A Tofaneli. Modeling of double-diffusive turbulent natural convection in porous media. *International journal of heat and mass transfer*, 47(19):4233–4241, 2004.

[139] Marcelo Assato, Marcos HJ Pedras, and Marcelo JS De Lemos. Numerical solution of turbulent channel flow past a backward-facing step with a porous insert using linear and nonlinear κ–ε models. *Journal of Porous Media*, 8 (1), 2005.

[140] Nicolau B Santos and Marcelo JS de Lemos. Flow and heat transfer in a parallel-plate channel with porous and solid baffles. *Numerical Heat Transfer, Part A: Applications*, 49(5):471–494, 2006.

[141] Marcelo JS de Lemos. Turbulent kinetic energy in a moving porous bed. *International Communications in Heat and Mass Transfer*, 35(9):1049–1052, 2008.

[142] Marcelo JS de Lemos and Marcelo B Saito. Computation of turbulent heat transfer in a moving porous bed using a macroscopic two-energy equation model. *International Communications in Heat and Mass Transfer*, 35(10): 1262–1266, 2008.

[143] Fujio Kuwahara, Mitsuhiro Shirota, and Akira Nakayama. A numerical study of interfacial convective heat transfer coefficient in two-energy equation model for convection in porous media. *International journal of heat and mass transfer*, 44(6):1153–1159, 2001.

[144] Marcelo B Saito and Marcelo JS De Lemos. A correlation for interfacial heat transfer coefficient for turbulent flow over an array of square rods. *Journal of Heat Transfer*, 128(5):444–452, 2006.

[145] WH MacAdams. Heat transmission. *McGraw-Hill series in chemical engineering*, 1954.

[146] Blas Melissari and Stavros A Argyropoulos. Development of a heat transfer dimensionless correlation for spheres immersed in a wide range of Prandtl number fluids. *International journal of heat and mass transfer*, 48(21):4333–4341, 2005.

[147] MM Yovanovich. Natural convection from isothermal spheroids in the conductive to laminar flow regimes. In *AIAA, 22nd Thermophysics Conference*, volume 1, 1987.

[148] MM Yovanovich and CA Vanoverbeke. Combined natural and forced convection heat transfer from isothermal spheres. In *AIAA, Thermophysics, Plasmadynamics and Lasers Conference*, volume 1, 1988.

[149] M Michael Yovanovich. General expression for forced convection heat and mass transfer from isopotential spheroids. In *26th AIAA Aerospace Sciences Meeting*, volume 1, 1988.

[150] Frank P Incropera. *Fundamentals of heat and mass transfer*. John Wiley & Sons, 2011.

[151] Gazy F Al-Sumaily, John Sheridan, and Mark C Thompson. Analysis of forced convection heat transfer from a circular cylinder embedded in a porous medium. *International Journal of Thermal Sciences*, 51:121–131, 2012.

[152] Gazy F Al-Sumaily, Akira Nakayama, John Sheridan, and Mark C Thompson. The effect of porous media particle size on forced convection from a circular cylinder without assuming local thermal equilibrium between phases. *International Journal of Heat and Mass Transfer*, 55(13):3366–3378, 2012.

[153] Yaser Hadad and Khosrow Jafarpur. Modeling of laminar forced convection heat transfer in packed beds with pebbles of arbitrary geometry. *Journal of Porous Media*, 16(11), 2013.

[154] Yaser Hadad and Khosrow Jafarpur. Laminar forced convection heat transfer from isothermal bodies with unity aspect ratio in coaxial air flow. *Heat Transfer Engineering*, 33(3):245–254, 2012.

[155] D Handley and PJ Heggs. Momentum and heat transfer mechanisms in regular shaped packings. *Transactions of the Institution of Chemical Engineers and the Chemical Engineer*, 46(9):T251, 1968.

[156] LR Galloway, W Komarnicky, and N Epstein. Effect of packing configuration on mass and heat transfer in beds of stacked spheres. *Can. J. Chem. Eng*, 35:139–150, 1957.

[157] James De Acetis and George Thodos. Mass and heat transfer in flow of gases through spherical packings. *Industrial & Engineering Chemistry*, 52 (12):1003–1006, 1960.

[158] Ashis Sen Gupta and George Thodos. Direct analogy between mass and heat transfer to beds of spheres. *AIChE Journal*, 9(6):751–754, 1963.

[159] GF Malling and George Thodos. Analogy between mass and heat transfer in beds of spheres: Contributions due to end effects. *International Journal of Heat and Mass Transfer*, 10(4):489–498, 1967.

[160] AV Bradshaw, A Johnson, NH McLachlan, and YT Chiu. Heat transfer between air and nitrogen and packed beds of non-reacting solids. *Trans. Inst. Chem. Eng*, 48:T77–T84, 1970.

[161] Kambiz Vafai. *Handbook of porous media*. Crc Press, 2010.

[162] H Inaba, T Fukuda, H Saito, and F Mayinger. Transient behavior of heat removal from a cylindrical heat storage vessel packed with spherical porous particles. *Wärme-und Stoffübertragung*, 22(6):325–333, 1988.

[163] Jamil A Khan, Donald E Beasley, and Bulent Alatas. Evaporation from a packed bed of porous particles into superheated vapor. *International journal of heat and mass transfer*, 34(1):267–280, 1991.

[164] GD Raithby and ERG Eckert. The effect of turbulence parameters and support position on the heat transfer from spheres. *International Journal of Heat and Mass Transfer*, 11(8):1233–1252, 1968.

[165] Sebastian Schulze, Petr A Nikrityuk, and Bernd Meyer. Porosity Distribution in Monodisperse and Polydisperse Fixed beds and Its Impact on the Fluid Flow. *Particulate Science and Technology*, (just-accepted), 2014.

[166] Ansys Fluent. Ansys fluent theory guide. *ANSYS Inc., USA*, 2011.

[167] Petr A Nikrityuk and Bernd Meyer. *Gasification Processes: Modeling and Simulation*. John Wiley & Sons, 2014.

[168] Gregor D Wehinger, Thomas Eppinger, and Matthias Kraume. Detailed numerical simulations of catalytic fixed-bed reactors: Heterogeneous dry reforming of methane. *Chemical Engineering Science*, 122:197–209, 2015.

[169] DL Hartmann, AMG Klein Tank, M Rusicucci, LV Alexander, B Broenniman, Y Charabi, FJ Dentener, EJ Dlugokencky, DR Easterling, A Kaplan, et al. Observations: atmosphere and surface. 2013.

[170] De Chen, Rune Lødeng, Arne Anundsk ås, Ola Olsvik, and Anders Holmen. Deactivation during carbon dioxide reforming of methane over Ni catalyst: microkinetic analysis. *Chemical Engineering Science*, 56(4):1371–1379, 2001.

[171] Jason M Ginsburg, Juliana Piña, Tarek El Solh, and Hugo I de Lasa. Coke formation over a nickel catalyst under methane dry reforming conditions: thermodynamic and kinetic models. *Industrial & engineering chemistry research*, 44(14):4846–4854, 2005.

[172] Jianjun Guo, Hui Lou, and Xiaoming Zheng. The deposition of coke from methane on a $Ni/MgAl_2O_4$ catalyst. *Carbon*, 45(6):1314–1321, 2007.

[173] Steven Corthals, Toon Witvrouwen, Pierre Jacobs, and Bert Sels. Development of dry reforming catalysts at elevated pressure: D-optimal vs. full factorial design. *Catalysis Today*, 159(1):12–24, 2011.

[174] Xuli Zhai, Shi Ding, Yinhong Cheng, Yong Jin, and Yi Cheng. CFD simulation with detailed chemistry of steam reforming of methane for hydrogen production in an integrated micro-reactor. *international journal of hydrogen energy*, 35(11):5383–5392, 2010.

[175] John N Armor. The multiple roles for catalysis in the production of H_2. *Applied Catalysis A: General*, 176(2):159–176, 1999.

[176] Yunhua Li, Yaquan Wang, Xiangwen Zhang, and Zhentao Mi. Thermodynamic analysis of autothermal steam and CO_2 reforming of methane. *International Journal of Hydrogen Energy*, 33(10):2507–2514, 2008.

[177] AM Adris, BB Pruden, CJ Lim, and JR Grace. On the reported attempts to radically improve the performance of the steam methane reforming reactor. *The Canadian Journal of Chemical Engineering*, 74(2):177–186, 1996.

[178] L Kepiński, B Stasińska, and T Borowiecki. Carbon deposition on Ni/Al_2O_3 catalysts doped with small amounts of molybdenum. *Carbon*, 38(13):1845–1856, 2000.

[179] Ta-Jen Huang and Meng-Chin Huang. Effect of Ni content on hydrogen production via steam reforming of methane over Ni/GDC catalysts. *Chemical Engineering Journal*, 145(1):149–153, 2008.

[180] Mohammad Irani, Asghar Alizadehdakhel, Ali Nakhaei Pour, Nasibeh Hoseini, and Morteza Adinehnia. CFD modeling of hydrogen production using steam reforming of methane in monolith reactors: Surface or volume-base reaction model? *international journal of hydrogen energy*, 36(24):15602–15610, 2011.

[181] Mustafa Balat. Potential importance of hydrogen as a future solution to environmental and transportation problems. *International Journal of Hydrogen Energy*, 33(15):4013–4029, 2008.

[182] MEE Abashar. Coupling of steam and dry reforming of methane in catalytic fluidized bed membrane reactors. *International Journal of Hydrogen Energy*, 29(8):799–808, 2004.

[183] OL Ding and SH Chan. Autothermal reforming of methane gas- modelling and experimental validation. *International Journal of Hydrogen Energy*, 33 (2):633–643, 2008.

[184] Pradeepkumar O Sharma, Martin A Abraham, and Sudipta Chattopadhyay. Development of a novel metal monolith catalyst for natural gas steam reforming. *Industrial & Engineering Chemistry Research*, 46(26):9053–9060, 2007.

[185] I-Tso Chen. Steam Reforming of Methane.

[186] Alireza Behroozsarand and Ali Nakhaei Pour. Modeling of microreactor for methane dry reforming: Comparison of Langmuir–Hinshelwood kinetic and microkinetic models. *Journal of Natural Gas Science and Engineering*, 20: 99–108, 2014.

[187] WP Jones and RP Lindstedt. Global reaction schemes for hydrocarbon combustion. *Combustion and Flame*, 73(3):233–249, 1988.